Monitoring restoration and aboveground biomass in tropical peat swamp forests on Borneo using multi-sensoral remote sensing data

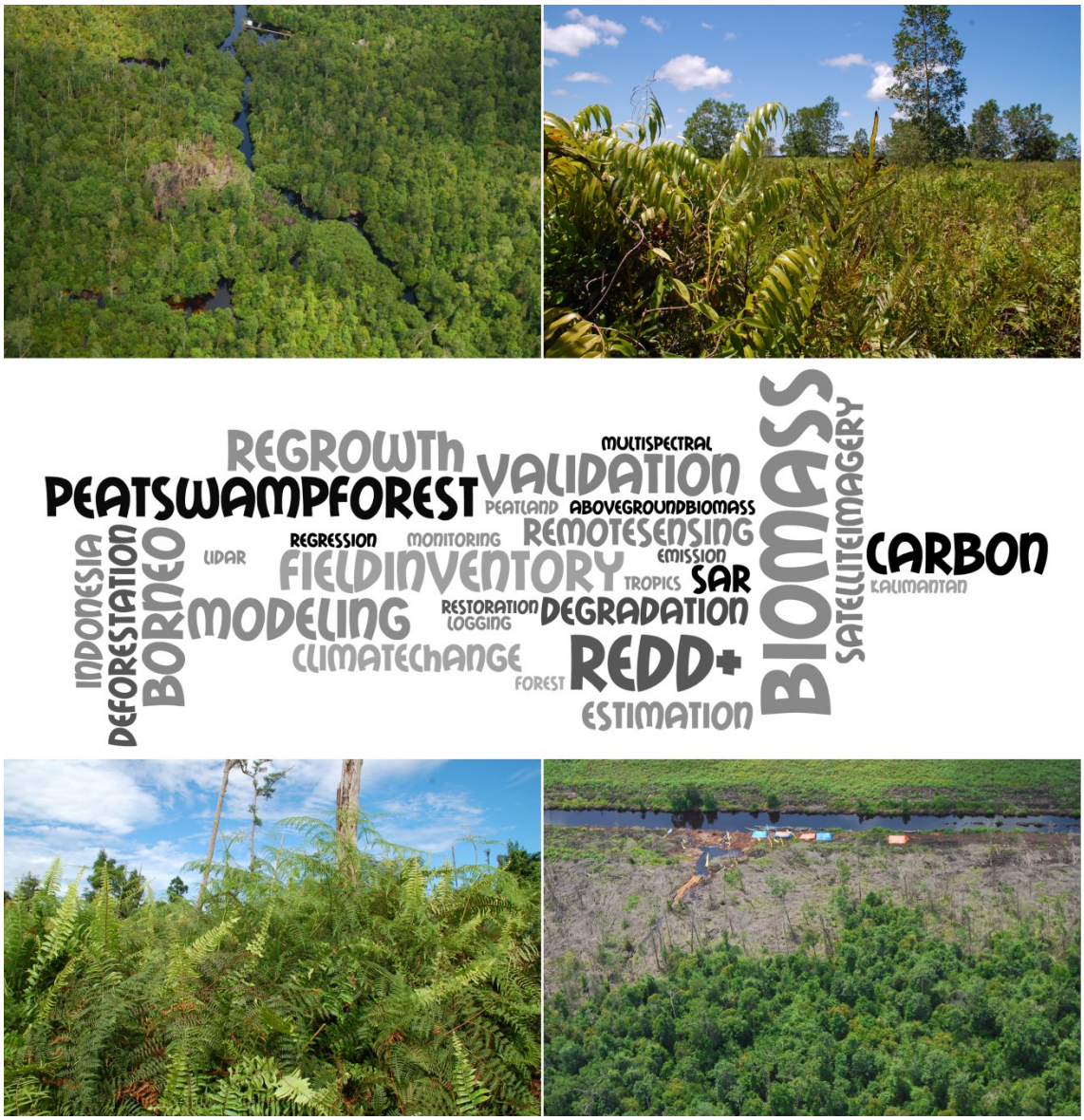

Sandra Englhart

München 2012

Monitoring restoration and aboveground biomass in tropical peat swamp forests on Borneo using multi-sensoral remote sensing data

Dissertation der Fakultät für Biologie
der Ludwig-Maximilian-Universität München

vorgelegt von
Sandra Englhart

München, 15. November 2012

Erstgutachter: Prof. Dr. Florian Siegert

Zweitgutachter: PD Dr. Martin Heß

Tag der Abgabe: 15. November 2012

Tag der mündlichen Prüfung: 21.Mai 2013

ACKNOWLEDGEMENTS

First of all, I would like to thank my supervisor Prof. Dr. Florian Siegert for giving me the opportunity to realize this dissertation at the Remote Sensing Solutions GmbH, Baierbrunn. He supported my work and ideas and always provided helpful comments to my work. I appreciate the participation in conferences and summer schools. Furthermore, I am thankful for the great experience of field trips to Central Kalimantan on Borneo. It was very valuable for me to discover the study area and to get to know the Dayak way of life.

I thank PD Dr. Martin Heß very much for being the second referee of this thesis and for showing interest in my topic.

Suwido Limin and the team from CIMTROP (Centre for International Co-operation in sustainable Management of Tropical Peatland), University of Palangka Raya are acknowledged for the logistical support during the field surveys. Special thanks to Agung Susanto for taking care of me and for having a great time.

Furthermore, I would like to express my gratitude to my colleagues and former colleagues Peter, Julia, Vanessa, Jonas, Karin, Uwe, Juilson, Iris, Tanja, and Keith for being so helpful and supportive. Thanks for the nice and relaxed working atmosphere. Many thanks to Vanessa for helping me with all kind of questions and for always providing valuable input and helpful comments to my work. Her support helped me through the most difficult parts of my work. Special thanks to Julia for always encouraging me.

This dissertation would not have been possible without my family and friends. Thanks to all my friends who accompanied me during my doctoral studies. I greatly value your friendship and support. Very special thanks go to my boyfriend Thomas for his never ending love and support in all respects, especially the immediate computer technical help. Thank you for being always there for me. Finally, I would like to express my deepest gratitude to my parents Brigitte and Bernd for your unconditional love, amazing support and everything you did for me. From you I learned to believe in me and to go my own way. You gave me so much strength.

ABSTRACT

Tropical forests store huge amounts of carbon and are responsible for high annual emissions rates. Deforestation and forest degradation in the tropics contribute 6 - 17% of global anthropogenic carbon dioxide emissions. Additionally, tropical peatlands make a significant contribution to the terrestrial carbon stock in terms of thick belowground peat deposits (up to 20 m) and aboveground forests. The largest share of tropical peat swamp forest occurs in Indonesia and is a huge carbon sink due to the amount of carbon stored in the peat. The forests are under severe anthropogenic pressure, mainly for the needs of logging activities and large scale plantation development (mostly oil palm). The peat is being drained and the forest cover is being reduced resulting in a high susceptibility to fire which is commonly used to clear forested areas. Between 1990 and 2010, Borneo lost approximately half of its initial peat swamp forest cover mainly caused by legal and illegal logging, extensive plantation development, enormous drainage, land-development projects, and a very strong El Niño episode in 1997/1998 being responsible for a prolonged drought period. Hence, Indonesia became one of the largest greenhouse gas emitters worldwide and is therefore in the focus of REDD+ projects which aim at reducing emissions from deforestation and forest degradation. These projects require a precise monitoring of national forest carbon stocks which are generally derived from aboveground biomass (AGB) estimations. Remote sensing has been identified as the most cost effective way to monitor these remote and hardly accessible forests. Even though field inventory measurements are laborious, time consuming and, they are mandatory to calibrate satellite or airborne signals to estimate AGB.

The main goals of this thesis are to monitor hydrological effects of peat restoration measurements with continuous SAR (synthetic aperture radar) imagery and to evaluate the potential and accuracy of multi-frequency SAR, multispectral RapidEye, and multi-temporal airborne LiDAR (light detection and ranging) data for AGB retrieval. The study area is located in Central Kalimantan on Borneo, Indonesia, and is dominated by peat swamp forests. Analysis of multi-temporal combined X- and L-band SAR imagery showed promising results for estimating AGB up to 300 t/ha. A comparison of methods revealed that artificial neural network (ANN) was superior to multivariate linear regression (MLR) and support vector regression (SVR) models. AGB estimations based

on spectral unmixed RapidEye data were more accurate than using multi-frequency SAR data but were affected by frequent cloud cover and saturation of the satellite signal. Multi-temporal airborne LiDAR (light detection and ranging) measurements successfully proved to precisely quantify even small scale AGB dynamics without the constraint of saturation due to the detailed determination of the vertical vegetation structure. This evaluation of different sensors for AGB retrieval in tropical peat swamp forests is very important, especially in the context of REDD+.

ZUSAMMENFASSUNG

Tropische Wälder bilden einen großen Kohlenstoffspeicher und setzen jedes Jahr große Mengen davon frei. Entwaldung und Walddegradierung in den Tropen trägt jährlich 6 - 17% zu den anthropogenen Kohlenstoffdioxidemission bei. Tropische, bewaldete Torfgebiete leisten durch tiefe, unterirdische Torfvorkommen (bis zu 20 m) und darauf wachsende Wälder einen besonderen Beitrag zum terrestrischen Kohlenstoffspeicher. Das größte Vorkommen tropischer Torfsumpfwälder befindet sich in Indonesien und bildet durch den im Torf gebundenen Kohlenstoff einen enormen Speicher. Diese Wälder sind starken anthropogenen Einflüssen ausgesetzt, hauptsächlich aufgrund von Holzeinschlag und großflächigen Plantangen (überwiegend für Palmöl). Der Torf wird dabei trockengelegt und der Waldbestand reduziert. Dies führt zu einer hohen Anfälligkeit für Feuer, welches üblicherweise dazu genutzt wird, bewaldete Flächen zu roden. Zwischen 1990 und 2010 hat Borneo ungefähr die Hälfte des ursprünglichen Torfsumpfwaldes verloren, vorwiegend aufgrund von legalem und illegalem Holzeinschlag, großflächigen Plantagen, massiver Trockenlegung des Torfes, sowie einer extremen El Niño Trockenperiode in den Jahren 1997/1998. Dadurch wurde Indonesien zu einem der größten Treibhausgasemittenten weltweit und rückte daher in den Fokus von REDD+ Projekten, die auf eine Verringerung der Emissionen durch Entwaldung und Walddegradierung abzielen. Diese Projekte benötigen eine genaue Kontrolle der nationalen Kohlenstoffbestände der Wälder, welche im Allgemeinen von der Biomasse abgeleitet werden. Die Analyse von Fernerkundungsdaten erwies sich als die wirtschaftlichste Methode diese abgelegenen und kaum zugänglichen Wälder zu überwachen. Auch wenn die Erhebung von Felddaten arbeitsintensiv, zeitaufwendig und teuer ist, ist dies dennoch zwingend erforderlich für die Kalibrierung von luft- oder satellitengestützten Fernerkundungsdaten im Hinblick auf die Bestimmung der Biomasse.

Das Hauptziel dieser Arbeit ist eine Evaluation der hydrologischen Effekte der Torfrenaturierung mithilfe von Radardatenzeitreihen sowie die Möglichkeit und Genauigkeit der Biomassebestimmung auf Basis von Radardaten verschiedener Frequenzen, multispektralen RapidEye und multitemporalen flugzeuggetragenen LiDAR (light detection and ranging) Messungen. Das Untersuchungsgebiet liegt in Zentral Kalimantan auf Borneo, Indonesien, und wird von Torfsumpfwälder dominiert.

Die Verwendung von multitemporalen kombinierten X- und L-Band Radardaten zeigte vielversprechende Ergebnisse für eine Bestimmung der Biomasse bis zu 300 t/ha. Ein Methodenvergleich demonstrierte, dass künstliche neuronale Netze besser geeignet waren als multivariate lineare Regressionen oder Support Vektor Regressionen. Biomassebestimmungen basierend auf optischen, spektral entmischten RapidEye Daten erzielten eine höhere Genauigkeit als die Verwendung von Radardaten verschiedener Frequenzen. Nachteile sind jedoch die häufige Bewölkung in tropischen Regionen sowie eine Sättigung des Satellitensignal. Mithilfe von multitemporale flugzeuggetragenen LiDAR Messungen konnten auch kleinräumige Änderungen der Biomasse beobachtet werden, was durch die detailgetreue Darstellung der vertikalen Vegetationsstruktur ermöglicht wird. Diese Evaluierung verschiedener Sensoren zur Bestimmung der Biomasse in tropischen Torfsumpfwäldern ist besonders für REDD+ Projekten sehr bedeutend.

LIST OF ORIGINAL ARTICLES

CHAPTER II

Jaenicke J., **Englhart S.** & Siegert F. (2011) Monitoring the effect of restoration measures in Indonesian peatlands by radar satellite imagery. *Journal of Environmental Management,* 92, 630-380.

CHAPTER III

Englhart S., Keuck V. & Siegert F. (2011) Aboveground biomass retrieval in tropical forests - the potential of combined X- and L-band SAR data. *Remote Sensing of Environment,* 115, 1260-1271.

CHAPTER IV

Englhart S., Keuck V. & Siegert F. (2012) Modeling aboveground biomass in tropical forests using multi-frequency SAR data - a comparison of methods. *IEEE Journal of Selected Topics in Applied Earth Observation and Remote Sensing,* 5, 298-306.

CHAPTER V

Englhart S., Franke J., Keuck V. & Siegert F. (2012) Carbon stock monitoring of tropical forests on Borneo, Indonesia, and related REDD+ requirements. *EARSeL-Springer Book 'Land use and land cover mapping in Europe',* submitted.

CHAPTER VI

Englhart S., Jubanski J. & Siegert F. (2012) Quantifying dynamics in tropical peat swamp forest biomass with multi-temporal LiDAR datasets. Manuscript in preparation for *Remote Sensing.*

CONTRIBUTION OF THE AUTHORS

CHAPTER II

Dr. Julia Jaenicke planned the study, developed the methodology for image processing and change detection analysis and Sandra Englhart processed the large amount of remote sensing data and helped with the analysis. Prof. Dr. Florian Siegert revised the manuscript.

CHAPTER III

Sandra Englhart planned the study, developed the methodology and analyzed the data. Dr. Vanessa Keuck helped with the statistics and SAR data processing. Dr. Vanessa Keuck and Prof. Dr. Florian Siegert participated in planning the study and revised the manuscript.

CHAPTER IV

Planning of the study and evaluating different methods for biomass estimation was conducted by Sandra Englhart. Dr. Vanessa Keuck helped to plan the study and introduced the neural networks and support vector machines. Dr. Vanessa Keuck and Prof. Dr. Florian Siegert revised the manuscript.

CHAPTER V

Sandra Englhart developed the methodology, conducted field inventory work in Central Kalimantan (Indonesia), and analyzed the results. Dr. Jonas Franke introduced the methodology of the spectral mixture analysis and processed the RapidEye data. Dr. Jonas Franke, Dr. Vanessa Keuck and Prof. Dr. Florian Siegert helped to plan the study and revised the manuscript.

CHAPTER VI

Sandra Englhart planned the study, conducted field inventory work in Central Kalimantan (Indonesia), calculated canopy height models, conducted the change analyses, and evaluated the results. Dr. Juilson Jubanski processed the LiDAR data, managed the data base, and helped with the implementation of the regressions. Prof. Dr. Florian Siegert helped to plan the study and revised the manuscript.

I hereby confirm the above statements.

Munich, 15 November 2012

_____	_____
Sandra Englhart	Prof. Dr. Florian Siegert

TABLE OF CONTENTS

LIST OF FIGURES

LIST OF TABLES

LIST OF ACRONYMS

3D	Three-dimensional
AGB	Aboveground biomass
ALOS	Advanced Land Observation Satellite
ANN	Artificial neural network
AP	Alternating polarization
ASAR	Advanced Synthetic Aperture Radar
AVHRR	Advanced Very High Resolution Radiometer
AVNIR-2	Advanced Visible and Near Infrared Radiometer type 2
C	Carbon
CH	Centroid height
CHM	Canopy height model
CKPP	Central Kalimantan Peatland Project
CO_2	Carbon dioxide
CPC	Climate Prediction Center
DBH	Diameter at breast height
DEM	Digital elevation model
dGPS	Differential Global Positioning System
DN	Digital numbers
DSM	Digital surface model
ENVISAT	Environmental Satellite
ETM+	Enhanced Thematic Mapper Plus
FAO	Food and Agriculture Organization
FBD	Fine beam dual
FBS	Fine beam single
FIRMS	Fire Information For Resource Management System
GLAS	Geoscience Laser Altimeter System
GOFC-GOLD	Global Observation for Forest and Land Cover Dynamics
GPCP	Global Precipitation Climatology Project
GPS	Global Positioning System
GV	Green vegetation

GWL	Ground water level
H	Horizontal
ICESat	Ice, Cloud, and land Elevation Satellite
IPCC	Intergovernmental Panel on Climate Change
JERS-1	Japanese Earth Resource Satellite 1
LiDAR	Light detection and ranging
MAE	Mean absolute error
ME	Mean error
MLP	Multilayer perceptron
MLR	Multivariate linear regression
MODIS	Moderate Resolution Imaging Spectroradiometer
MRP	Mega Rice Project
MTMF	Mixture Tuned Matched Filtering
NASA	National Aeronautic and Space Administration
NOAA	National Oceanic and Atmospheric Administration
NPV	Non-photosynthetic vegetation
PALSAR	Phased Array type L-band Synthetic Aperture Radar
REDD	Reducing emissions from deforestation and forest degradation
RMSE	Root mean square error
SAR	Synthetic aperture radar
SLC	Scan Line Corrector
SMA	Spectral mixture analysis
SRTM	Shuttle Radar Topography Mission
STD	Standard deviation
SVM	Support vector machine
SVR	Support vector regression
USD	United States Dollar
USGS	United States Geological Survey
UV	Ultraviolet
V	Vertical

I. Introduction

1. Importance of tropical forest monitoring

Tropical forests are among the most carbon (C) rich and structurally complex ecosystems in the world and are therefore in the focus of climate change mitigation mechanism projects (Streck et al. 2008). Deforestation and forest degradation of tropical forests contribute to atmospheric greenhouse gas emissions through combustion of forest biomass and decomposition of remaining plant material and soil carbon. In total, 228.7 Gt of carbon is stored in tropical woody vegetation and the total net emission of carbon from tropical deforestation is estimated at 1.0 Gt of carbon per year annualized over the period from 2000-2010 (Baccini et al. 2012). These activities are responsible for 6 - 17% of global anthropogenic carbon dioxide (CO_2) emissions (van der Werf et al. 2009). Considering also carbon emissions from tropical peatland burning and oxidation in Southeast Asia, the contribution of forest and peatland decline amounted even to 23% of global anthropogenic CO_2 emissions (van der Werf et al. 2009).

Tropical peatlands make an important contribution to the terrestrial carbon storage not only in terms of their forests but also in terms of their underlying thick peat deposits (Page et al. 1999). The total area of tropical peatland is estimated at 441.025 km² whereby Southeast Asia encompasses the largest portion (247.778 km², 56%). Indonesia comprises the largest area of peat within Southeast Asia (206.950 km², 47% of total tropical peatland area) and contains a total carbon stock of approximately 74 Gt of which 19 Gt is stored aboveground in forests and 55 Gt belowground in peat deposits (Baccini et al. 2012; Jaenicke et al. 2008; Page et al. 2011).

Due to widespread felling and burning of rain forests and carbon rich peat swamp forests, Indonesia became one of the world's largest greenhouse gas emitter and moved therefore into focus of climate change mitigation mechanisms aiming at avoided deforestation (Sloan et al. 2012). REDD+ is an example for such a mechanism and deals with reducing emissions from deforestation and forest degradation, conservation of forest carbon stocks, sustainable management of forest land and enhancement of forest carbon stocks (Campbell 2009). Deforestation is defined as conversion from forest land to non-forest land which means a reduction in crown cover below a certain threshold (typically between 10% and 30%) (GOFC-GOLD 2011). Deforestation typically results from conversion of forest to annual crop land, conversion to perennial plants (oil palm

or shrubs) and conversion to urban lands or other human infrastructure (GOFC-GOLD 2011). Forest degradation is defined as decrease in canopy cover or biomass density, mainly caused by selective logging or understory fire (DeFries et al. 2007). REDD+ was approved at the United Nations Climate Change Conferences in 2009 and 2010, and the year 2011 provided the starting point for the development of a worldwide forest monitoring system. The aim of the REDD+ mechanism is to rapidly and radically reduce the rate of deforestation and degradation across the tropics via performance related payments to countries that reduce these emissions. The financing needs for 2010 to 2015 are estimated at 20 - 30 billion USD. Developed countries made an initial payment of 4 billion USD for the years 2010 to 2012 (Clements 2010). Norway and Indonesia concluded a landmark deal which obligated Norway to provide 1 billion USD for Indonesia's advancing forest emission reduction. A major component is a moratorium on new agricultural and logging licenses which aims to support Indonesia's goal of reducing national emissions by 26% until 2020 and to prepare Indonesia to draw payments from industrial nations via the REDD+ scheme (Sloan et al. 2012).

REDD+ is promoted as a win-win situation for climate change mitigation and tropical forest conservation. It could end up contributing to a global economy based on carbon and ecosystem services (Asner 2011). Co-benefits of REDD+ are supposed to be conserving biodiversity, alleviating poverty, and climate change adaptation. However, there are also REDD+ related problems, such as leakage or displacement of carbon emissions within a country. Therefore, a nationwide carbon stock monitoring is needed to prevent that reduced deforestation or forest degradation could occur in one part of the country but increase in another one (DeFries et al. 2007). A challenge for REDD+ projects is to accurately estimate the carbon stock and to monitor its changes. Remote sensing has been identified as a very efficient and cost effective method (Herold et al. 2007).

2. Tropical carbon stock monitoring using remote sensing

The amount of carbon stored in vegetation is generally derived from aboveground biomass (AGB) estimates by assuming a carbon content of dry biomass of 50% (Goetz et al. 2009). Field inventory measurements are the most accurate way to retrieve AGB but they are difficult to obtain because their collection is laborious and expensive, especially in remote and highly inaccessible tropical forests. Therefore, remote sensing

is an effective way to retrieve spatially explicit AGB estimation maps. However, field inventory derived AGB data are mandatory as reference for remote sensing based AGB estimations.

Different kinds of approaches have been developed to retrieve AGB estimation maps from remote sensing data. The indirect approach is based on a land cover classification whereby a certain AGB value or range is linked to each of the land cover classes. This approach is limited by the wide range of AGB variability within any land cover class and by ambiguities in the definition of those classes. A more sophisticated way to produce carbon stock maps is the direct AGB estimation method in which satellite measurements are calibrated directly to field inventory AGB data (Goetz et al. 2009). The direct AGB estimation adapted from optical, SAR (synthetic aperture radar) and LiDAR (light detection and ranging) data as well as the sensor basics are described in detail in the following chapters. Table I-1 provides an overview of the different sensors and their characteristics. A general distinction is made between active and passive systems. Active systems emit energy and measure the radiation that is reflected or scattered back, whereas passive systems detect the natural available radiation that is emitted or reflected.

Table I-1: Overview of different remote sensing sensors and their characteristics.

	Optical	**SAR**	**LiDAR**
System	passive	active	active
Radiation	reflected sunlight	microwave pulses	pulses of infrared light
Spectrum	UV - infrared	microwave	infrared
Wavelengths	0.3 – 14 µm	0.75 – 100 cm	around 1 µm
Acquisition time	day	day & night	day & night
Signal dependence on weather	blocked by clouds	penetrate clouds	blocked by clouds

2.1. Optical data

Optical remote sensing is a passive system which makes use of electromagnetic radiation which is emitted by the sun and reflected off the earth's surface. The optical spectrum includes ultraviolet (UV), visible, near-, mid-, and thermal-infrared

wavelengths which range from 0.3 - 14 µm (Lillesand et al. 2008). The acquisition depends on daylight and can be hindered by clouds, haze or smoke. The different materials on the earth's surface have different characteristics of reflection and absorption at different wavelengths which means that targets can be differentiated by their spectral reflectance signatures. Multispectral sensing includes data which are acquired simultaneously in several spectral bands.

AGB estimations derived from optical imagery are mostly based on spectral reflectance collected by moderate or medium resolution sensors, e.g. MODIS (Moderate Resolution Imaging Spectroradiometer) (1 km) or Landsat (30 m) imagery (Avitabile et al. 2012; Baccini et al. 2008; Li et al. 2010; Tangki et al. 2008).

Vegetation indices are combinations of two or more spectral bands and can be calculated by rationing, differencing, rationing differences and sums, and by forming linear combinations. Vegetation indices are intended to highlight a particular property of the vegetation signal, while minimizing solar irradiance and soil background effects. AGB estimations derived from Landsat vegetation indices were conducted by Foody et al. (2001) and Freitas et al. (2005), for example. Boyd et al. (1999) estimated AGB from a combination of spectral reflectance and vegetation indices of moderate resolution (1 km) NOAA AVHRR (National Oceanic and Atmospheric Administration, Advanced Very High Resolution Radiometer) imagery.

Image texture is another method to derive AGB estimations from optical data and is defined by the multi-dimensional variance observed in a moving window passed through the image (e.g. 3 x 3 pixels window). Sarker et al. (2011) found image texture superior to using vegetation indices or spectral reflectance at high resolution (10 m) ALOS AVNIR-2 (Advanced Land Observation Satellite, Advanced Visible and Near Infrared Radiometer type 2) data. Eckert (2012) also found a superior performance of image texture to estimate AGB from very high resolution (0.5 m) WorldView-2 imagery. Lu (2005) and Lu et al. (2012) retrieved best results in estimating AGB on the basis of Landsat spectral signatures and image texture.

Spectral mixture analysis (SMA) is a technique for comparing mixed spectral signatures to "pure" reference data, e.g. bare soil, green vegetation (GV), non-photosynthetic vegetation (NPV), or shade. Mixed pixels include more than one reference spectrum or land cover type on ground. The result is an estimate of the approximate proportions of the ground area of each pixel that are occupied by each of the reference class. For

example, Lu et al. (2005) and Clark et al. (2011) used SMA to estimate AGB in tropical forests.

AGB estimations derived from optical imagery are limited in high biomass ranges by the saturation of the satellite signal. Generally, the saturation level strongly depends on forest structure, vegetation characteristics as well as quality of reference and remote sensing data. Different saturation levels have been reported in tropical forests. Reported saturation levels for AGB estimations based on Landsat imagery range from 150 t/ha to 300 t/ha (Avitabile et al. 2012; Li et al. 2010; Lu et al. 2012). MODIS data were capable to retrieve AGB even up to 450 t/ha (Baccini et al. 2008).

2.2. SAR data

SAR is an active remote sensing instrument which transmits microwave pulses towards the earth's surface and measures the backscattered energy to the sensor. An important advantage of the SAR system is the daylight and weather independence as the signal can penetrate through clouds, haze and smoke. SAR systems have different band designations which indicate their wavelengths of operation. The wavelengths range from 0.75 cm to 100 cm (Lillesand et al. 2008). The longer the wavelength, the deeper is the penetration into the vegetation. An overview of the most important SAR bands and their characteristics is given in Table I-2. At X-band, the sources of scattering are leaves and twigs from the upper part of the canopy (Le Toan et al. 1992). The scatter targets of the C-band are leaves and small branches, whereas branches and trunks build the main scatterers of L- and P-band (Le Toan et al. 2001). Principally, longer wavelengths are more sensitive to AGB and the saturation level increases with decreasing frequencies. However, AGB estimations are also sensitive on forest structure, incidence angle, and polarization of the radar signal (Koch 2010; Le Toan et al. 2001).

Table I-2: Characteristics of SAR bands commonly used for AGB estimations.

Band designation	Wavelength [cm]	Frequency [GHz]	Penetration depth [cm]	Scatter objects	Examples of satellites
X-band	2.40 - 3.75	12.5 - 8.0	3	leaves, twigs	TerraSAR-X
C-band	3.75 - 7.50	8.0 - 4.0	5	leaves, branches	ENVISAT ASAR, RADARSAT-2
L-band	15.0 - 30.0	2.0 - 1.0	25	branches, trunk	JERS-1, ALOS PALSAR

SAR signals can be transmitted and received in different modes of polarizations, either horizontal (H) or vertical (V) which results in four typical polarization combinations (HH, HV, VV, VH) where the first letter indicates the transmitted polarization and the second indicates the received polarization (Lillesand et al. 2008). In most cases, cross-polarized backscatter is more sensitive to variations in forest biomass (Hamdan et al. 2011; Le Toan et al. 1992; Mitchard et al. 2012; Pandey et al. 2010; Wijaya et al. 2009). SAR backscatter is generally affected by soil roughness (as it changes the directionality of scattering), moisture (it changes the total proportion of scattering) as well as other environment factors and thus influences AGB analyses (Ryan et al. 2012).

X-band SAR data has found up to date only little application for AGB estimations in tropical forests. Low or negligible correlation has been most often detected between AGB and C-band backscatter (Lu 2006). In contrast to that, Pandey et al. (2010) found a correlation between C-band ENVISAT ASAR (Environmental Satellite, Advanced Synthetic Aperture Radar) backscatter and AGB up to 250 t/ha. Most AGB studies in tropical forests were conducted on the basis of L-band SAR data (Hamdan et al. 2011; Mitchard et al. 2011; Ryan et al. 2012; Wijaya et al. 2009). Sarker et al. (2012) successfully predicted AGB in a subtropical forest on the basis of L-band ALOS PALSAR texture. P-band backscatter has proven to allow more accurate AGB predictions than L-band backscatter (Saatchi et al. 2011b).

Also SAR based AGB retrieval suffers from saturation of the backscatter signal in the higher biomass range. The saturation level of L-band SAR is between 50 t/ha and 200 t/ha, whereby HV polarized data featured higher saturation levels than HH polarized data (Hamdan et al. 2011; Mitchard et al. 2012; Mitchard et al. 2009; Saatchi et al. 2007; Saatchi et al. 2011b). P-band SAR backscatter has been found to saturate at approximately 300 t/ha (Saatchi et al. 2011b).

2.3. LiDAR data

LiDAR is an active remote sensing technique that sends out pulses of light, usually in a narrow wavelength in the infrared spectrum, and records the time it takes for each pulse of light to return to the sensor (Gleason et al. 2011). The return time is used to calculate the distances between the sensor and the various surfaces on or above the ground (Lillesand et al. 2008). The LiDAR signal is prepared as three-dimensional (3D) coordinates which have the ability to estimate the height and to map the three-dimensional structure of the vegetation.

Airborne LiDAR data acquisition is costly and requires processing of large data volumes. Currently, the capacity to collect annual data over whole countries does not exist currently (Mitchard et al. 2012). GLAS (Geoscience Laser Altimeter System) onboard NASA ICESat (Ice, Cloud, and land Elevation Satellite), was the first spaceborne LiDAR system, capable of providing global datasets of the earth's topography with a footprint of 65 m and data is available from 2003 to 2009 (Schutz et al. 2005).

Many studies demonstrated the great potential of airborne LiDAR measurements to precisely predict AGB of tropical forests (Asner et al. 2010; Asner et al. 2012; Clark et al. 2011; Mascaro et al. 2011b). Kronseder et al. (2012) estimated AGB from in-situ data and airborne LiDAR measurements in Central Kalimantan on Borneo for lowland dipterocarp forests and peat swamp forests.

Ballhorn et al. (2011) used airborne LiDAR AGB estimations based on field inventory measurements to estimate AGB from ICESat GLAS data. Baccini et al. (2008) and Lefsky et al. (2005) are further examples of AGB estimations in tropical forests on the basis of ICESat GLAS.

As LiDAR instruments are able to map the three-dimensional structure and height of the vegetation in great detail, AGB estimations are not restricted in terms of saturation in high biomass ranges.

3. Tropical peat swamp forests

3.1. Characteristics

Peatlands are terrestrial ecosystems in which the production of organic matter exceeds its decomposition (Page et al. 2006). Approximately 11% of the global peatland areas occur in the tropics in Southeast Asia, Africa, the Caribbean, Central and South America and are predominantly located at low altitude, although some can be found in the mountains of Africa, South America, and Papua New Guinea (Page et al. 2011). Most of them have developed in Southeast Asia and are domed, ombrogenous systems (Page et al. 2006).

Lowland tropical peat is relatively homogenous and mainly consists of slightly or partially decomposed debris of the former forest vegetation. Well preserved tree trunks, branches, twigs and coarse roots are found within a matrix of dark brown, amorphous organic material in various stages of humification (Page et al. 2006) (Figure I-1A). Peat swamp forests are moist tropical forests growing on peat and are oligotrophic (deficient in nutrients) because the lack of mineral input and leaching of organic compounds causes the water to become extremely acidic (pH 4 or less) (Posa et al. 2011).

There are two major categories of peat swamp forests: topogenous and ombrogenous. Topogenous peat swamp forests are characterized by a shallow accumulation of organic material (< 50 cm) and are flooded by a river in the wet season and are formed in areas with high water table where nutrients are available from seasonal flooding or underlying mineral soils. Ombrogenous peat swamp forests, which occur within the study area, have peat deposits which are deeper than 50 cm and water and nutrient supply is only derived from aerial depositions. Ombrogenous peat swamp forests develop inland on flat or gently convex areas between rivers in places with year-round rainfall (Rieley et al. 1997).

Peat swamp forests find their origin at the beginning of the Holocene, approximately 11,000 years before present, where the sea level rose and the temperatures and rainfall increased. Swamps and lakes became gradually filled. Decomposers, i.e. microorganisms, could not thrive in these wet environments and organic material began to accumulate. Thus peat swamp forests could evolve. The peat grew in depth and the water table rose aboveground water level and the plant community became solely

dependent on rain water for nutrient input, and so ombrogenous peat swamp forests evolved (Sorensen 1993).

The vegetation of tropical peat swamp forests is dominated by trees. Many of them have buttress or stilt root that provide stability on the waterlogged peat. Breathing roots (pneumatophores) that protrude above the peat surface enable respiratory gas exchange (Figure I-1B) (Page et al. 2006). Peat swamp forests in Southeast Asia support unique flora and fauna that are partially endemic and contribute to the exceptionally high levels of biodiversity (Miettinen et al. 2012).

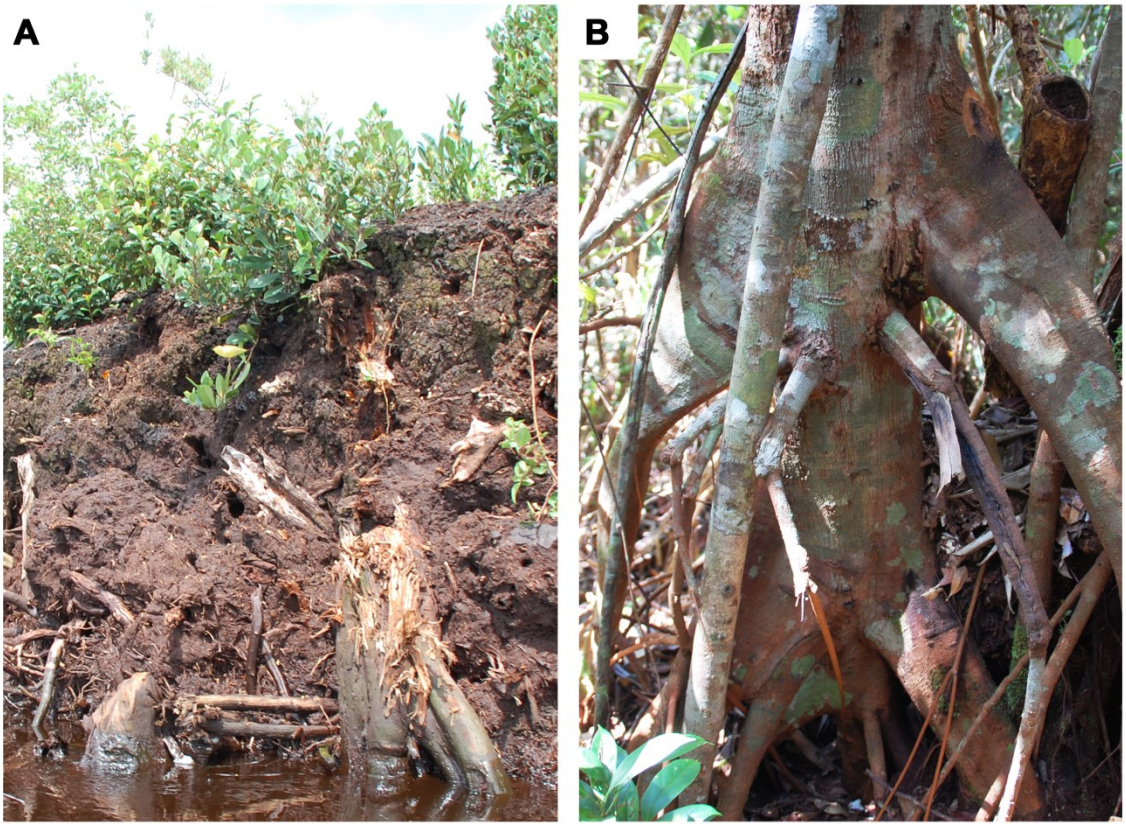

Figure I-1: (A) Peat layer of a disturbed area viewed from a drainage canal. (B) Typical stilt roots of peat swamp forest trees (© S. Englhart).

Vegetation is not only influenced by the total annual rain, which generally exceeds 2,500 mm, but also by the rainfall distribution throughout the year (Page et al. 2006). The annual pattern of precipitation is characterized by a dry season from May to October and a wet season from November to April (MacKinnon et al. 1996). Periodic El Niño events appearing in intervals of two to seven years prolong the dry season. The

last El Niño events occurred in 2006/2007 and in 2009/2010. The next one is expected in 2012/2013 (NOAA Climate Prediction Center 2012).

3.2. Threats

Due to the balance that exists between vegetation, peat and hydrology, peat swamp forests are highly susceptible to disturbance. There is a positive feedback loop among deforestation, drainage and fire which means that peatlands are easily degraded once the balance is upset (Hoscilo et al. 2011). This feedback is disrupted once the area is highly degraded. After a few consecutive fires, most of the aboveground vegetation is eliminated and many years are required before the vegetation regrowths sufficiently. Hence, there is a lot of fuel load which sustains new fires (Hoscilo et al. 2011).

3.2.1. Logging

Peat swamp forests contain a number of valuable timber species and have been intensively exploited (Posa et al. 2011). Roads and drainage channels allow loggers access into previously highly inaccessible forests (Boehm et al. 2004). Logging operations are possible though exhausting manual labor. Valuable trees are felled, cut into manageable pieces and then dragged along skid trails to the nearest river or canal where the logs can be floated away (Figure I-2). Logging creates gaps in the forest canopy which dries out the forest microclimate. Additionally, canals, which are used for transportation, further drain the peat. The resulting low water table in the peat causes trees to die and the forests become susceptible to fires (Boehm et al. 2004). Even where hydrology is not comprised, impacts of logging are noticeable in flora and fauna. Selective logging causes changes in forest structure and composition as well as in orangutan densities (Hadisuparto 1996; Morrogh-Bernard et al. 2003).

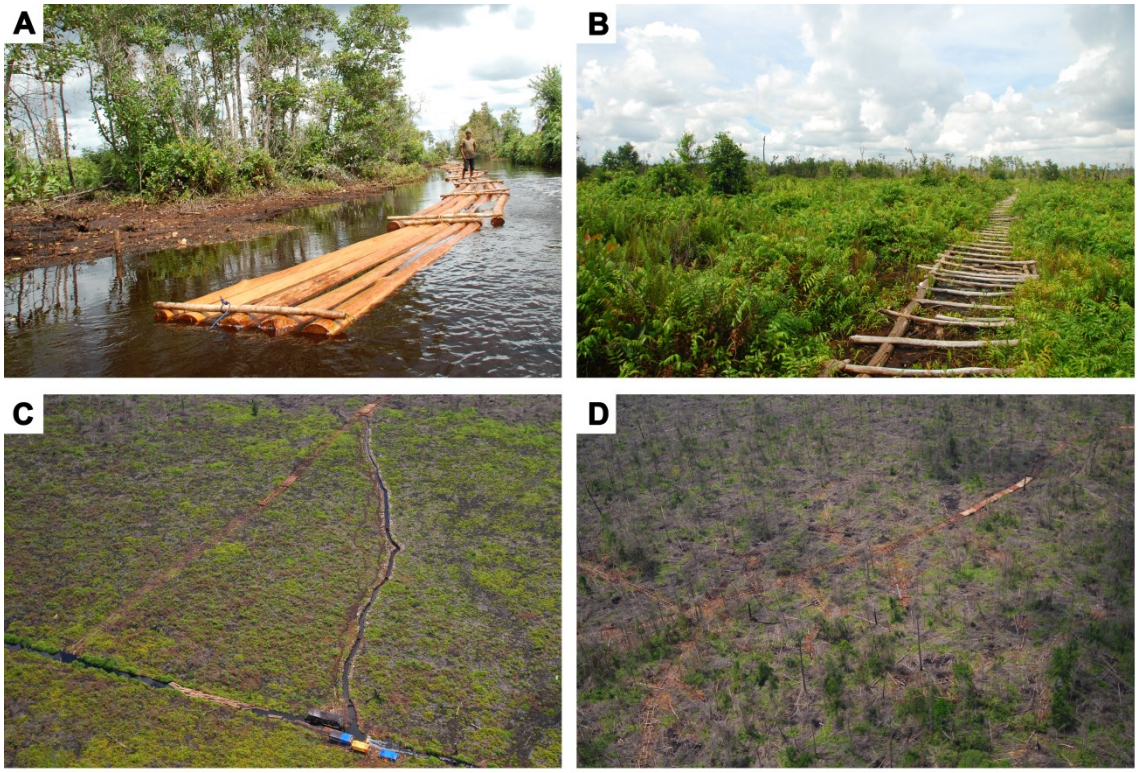

Figure I-2: Logging within Central Kalimantan. (A) Transportation of logs on a drainage canal. (B) Logging skid trail. (C) Illegal logging camp on a canal with skid trail. (D) Old logging skid trails within a burned forest (© S. Englhart, P. Navratil, F. Siegert).

3.2.2. Land conversion

Large scale conversions of infertile peatlands into agricultural land requires clearance, drainage, fertilizer application and liming in order to increase the pH value and to boost microbial activity (Posa et al. 2011). Construction of canal systems for drainage and water table management are often the first steps. Next, fire is a cheap method for land clearing. Often no efforts are made to control the area burned. Thus, fires easily spread and run out of control (Page et al. 2009a).

The most severe peatland conversion was caused by the Mega Rice Project (MRP) in Central Kalimantan which was established by the Government of Indonesia in 1995. It was planned to convert one million hectare of tropical forest, mostly peatland (61%), to cultivated land, e.g. rice fields. More than 4,500 km of drainage and irrigation canals were built. Finally, the project was officially terminated in 1999. Between 1990 and 2010, 40% of the initial forest cover was deforested whereby 31% was lost during the

1990s, partly facilitated by the severe El Niño event in 1997/1998 and the drained MRP area was particularly effected (Miettinen et al. 2012).

Forested peatlands are still being deforested, drained and burned for agricultural development, mainly oil palm and pulpwood plantations (Figure I-3). Especially domestic and international interests in oil palm for biofuel production are a driving force.

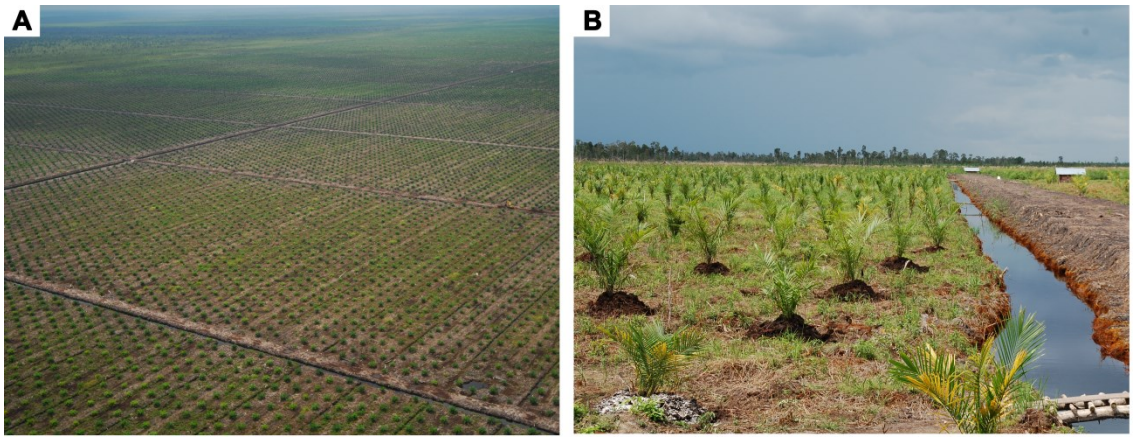

Figure I-3: (A) Aerial and (B) ground photo of a large scale oil palm plantation in Central Kalimantan (© F. Siegert, P. Navratil).

3.2.3. Fire

Forest fires are playing an important role in deforestation. The increase of fire occurrence is strongly related to peat swamp forest disturbance, as intact forests are unlikely to burn because they retain large amounts of moisture (Langner et al. 2007; Langner et al. 2009). The effects of fire are lower canopy cover, decreased species richness, and reduced tree and sapling density (Yeager et al. 2003). Due to the high combustibility of drained peat, fires can burn both above- and belowground (Page et al. 2009a). Deep peat fires can smolder below the surface for months and are difficult to extinguish. These subsurface fires affect the seed bank and cause the collapse of overlying material, creating additional tree mortality (Posa 2011).

During extreme droughts, often associated with strong El Niño events, peat swamps are extremely prone to burning, as evidenced by recent large wildfires that have destroyed hundreds of thousands of hectares on Borneo (Langner et al. 2009; Page et al. 2009a). Previous disturbance increases the susceptibility to fire. For instance, logging creates

gaps in the canopy, which dries out the forest microclimate and thus increases the temperature of the peat surface. Whereas drainage causes a decrease in the water table which can result in shrinkage and irreversible drying out of the peat (Wosten et al. 2006). Repeated and extensive peatland fires in Central Kalimantan follow drainage as well as selective logging and played an important role in land cover dynamics and forest loss from 1973 to 2005 (Hoscilo et al. 2011). Additionally, peat swamp forest that has burned once has a high probability of burning again because of the accumulation of unburned dead biomass and the regrowth of fire-prone vegetation (fuel load) (Page et al. 2009a; Siegert et al. 2001).

3.3. Restoration

Restoration attempts to recover the natural resource functions of degraded ecosystems. There are different measures of peatland restoration, for example restoration of hydrology, restoration of vegetation cover in order to protect the peat surface from direct sunlight and to reduce water streams at the surface level caused by drainage canals. Rewetting of peat is the most effective way to prevent peat decomposition, soil subsidence and annual fires (Page et al. 2009b). To achieve this, blocking of drainage canals by dam building is necessary in order to raise the water level of the surrounding peat (Jaenicke et al. 2010; Page et al. 2009b). The resultant reduced water flow in the canals allows sedimentation of organic and mineral material upstream of the dam which in turn facilitates the regrowing of vegetation. Some drainage canals are used for navigation and transportation by local people, which sometimes results in dam damages (Figure I-4). Therefore, planning, monitoring and maintenance of dams is very important ofr a successful peatland restoration (Jaenicke et al. 2010).

Figure I-4: Broken dam due to transportation needs (© P. Navratil).

4. Objectives of this thesis

In the context of climate change mitigation, restoration of degraded tropical peatlands and conservation of peat swamp forests are crucial elements. The peat swamp forests on Borneo, Indonesia, are threatened by different human activities. Enormous amounts of CO_2 and other greenhouse gases have already been released into the atmosphere. Therefore, it is crucial to rehabilitate degraded peatlands with restoration measures and to monitor the success. Furthermore, tropical peat swamp forests must be protected, for example through REDD+ projects which require accurate carbon stock estimations in order to assign carbon credits.

In Chapter II, continuous C-band ENVISAT ASAR data from 2004 to 2009 and L-band ALOS PALSAR data from 2007 to 2009 were used to monitor the hydrological effects of restoration measurements, more precisely blocking of drainage canals through dam construction. The sensitivity of SAR data to soil moisture was utilized to monitor hydrological changes in the peat soil and vegetation.

Chapter III and IV aimed at an intensive examination of the potential of X-band TerraSAR-X and L-band ALOS PALSAR imagery for AGB retrieval in intact and degraded peat swamp forests on Borneo. Field inventory data were first related to

airborne LiDAR measurements to estimate AGB across large areas and ecosystems. These LiDAR based AGB estimations were then related to SAR backscatter. This upscaling approach from field inventory to LiDAR AGB estimations was used because it provided numerous AGB reference data over the whole biomass range from woody regrowth to pristine forest. The mono- and multi-temporal relationships of SAR signals and biomass were analyzed in Chapter III. Single as well as combined frequencies were considered to develop regression models for AGB estimation and evaluate the saturation. On the basis of the results achieved so far, three different methods were analyzed and compared for AGB estimation based on multi-temporal combined TerraSAR-X and ALOS PALSAR in Chapter IV, namely multivariate linear regression (MLR), artificial neural network (ANN) and support vector regression (SVR).

Chapter V reveals the direct relationship between field inventory derived AGB and different SAR frequencies or multispectral RapidEye data. On the one hand, different polarizations of X-band TerraSAR-X, C-band RADARSAT-2 and L-band ALOS PALSAR data were analyzed for their correlation to AGB. On the other hand, multispectral RapidEye imagery was evaluated for its potential to estimate AGB using spectral mixture analysis (SMA). Furthermore, the direct AGB estimation approach, i.e. calibrating RapidEye signals to field inventory measurements, was compared to the indirect AGB estimation approach, i.e. linking specific AGB values to each land cover class of a detailed RapidEye land cover classification.

In Chapter VI, multi-temporal airborne LiDAR measurements from 2007 and 2011 were analyzed to quantify small scale AGB and canopy height dynamics. Canopy height models (CHMs) were created and AGB regression models were developed on the basis of field inventories and LiDAR height histogram metrics. Finally, changes in canopy height and AGB were evaluated with a special focus on unaffected, selective logged and burned peat swamp forests.

II. Monitoring the effect of restoration measures in Indonesian peatlands by radar satellite imagery

J. Jaenicke [a,b], S. Englhart [a,b], F. Siegert [a,b]

Journal of Environmental Management 92 (2011) 630 - 638

[a] *Biology Department II, GeoBio Center, Ludwig-Maximilians-University, Großhaderner Straße 2, D-82152 Planegg-Martinsried, Germany*

[b] *Remote Sensing Solutions GmbH, Isarstr. 3, D-82065 Baierbrunn, Germany*

1. Abstract

In the context of the ongoing climate change discussions the importance of peatlands as carbon stores is increasingly recognized in the public. Drainage, deforestation and peat fires are the main reasons for the release of huge amounts of carbon from peatlands. Successful restoration of degraded tropical peatlands is of high interest due to their huge carbon store and sequestration potential. The blocking of drainage canals by dam building has become one of the most important measures to restore the hydrology and the ecological function of the peat domes. This study investigates the capability of using multi-temporal radar remote sensing imagery for monitoring the hydrological effects of these measures. The study area is the former Mega Rice Project area in Central Kalimantan, Indonesia, where peat drainage and forest degradation is especially intense. Restoration measures started in July 2004 by building 30 large dams until June 2008. We applied change detection analysis with more than 80 ENVISAT ASAR and ALOS PALSAR images, acquired between 2004 and 2009. Radar signal increases of up to 1.36 dB show that high frequency multi-temporal radar satellite imagery can be used to detect an increase in peat soil moisture after dam construction, especially in deforested areas with a high density of dams. Furthermore, a strong correlation between cross-polarized radar backscatter coefficients and groundwater levels above -50 cm was

found. Monitoring peatland rewetting and quantifying groundwater level variations is important information for vegetation re-establishment, fire hazard warning and making carbon emission mitigation tradable under the voluntary carbon market or REDD (Reducing Emissions from Deforestation and Degradation) mechanism.

Keywords: ALOS PALSAR; Canal blocking; Carbon dioxide mitigation; ENVISAT ASAR; Hydrology; Restoration; Soil moisture; Tropical peat

2. Introduction

Natural lowland tropical peatlands are covered with trees (peat swamp forests) and are important reservoirs of biodiversity, carbon and water. With an average peat thickness of 4.5 m and an estimated amount of 55 Gt carbon stored, the Indonesian peatlands are one of the largest near-surface reserves of terrestrial organic carbon (Jaenicke et al. 2008). On average, the Indonesian peat swamp forests store about 2800 tons carbon per hectare which is 20 times as much as tropical rainforest of the same size without peat soil. European peatlands, which mainly developed from loose mosses and grasses, have an average thickness of only 1.75 m (Byrne et al. 2004), and the carbon storage of German peat is about 1.6 Gt (Höper 2007). However, in the past decade, large areas of the Indonesian peatlands have experienced serious damage as a result of human activities such as logging and drainage. Peatland site development is often associated with the construction of drainage canals in order to make the land useable for agriculture or more often for oil palm and pulp wood plantations. The forest clearing rate in Indonesia is the second highest worldwide, after Brazil (FAO 2006); an areal reduction of lowland forest extent by 41.3% in 15 years (1990-2005) for the Indonesian islands of Sumatra and Borneo (Kalimantan) indicates a highly unsustainable rate of deforestation (Hansen et al. 2009). A recent study of the province of Riau, Sumatra, showed that deforestation is decreasing in dryland forest due to depletion but is accelerating in peat swamp forests (Uryu et al. 2008). Increased pressure on the wet, acid and nutrient poor peatlands is caused by the currently raised demand for biofuel in Europe and the US. Of the 22 million ha of peatlands in Indonesia, about 60% are forested but mainly logged (illegally) and drained, 5% are cultivated and managed, and

35% are a mixture of small scale agriculture and severely degraded "wasteland" (Hooijer et al. 2006).

Canals and ditches are not only built to control and lower the groundwater level for agriculture but also to facilitate access to the peat swamp forest and to extract timber. Naturally, the groundwater level is close to the peat surface throughout the year and fluctuates with the intensity and frequency of rainfall. Once peat is drained, it oxidizes due to microbial activity and releases stored carbon to the atmosphere as carbon dioxide. This ongoing rapid peat decomposition leads to the irreversible process of peatland subsidence (Furukawa et al. 2005; Wösten et al. 1997). Another severe consequence of drainage is that the peat surface becomes dry and thus susceptible to fire during the dry season, which usually lasts from May until October. During prolonged El Niño related droughts fires are most severe, as in 1997/98 when about 2.4 - 6.8 million ha of peatlands burnt in Indonesia, releasing huge amounts of the greenhouse gas CO_2 (Page et al. 2002; van der Werf et al. 2008). The water absorption and retention properties of these degraded peatlands are impaired, and hence cause vast flooding during the rainy season with impacts on downstream habitations (Wösten et al. 2008). Mainly due to peat fires, Indonesia became one of the largest producer of greenhouse gases worldwide (Hooijer et al. 2006). Therefore, restoration and conservation of tropical peatlands play a crucial role in global climate change mitigation.

Restoration of the hydrological functions is a pre-requisite for the establishment of a positive or, at least, neutral peatland carbon balance and for the re-establishment of forest vegetation (Page et al. 2009b). Complete rewetting is the only way to prevent fires and peat oxidation. One of the most important restoration measures of tropical peatlands is blocking of drainage canals with dams and thus raising the groundwater level of the surrounding peatland (CKPP 2008; Jaenicke et al. 2010; Jauhiainen et al. 2004; Suryadiputra et al. 2005). The dam construction must be designed to cope with the high hydraulic conductivity and low load bearing capacity of tropical peat (Salmah 1992; Wösten et al. 2001). The dams mainly act as barriers to prevent water flow but cannot store water for long periods because it seeps away through the surrounding peat. The blocking of a canal can be regarded as successful if the blocked canal sections continue to hold water during the dry season. Damming activities in Central Kalimantan have led to an increase in canal surface water levels between 50 cm to over 1 m (CKPP 2008). Jauhiainen et al. (2008) reported a raise of groundwater levels in a deforested

and forested area near the city of Palangka Raya, Central Kalimantan, after dam construction. In the field, peat groundwater levels are measured by using tube wells; for monitoring the effect of dam constructions it is recommended to install these in transects perpendicular to the blocked canals (Jaenicke et al. 2010). Studies of tropical peatland restoration are at an early stage (Page et al. 2009b). Therefore, monitoring the effects of hydrological restoration measures is essential in order to optimize the techniques applied. Since tropical peatlands have been recognized as major sources of carbon dioxide emissions peatland rehabilitation projects are of high interest for carbon trading, especially on the growing voluntary carbon market (Couwenberg et al. 2010; Jaenicke et al. 2010; van der Werf et al. 2009). Quantifying the rise in groundwater level, which is the main control on carbon dioxide emissions from peatlands, is important information to make greenhouse gas emission mitigation tradable under the voluntary carbon market or REDD (Reducing Emissions from Deforestation and Degradation) mechanism.

In situ groundwater level measurements are laborious and very time-consuming since access to the wet and densely vegetated tropical peatlands is difficult. Therefore, this paper aims to investigate the capabilities of radar remote sensing for monitoring the effects of tropical peatland restoration by canal blocking. The study area is the Mega Rice Project area in Central Kalimantan, Indonesia, a severely drained and degraded peatland where dam constructions started in July 2004. The principal advantage of remote sensing over field measurements is the possibility of continuously monitoring vast areas. Compared to optical satellite data, radar imagery is available at high temporal frequency due to cloud penetration and daylight independency and is sensitive to changes in soil moisture. In general, vegetation or soil with high moisture content returns more energy to the radar sensor than if it is dry (Lillesand et al. 2008). Several studies have demonstrated the relationship between radar backscatter and surface soil moisture content under varying terrain conditions (Dubois et al. 1995; Paloscia et al. 2005; Ulaby et al. 1982). Hashim et al. (2002) found a strong correlation between radar backscatter (L-band) and soil moisture as well as groundwater level in drained tropical peatland in Malaysia. We applied change detection analysis with a time series of ENVISAT ASAR and ALOS PALSAR radar imagery, acquired before and after rewetting measures (2004 - 2009). Mean radar backscatter values of more than 40 deforested and forested test sites near the dams were compared with reference test sites

in undrained regions. Square "test sites" of 220 m - 550 m in size, depending on the radar sensor used, were chosen. Changes in radar backscatter were validated with in situ groundwater level measurements and with rainfall data. Radar backscatter variations resulting from vegetation cover changes were considered by analyzing optical Landsat satellite imagery and MODIS fire hotspot data.

3. Study area and materials

3.1. The Mega Rice Project area

The study area is located within the so called Mega Rice Project area, which extends south east of the city of Palangka Raya in the southern lowlands of the Indonesian province of Central Kalimantan on Borneo (Figure II-1). The landscape comprises flat alluvial plains with dome-shaped peat deposits that have accumulated to a thickness of more than 10 m (Jaenicke et al. 2008; Rieley et al. 2005). In 1995, the Mega Rice Project (MRP) was initiated by the Indonesian government under President Suharto. Despite warnings by scientists, it was planned to convert 1 million ha of peatlands for rice cultivation, accompanied by a transmigration program. A massive network of drainage canals was built, with a combined length of 4,500 km and depth of up to 10 m, but rice production appeared to be impossible. Intensive deforestation took place during the El Niño induced drought in 1997/98. Fifteen years of drainage and recurrent fires in 2002, 2004, 2006 and 2009 have severely degraded the MRP area (Langner et al. 2009). The MRP is the most disastrous example of unsustainable peatland management (Muhamad et al. 2002).

The MRP area is divided into different "Blocks" (A, B, C, D and E). This study focuses on Block A and C, where peatland restoration has been conducted in the course of different projects. In July 2004, hydrological restoration measures started in Block A under the CCFPI (Climate Change Forests and Peatlands in Indonesia) project by building 5 large dams (Figure II-1).

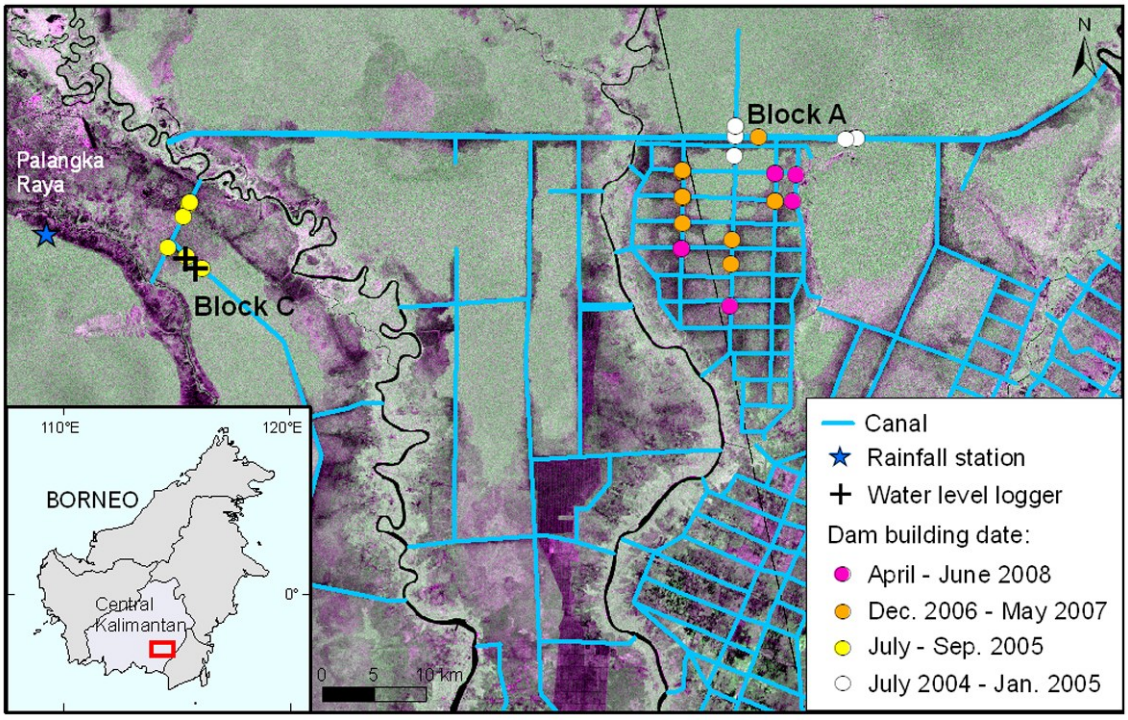

Figure II-1: ALOS PALSAR satellite image (HH, HV) from June 2009 showing the study area located in Central Kalimantan on the island of Borneo, Indonesia. Peat swamp forests appear in green, fire scars in purple. Not all of the 30 dams are shown due to very small distances between some of them.

Financed by the Central Kalimantan Peatland Project (CKPP), 19 additional dams were constructed in this area in 2007 and 2008. Within the framework of the Academy of Finland funded project "Keys for Securing Tropical Peat Carbon" (KEYTROP) and the EU funded RESTORPEAT (Restoration of Tropical Peatland for Sustainable Management of Renewable Natural Resources) project, 6 dams were built in 2005 in the drainage canals of Block C, which is located in the most western part of the MRP area (Figure II-1). Adjacent to two of these dams automatic groundwater level loggers were placed. The dams in Block C are up to 25 m long, 4 m wide and 3 m high, and were made of a timber frame which was sealed with plastic sheeting and filled with peat (Figure II-2). Trees were planted on top and behind the dams to increase resistance. The water flow reduction capability increases with time because organic sediments accumulate upstream of the dams. The dams in Block A are very similar to those in Block C in terms of size and design (CKPP 2008).

Figure II-2: Large dam constructed across a drainage canal in degraded peatland in Block C, Mega Rice Project area. A timber frame was sealed with plastic sheeting and then filled with peat (© K. Kusin).

3.2. Radar imagery

The Indonesian peatlands are covered by clouds 70-80% of the year; in addition haze from smoldering fires during the dry period often impedes the visibility (Langner et al. 2007). Therefore, continuous and cost-efficient monitoring is only possible with radar satellite remote sensing. The Advanced Synthetic Aperture Radar (ASAR) instrument onboard ENVISAT satellite, which was launched by the European Space Agency in March 2002, provides radar data in different modes with varying spatial and temporal resolution and alternating polarization at C-Band wavelength (5.6 cm). Twenty-eight ASAR scenes, acquired between July 2004 and March 2009 in dual polarization mode (VV, VH) and with an incidence angle of 23°, were available for monitoring the dams in Block C (Table II-1). The pixel spacing is 12.5 m and the temporal resolution 35 days. No ASAR imagery was available for monitoring Block A. The Phased Array type L-band (23.6 cm wavelength) Synthetic Aperture Radar (PALSAR) was launched onboard the Japanese ALOS satellite in January 2006. Four scenes are required to cover the whole study area (Block A and C) and were available at an incidence angle of 38.8° since the beginning of 2007 (Table II-1). The polarization mode is switched periodically between single mode (HH) during the wet season and dual mode (HH, HV) during the dry season, with a temporal resolution of 46 days. The pixel spacing is 6.25 m for single

and 12.5 m for dual polarization. Altogether 58 PALSAR scenes acquired between January 2007 and October 2009 were analyzed in this study. The absolute calibration accuracy of PALSAR data is 0.219 dB, using the Amazon rainforest as calibration target (Shimada et al. 2009), and it is 0.31 dB for the ASAR data used, using ASAR transponders as calibration targets (Rosich et al. 2007).

Table II-1: Description of radar imagery available for this study.

Sensor	Period	Path/Frame	Incidence Angle	Wave-length (cm)	Polari-zation	Pixel spacing (m)
ASAR AP*	2004-2009	-2.29; 114.13 (scene centre)	23°	5.6	VV, VH	12.5
PALSAR FBS**	2007-2009 (wet season)	421-422/ 7130-7140	38.8°	23.6	HH	6.25
PALSAR FBD***	2007-2009 (dry season)	421-422/ 7130-7140	38.8°	23.6	HH, HV	12.5

* AP = Alternating Polarization, ** FBS = Fine Beam Single, *** FBD = Fine Beam Dual.

3.3. Auxiliary data

When analyzing radar imagery it is essential to consider the weather conditions because rain occurring at the time of data acquisition can change the physical and dielectric properties of the surface soil and vegetation, thus affecting backscatter. Daily precipitation data collected by a weather station near Palangka Raya (Figure II-1) between 1997 and February 2008 as well as data from the Global Precipitation Climatology Project (GPCP) were analyzed for this purpose. Due to problems with the data logger, in situ rainfall measurements were available only until February 2008 and thus complemented with GPCP data. GPCP data incorporates infrared and microwave satellite retrievals and rain gauge observations. It is freely available since 1997 with a spatial resolution of 1 degree latitude and longitude. Daily mean groundwater level data were recorded at a forested and deforested area next to dams in Block C between April 2004 and November 2007 (see Figure II-1), and were used for comparison with radar backscatter. The "deforested area" was burnt down in 1998 and now mainly consists of ferns, sedges and scrub. No in situ groundwater level measurements were available for

Block A. Another important parameter for monitoring the effect of damming is the flow direction of the canal water. This information was derived from a digital elevation model of the whole study area and from punctual in situ measurements. Since changes in surface roughness, e.g. by burning or vegetation regrowth, can alter the radar backscatter, fire events in the study area were analyzed with Landsat optical satellite imagery, acquired between June 1991 and October 2009 (seventeen 80% cloud-free scenes). Active fires were analyzed using the thermal infrared MODIS sensor onboard TERRA satellite (FIRMS 2009).

4. Methods

4.1. Image processing

The radar imagery was calibrated using ERDAS Imagine 9.3 software by Leica Geosystems and a digital elevation model (DEM) from the Shuttle Radar Topography Mission (SRTM) with 90 m pixel spacing. This DEM resolution is sufficient because tropical peatlands are very flat, with elevation gradients of only 0.2 m - 1 m per kilometer in the centre (Rieley et al. 2005). ASAR data was calibrated to radar backscatter coefficients (σ^0) using an algorithm implemented in the Imagine software. The PALSAR digital numbers (DN) were transformed into backscatter coefficients applying the following equation (Shimada et al. 2009):

$$(1)\quad \partial^0(dB) = 10 * \log_{10}(DN^2) + CF$$

where CF is the calibration factor which varies between -80.2 and -83.4, depending on the processing date, incidence angle and polarization mode. The JAXA PALSAR product has already included the correction of the local incidence angle during the SAR image production. The multi-temporal radar imagery was co-registered with an accuracy of less than one pixel, using a Landsat ETM+ image from August 2007 as master. The Landsat dataset used for validation of the radar backscatter analysis and acquired after May 2003 had to be "de-striped", i.e. scan gaps due to Scan Line Corrector (SLC) malfunction were filled. This was done by 1) image registration of the *primary* scene and *fill* scenes and 2) histogram-matching (USGS 2009).

4.2. Change detection analysis

The intensity of radar returns is determined by several surface parameters such as dielectric constant and roughness. The dielectric constant is highly dependent on soil moisture because there is a large difference between dry soil (typically 2-3) and water (approximately 80). The C-Band ASAR sensor is able to penetrate regenerating tropical forest and to detect soil moisture variations underneath (Grover et al. 1999), while the longer wavelength L-Band ALOS sensor is even capable of observing soil moisture fluctuations and seasonal flooding dynamics under a closed peat swamp forest canopy (Aziz et al. 2003; Hoekman 2007; Romshoo 2004; Stahlhut et al. 2005). This forms the basis for measuring changes in peat moisture.

In this study, mean backscatter values of "test sites" located close to the dams and of reference "test sites" in undrained regions were analyzed before and after dam construction. Random interference of microwaves produces a characteristic backscatter fluctuation known as speckle noise on Synthetic Aperture Radar (SAR) data. To reduce radiometric resolution errors due to speckle, backscatter values of a certain amount of pixels were averaged (Laur et al. 1998). Baup et al. (2007) demonstrate that the backscattering coefficient σ^0 and the associated radiometric resolution vary as a function of the size of the sampling window. Therefore, by calculating the radiometric resolution, the optimal sampling window size of a "test site" can be determined. The radiometric resolution R_{rad} of the measured intensity is defined as (Laur et al. 1998):

$$(2)\quad R_{rad} = 10 * \log_{10}\left(1 + \frac{1}{\sqrt{ENL}}\right)$$

$$(3)\ \text{with}\quad ENL = N_{pixel\_az} * N_{pixel\_ra} * NL_{az} * \frac{NL_{ra}}{R}$$

where ENL is the equivalent number of looks, N_{pixel_az} and N_{pixel_ra} are the number of azimuth and range pixels of the sampling window, NL_{az} and NL_{ra} are the number of azimuth and range looks, and R is the number of pixels per independent pixel in the data product (Table II-2). R is calculated as follows:

$$(4)\quad R = \frac{\rho_{az}}{\Delta_{az}} * \frac{\rho_{ra}}{\Delta_{ra}}$$

where ρ_{az}, ρ_{ra} and Δ_{az}, Δ_{ra} denote the azimuth and ground range spatial resolution, and the azimuth and range pixel spacing, respectively (Table II-2).

Prerequisite for the calculation of image radiometric resolution is homogeneity within the test site. It was found that test site sizes of 550 m x 550 m for ASAR AP data, 220 m x 220 m for PALSAR FBS and 300 m x 300 m for PALSAR FBD data are large enough to obtain a good accuracy and to ensure homogeneity. With such windows, the radiometric resolution is ±0.14 dB (Table II-2). Forty-two test sites next to dams, i.e. with a distance of about 100 m minimum, and 10 reference test sites in undrained regions were investigated. Of the 42 test sites next to dams, 12 were placed in Block C (4 in the forest and 8 on degraded area) and 30 in Block A (10 in the forest and 20 on degraded area). The reference test sites were distributed over the whole study area of the MRP and placed where undrained, undisturbed peat swamp forest remained in order to check the stability of the radar backscatter over the whole time period analyzed. Some test sites were set with increasing distance to a dam in order to examine the extent of a possible rewetting effect by damming. Furthermore, the influence of the flow direction of the canal water was analyzed by placing test sites on both sides of a dam.

In addition to the evaluation of mean backscatter values of "test sites" up to 0.3 km² in size, a multi-temporal image stack was produced to visualize and investigate peat moisture changes in Block A on a regional scale. For this, three mosaic PALSAR images (6 scenes, 8,000 km² in size) acquired during the dry season of 2007, 2008 and 2009, respectively, were chosen. During dry conditions it can be assumed that there is no temporal variation in dielectric properties of the imaged surface due to rainfall. To reduce speckle in the radar scenes, a Lee-Sigma filter with a 5x5 and 9x9 moving-window was applied.

Table II-2: Radar image parameters to calculate the image radiometric resolution.

Sensor	Number of looks (azimuth x range)	Spatial resolution	R	Test site size	R_{rad} (dB)
ASAR AP*	4 x 1	22 x 25	3.52	550 x 550	±0.14
PALSAR FBS**	2 x 1	10 x 10	2.56	220 x 220	±0.14
PALSAR FBD***	4 x 1	20 x 20	2.56	300 x 300	±0.14

* AP = Alternating Polarization, ** FBS = Fine Beam Single, *** FBD = Fine Beam Dual.

5. Results

5.1. Rainfall and fire occurrence

The annual rainfall in Central Kalimantan varies between 2000 - 4000 mm and is influenced by periodic El Niño induced drought events. Figure II-3 shows daily precipitation measurements during times of radar image acquisition (2004 - 2009). The prolonged drought in 2006 is clearly visible and resulted in extremely low groundwater levels of up to -2 m in drained peat swamp forest. A comparison of the in situ and GPCP rainfall data showed that GPCP does not record precipitation events higher than 60 mm per day; however, the trend of monthly and yearly averages is the same. To date, GPCP data is processed and made available only until April 2009, but it is known from global weather observations (CPC 2009), local observations and from remotely sensed fire and burn scar detection that 2009 was an extremely dry year with many fire events occurring in the study area between mid-August and the end of September. With an annual average rainfall of about 3000 mm, 2004 and 2005 were normal precipitation years, whereas 2007 was an unusually wet La Niña influenced year (nearly 4000 mm) and 2008 slightly above average (ca. 3400 mm).

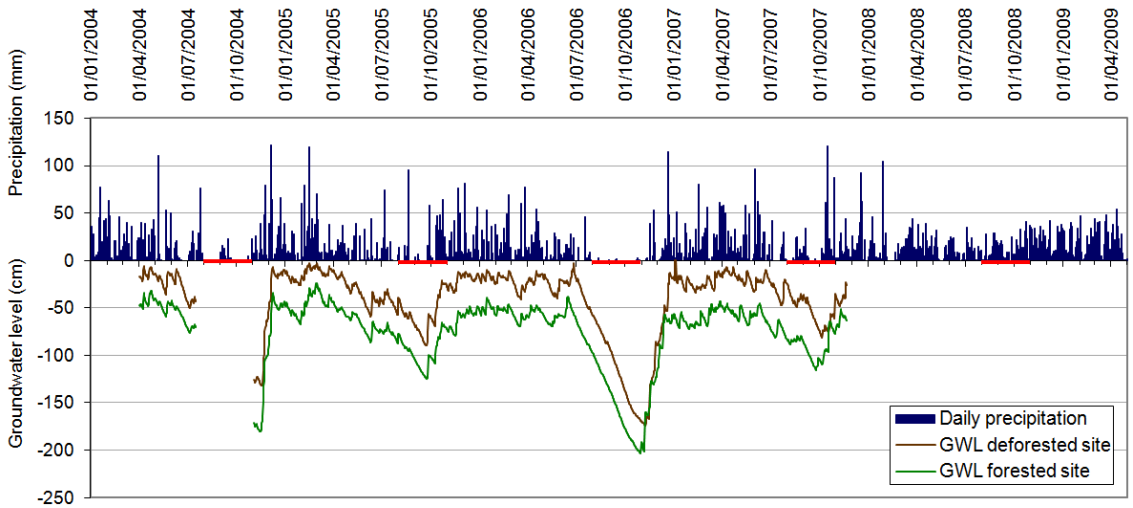

Figure II-3: Daily precipitation (in situ until February 2008, more recent satellite GPCP) and groundwater level data measured in the study area between 2004 and 2009. The dry months August – October are marked in red.

Landsat and MODIS fire hotspot analysis of the study area showed that in 2007 only one small fire event (400 m x 400 m) occurred in Block A, and no fires at all were recorded in 2008. Landsat imagery further revealed that the burn scars in the test site in Block C result from severe fires in 1997/98 and 2002, thereafter no fires occurred until September 2009. The burn scars in Block A originate mainly from the extremely dry years 1997/98 and 2006, with recurrent fires in between (Langner et al. 2007; Langner et al. 2009). The first vegetation after a severe fire event consists of ferns and sedges, which quickly cover the soil after the first rainfalls (Page et al. 2009b). Some few pioneer species will grow if the fire did not destroy all seeds. After 2 - 3 fires ferns and sedges set up as permanent vegetation.

5.2. Correlation of groundwater level and radar backscatter

The groundwater level (GWL) at the drained, deforested area in Block C varies between 0 cm, i.e. the peat surface, recorded after high rainfall events during the wet season and a minimum value of -174 cm in November 2006 (Figure II-3). At the forested area, generally lower GWLs were registered but show the same course over the years. A long-term comparison of in situ GWL measurements and radar backscatter was only possible with ASAR C-band data due to failure of the loggers at the end of 2007. A first, visual comparison of the GWL data at the degraded area with σ^0 backscatter coefficients averaged over a 550 m x 550 m test site at the logger station showed a positive relationship, i.e. higher σ^0 values occurred with higher GWLs, but linear regression revealed bad correlation coefficients. After excluding all GWL values less than -50 cm, correlation coefficients of r=0.44 for VH polarization and 0.35 for VV polarization were reached and further improved to 0.72 (VH) and 0.46 (VV), respectively, if a delay in groundwater level reaction of nine weeks was assumed (Figure II-4a). This high value of r=0.72 suggests that a relationship exists between VH C-band backscatter of degraded peatland and GWL values (up to -50 cm) recorded nine weeks after image acquisition. A similar time delay was found between rainfall and GWL (Figure II-4b). While a comparison of daily values was not significant (r=0.32), mean values of both variables were calculated and very high correlation (r=0.94) reached by averaging rainfall values over a period of the past nine weeks before GWL measurements. There is a time delay between rainfall and changes of the groundwater level because the peat layer with its high permeability acts like a sponge, slowly

"filling" and "emptying". The GWL threshold of -50 cm suggests that the sensitivity of the radar signal is not sufficient to detect changes in lower GWLs. Probably the roughness of the peat soil, in terms of L-band wavelength, prevents further decrease of the radar backscatter coefficients. At the forested area, no relationship between GWL and radar backscatter was found.

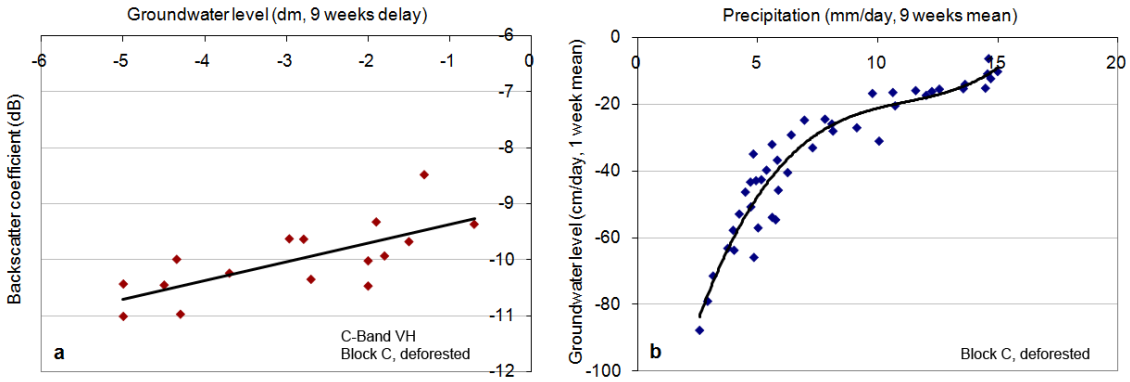

Figure II-4: (a) Linear relationship with r=0.72 exists between radar backscatter coefficients σ^0 (C-Band, VH) determined between July 2004 and October 2009 over deforested peatland and groundwater levels measured nine weeks later at the same area. (b) A similar time delay exists between rainfall and groundwater level; a very high correlation of r=0.94 is reached when comparing groundwater levels averaged over one week with precipitation averaged over the past nine weeks.

5.3. Evaluation of the "test sites"

Before evaluation of the test sites near dams, the temporal variability of the radar backscatter in undisturbed peat swamp forests was investigated, i.e. the reference test sites. Romshoo (2004) has shown that the L-Band (JERS-1 SAR) backscattering coefficient of dense, high biomass peat swamp forests is very constant. This was confirmed here by investigating 40 multi-temporal PALSAR scenes and ten reference test sites in undrained forests. Especially the cross-polarized HV backscatter is very stable; with a standard deviation (STD) of only 0.16 during the three year observation period, compared to 0.22 for like-polarized HH backscatter. The backscatter coefficient of primary forest in the study area does not vary more than 0.3 dB for HV polarization and 0.57 dB for HH, respectively. Thus, an increase or decrease of more than 0.3 dB in the HV backscattering coefficient could be reasonably attributed to anthropogenic or natural changes in the forest. The C-Band ASAR return from undisturbed peat swamp

forest shows no stability during the six year observation period (STD_{VH}=0.54, STD_{VV}=0.6). Due to signal instability, the ASAR data were not used to analyse forested test sites.

Figure II-5a shows the result of the evaluation of seven forested test sites next to dams completed in January 2005 in Block A, in comparison to reference test sites of undrained forest. Up to a distance of 1 km from the dams, a backscatter increase of 0.41 dB (PALSAR HV) was observed between May 2008 and August 2009. This increase, even though 2008 was a wet and 2009 a very dry year, suggests that the dams have a locally limited rewetting effect. In HH polarization mode no distinct increase (>0.57 dB) was detected. A distinct increase in L-band backscatter is observed at the forested test site in Block C which is located only about 200 m away from the dam (Figure II-5b). A comparison of a test site upstream and downstream of the dam clearly shows the influence of the water flow direction in canals. While there is a σ^0_{HH} backscatter increase of 0.86 dB between 9 July 2007 and 14 October 2009 upstream of the dam, the backscatter downstream the dam is very constant, except on 14 October 2009. At this date a very strong increase of 3.7 dB is observed, caused by a double bounce mechanism of the HH polarized radar signal due to fire impact in September 2009. Fire occurrence only downstream of the dam further suggests a (small scale) rewetting effect of the dam. In HV cross polarization mode a backscatter increase of even 1.36 dB was observed between 9 July 2007 and 14 October 2009 upstream of the dam.

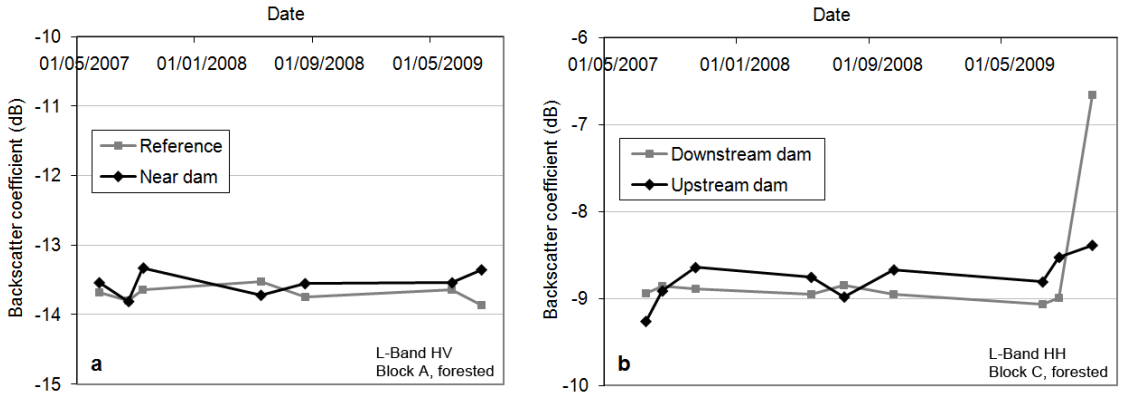

Figure II-5: Comparison of PALSAR radar backscatter from forested, rewetted test sites with forested, undrained test sites. (a) In Block A, only a slight HV backscatter increase is observed between May 2008 and August 2009, compared to the reference test sites in undrained forest. (b) In Block C, there is a HH backscatter increase of 0.86 dB upstream of the dam, compared to a very stable signal downstream of the dam (except of 14 October 2009, due to forest fire).

Test sites on deforested peatland in Block C were investigated with multi-temporal ASAR images, which allowed a comparison of the radar backscatter before and after dam constructions. Evaluation of the results shows a backscatter increase after completion of the dam construction in September 2005 and a small decrease before (Figure II-6). The increase of 0.9 dB observed between October 2005 and March 2009 is only visible in the cross-polarized VH imagery. During the wet seasons the radar backscatter is generally higher. The continuous backscatter increase after dam construction, even though 2006 had a very prolonged dry period, suggests successful peatland rewetting. Only two of the six dams in Block C show a rewetting effect, namely the most southern ones which have the highest water retention capability being at the end of a "cascade" of dams in terms of water flow direction.

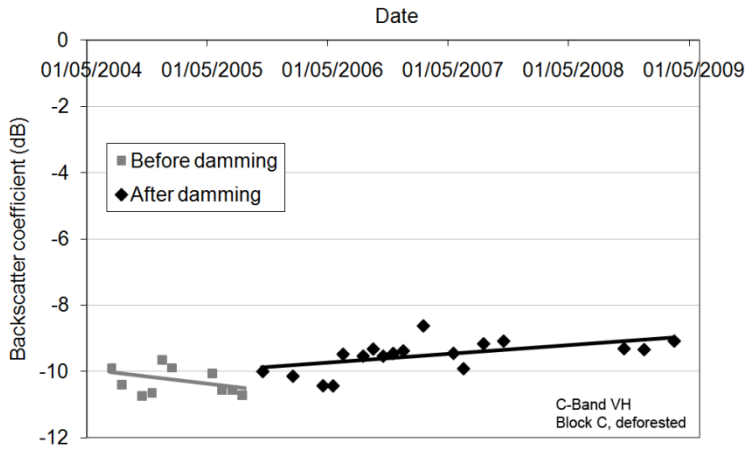

Figure II-6: ASAR C-Band VH backscatter analysis of a deforested test site in Block C over a six year period shows an increase of about 0.9 dB after completion of dam construction in September 2005.

5.4. Measuring peatland rewetting on a regional scale

In order to investigate the spatial pattern of rewetting in Block A, a multi-temporal image stack, i.e. red-green-blue (RGB) color composite of three images acquired during dry conditions in 2007, 2008 and 2009, respectively, was produced. HH polarized data was chosen because of a better discrimination between peat swamp forest and fresh burn scars. An optical Landsat ETM+ image from 5 August 2007 shows the condition of the peatland surface at the beginning of the change detection analysis; the landscape is determined by burn scars from 2006 (Figure II-7a). Figure II-7b illustrates the resulting RGB composite, in which the image from 7 August 2007 represents the red channel, the image from 9 August 2008 the green channel and the image from 12 August 2009 the blue channel. Areas that appear in grey (forests, burn scars) and white (riverine vegetation and some fresh burn scars in the southeast) show no significant changes among the three dates. Yellow areas indicate a backscatter decrease between 2007 and 2009 (ca. 1.3 dB); while blue areas reveal an increase in σ^0 values (ca. 0.7 dB), even though 2009 was an extremely dry El Niño year. This suggests that peatland rewetting was successful in a ca. 6 km² large area after the construction of dams in 2007 and 2008.

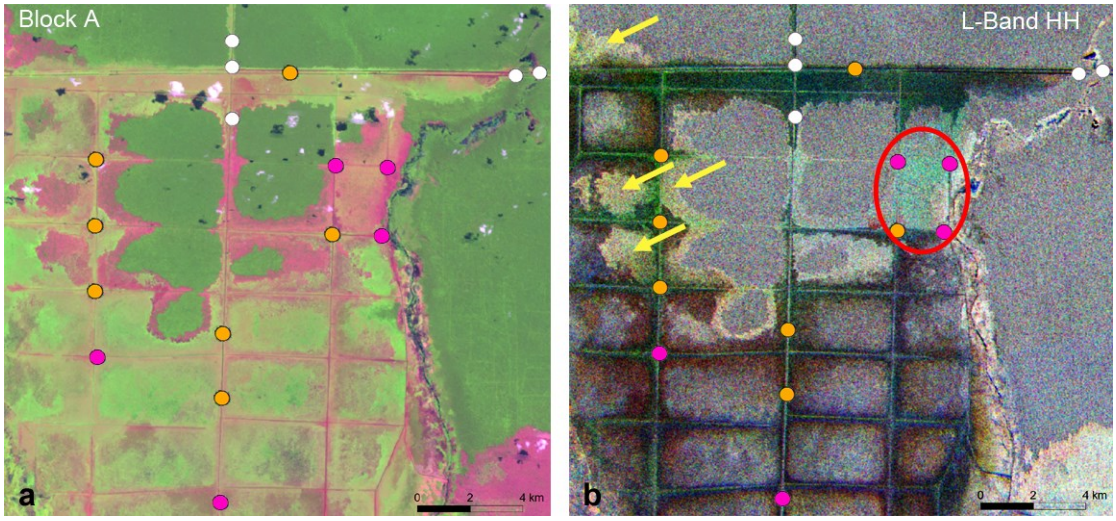

Figure II-7: (a) An optical Landsat ETM+ image shows the condition of the peatland surface in Block A at 5 August 2007; dark green: forested areas, red: burn scars from 2006; light green: vegetation regrowth. (b) RGB composite of three HH polarized PALSAR images (red: 7 August 2007, green: 9 August 2008, blue: 12 August 2009) showing relative changes over three years: marked with a red circle is the area where a significant backscatter increase occurred in 2009; marked with yellow arrows are areas where a backscatter decrease occurred between 2007 and 2009 (white dams completed in January 2005, orange in May 2007, pink in June 2008).

6. Discussion

This study shows that ASAR Alternating Polarization and PALSAR Fine Beam mode data are capable of monitoring peatland rewetting in Indonesia. Rewetting, which is achieved by damming drainage canals, is the most important restoration measure of tropical peatlands and a prerequisite for replanting trees and preventing carbon dioxide emissions. Relative changes in peat soil moisture before and after dam construction were observed with radar time series of up to six years. By calculating the radiometric resolution of the measured backscatter intensity, the optimal size of test sites for change detection analysis was determined. A multi-temporal stack of PALSAR images, acquired during dry weather conditions, proved to be successful in monitoring large scale temporal and spatial patterns of soil moisture. Variations in backscatter coefficients caused by changes in surface roughness could be excluded by analyzing optical Landsat imagery and MODIS fire hotspot data. Both radar wavelength bands investigated (C- and L-band) were able to penetrate post-fire regrowing vegetation, while only L-Band PALSAR data could detect soil moisture changes under a forest

canopy. Generally, cross polarization provided better results; probably because it is less sensitive to surface roughness and object orientation (Envisat 2007). A high correlation was found between C-band VH polarized backscatter and in situ groundwater level data above -50 cm, measured two months after image acquisition. This time delay also exists between rainfall and reaction of groundwater levels.

The rewetting of drained, forested and deforested peatland in Block C of the Mega Rice Project area in Central Kalimantan, as detected by ASAR and PALSAR imagery, is confirmed by in situ groundwater level measurements. After restoration, higher annual minimum GWLs prevailed on both areas and the GWL remained considerably longer near the peat surface (Jauhiainen et al. 2008). However, radar image analysis showed that an increase in soil moisture occurred only close to the dams and is strongly influenced by the water flow direction in the drainage canal. In the whole Block A, a relatively small area of ca. 6 km² showed a distinct increase in radar backscatter between 2007 and 2009 which can be reasonably associated with soil moisture variations. The occurrence of fires in the study area during the 2009 El Niño also suggests that the dams do not (yet) achieve large scale peatland rewetting. In contrast to its surroundings, the rewetted area in Block A was not affected by the severe 2009 fires. Usually, fires are ignited where the peat is dry and where there is access (mainly via drainage canals). The rewetted area is the only one in Block A which is bordered by dams at each canal junction. This, together with the observations in Block C, support the theory by Wösten et al. (2007) that a cascade of dams is most effective in canal water retention and hence rewetting of the surrounding peatland. The dense network and large size of canals in Block A make this a long-term and cost-intensive task. Furthermore, rising groundwater levels in Block A are restricted by severe peatland subsidence along the canals which has created a “mini-dome” topography (CKPP 2008). The 2009 El Niño fires make clear that peatland restoration must be accompanied by fire prevention, control and education, especially at the early stage.

Even though these first results of monitoring the effect of peatland restoration with radar imagery are very promising, in situ groundwater level measurements distributed over the whole study area should be investigated along with the acquisition of additional images. A longer time series of dual polarized PALSAR imagery, which proved to have best monitoring capabilities, is important to reduce uncertainties introduced by frequent short and long term changes of weather conditions in Central Kalimantan. This study

clearly shows the advantage of remote sensing data over in situ measurements which are laborious and cost-intensive due to difficult peatland accessibility and a high need for maintenance; destruction of measuring instruments by animals, humans and fires have been frequently reported from the study area. The identification of areas that have been successfully rewetted is essential for specifically planning the re-establishment of vegetation. In addition, groundwater level prediction is a key element for fire hazard warning systems. It is known that -40 cm is a critical threshold below which irreversible drying occurs; a layer of dry peat is created on the surface being very susceptible to fire (Takahashi et al. 2003; Usup et al. 2004; Wösten et al. 2008). Knowing the effect of peatland restoration measures as well as large scale groundwater levels is necessary to estimate carbon dioxide mitigation in view of carbon trading projects on the voluntary carbon market or under the REDD mechanism. Jaenicke et al. (2010) estimated that successful rewetting of a 590 km² large area of drained peat swamp forest could result in mitigated emissions of 1.4 - 1.6 Mt CO_2 yearly and Ballhorn et al. (2009) calculate that within a 27 900 km² large region in Central Kalimantan, including this study area, approximately 184 Mt CO_2 were released during the 2006 El Niño event, which equates to 20% of all carbon dioxide emissions from transport in the European Union in 2007. Carbon dioxide emissions of these orders can be avoided if large scale hydrological restoration measures are accompanied by an efficient monitoring program. Compared to carbon dioxide, other greenhouse gases such as methane (CH_4) and nitrous oxide (N_2O) are relatively unimportant in tropical peatlands (Furukawa et al. 2005; Strack 2008).

7. Acknowledgements

We thank the European Space Agency (ESA) for providing ENVISAT ASAR data within the EAO project 689, and the Japan Aerospace Exploration Agency (JAXA) for supplying ALOS PALSAR data within the PI project No. 211. FIRMS at the University of Maryland is gratefully acknowledged for their freely available fire hotspot data, the National Aeronautics and Space Administration (NASA) for providing GPCP rainfall data free of charge, and the U.S. Geological Survey (USGS) for supplying Landsat ETM+ Gap Filling Software. Special thanks to Dr. Jyrki Jauhiainen from the University of Helsinki and Kitso Kusin from CIMTROP, University of Palangka Raya, for making in situ groundwater level measurements available, which were very important for this study. We would like to thank Dr. Hidenori Takahashi, University of Hokkaido, for the

valuable rainfall measurements and Dr. Marcel Silvius, Wetlands International, for providing field data on water flow direction in drainage canals, collected within the CKPP project. Nyoman Suryadiputra from Wetlands International is gratefully acknowledged for providing geographical coordinates of the dams in Block A of the Mega Rice Project area, Central Kalimantan.

III. Aboveground biomass retrieval in tropical forests - the potential of combined X- and L-band SAR data use

S. Englhart [a], V. Keuck [b], F. Siegert [a,b]

Remote Sensing of Environment 115 (2011) 1260 - 1271

[a] *Biology Department II, GeoBio Center, Ludwig-Maximilians-University, Großhadener Str. 2, D-82152 Planegg-Martinsried, Germany*

[b] *Remote Sensing Solutions GmbH, Isarstr. 3, D-82065 Baierbrunn, Germany*

1. Abstract

In the context of reducing emissions from deforestation and forest degradation (REDD) and the international effort to reduce anthropogenic greenhouse gas emissions, a reliable assessment of aboveground forest biomass is a major requirement. Especially in tropical forests which store huge amounts of carbon, a precise quantification of aboveground biomass is of high relevance for REDD activities. This study investigates the potential of X- and L-band SAR data to estimate aboveground biomass (AGB) in intact and degraded tropical forests in Central Kalimantan, Borneo, Indonesia. Based on forest inventory data, aboveground biomass was first estimated using LiDAR data. These results were then used to calibrate SAR backscatter images and to upscale the biomass estimates across large areas and ecosystems. This upscaling approach not only provided aboveground biomass estimates over the whole biomass range from woody regrowth to mature pristine forest but also revealed a spatial variation due to varying growth condition within specific forest types. Single and combined frequencies, as well as mono- and multi-temporal TerraSAR-X and ALOS PALSAR biomass estimation models were analyzed for the development of accurate biomass estimations. Regarding the single frequency analysis overall ALOS PALSAR backscatter is more sensitive to AGB than TerraSAR-X, especially in the higher biomass range (>100 t/ha). However,

ALOS PALSAR results were less accurate in low biomass ranges due to a higher variance. The multi-temporal L- and X-band combined model achieved the best result and was therefore tested for its temporal and spatial transferability. The achieved accuracy for this model using nearly 400 independent validation points was $r^2 = 0.53$ with an *RMSE* of 79 t/ha. The model is valid up to 307 t/ha with an accuracy requirement of 50 t/ha and up to 614 t/ha with an accuracy requirement of 100 t/ha in flat terrain. The results demonstrate that direct biomass measurements based on the synergistic use of L- and X-band SAR can provide large scale AGB estimations for tropical forests. In the context of REDD monitoring the results can be used for the assessment of the spatial distribution of the biomass, also indicating trends in high biomass ranges and the characterization of the spatial patterns in different forest types.

Keywords: ALOS PALSAR, biomass, forest, Indonesia, REDD, TerraSAR-X

2. Introduction

Considering global climate change, carbon, as an element of the greenhouse gas carbon dioxide (CO_2), plays a major role in trapping thermal radiation from sunlight and reducing the Earth's space release of energy (Read et al. 2001). The rise of atmospheric CO_2 from about 280 ppm (in 1880) to 388 ppm (in 2009) was mainly caused by extensive burning of fossil fuels. Deforestation and land cover change caused 20% of global anthropogenic CO_2 emissions in the 1990s and 12% in 2008 (Le Quere et al. 2009). The total amount of global emissions from deforestation, forest degradation, and peatland fires is determined to be about 15% of global anthropogenic CO_2 emissions from 1997 to 2006 (van der Werf et al. 2009).

Tropical forests cover approximately 15% of the Earth's land surface (FAO 2009; Page et al. 2009a) and contain up to 40% of the terrestrial carbon (Page et al. 2009a). The main carbon pools are typically the living aboveground biomass (AGB) and the dead mass of litter, woody debris and soil organic matter (Gibbs et al. 2007). In Southeast Asia's peat swamp forests, both AGB and belowground thick peat deposits make a significant contribution to the carbon reservoir (Page et al. 2009a). Indonesia alone, where 48.8% of the land's surface is covered by forest, comprises a total carbon stock of

61 Gt to 63 Gt whereby aboveground forests store 6 Gt (FAO 2009) and belowground peatlands comprise between 55 Gt (Jaenicke et al. 2008) and 57 Gt (Page et al. 2011).

Southeast Asia features the highest rate of deforestation worldwide at 1.3% per year (Achard et al. 2002; FAO 2000; Langner et al. 2009) and is therefore a prime target for reducing emissions from deforestation and forest degradation (REDD) initiatives. REDD is a key element emphasized at the United Nations Climate Change Conference in Copenhagen in December 2009 for the reduction of CO_2 emissions. The most important requirements for a successful implementation of REDD are accurate biomass and carbon estimations and the subsequent monitoring of the forest carbon pool.

AGB or carbon stocks in tropical forests can be monitored in various ways (FAO 2000; Gibbs et al. 2007; Goetz et al. 2009). The most accurate way of AGB retrieval is destructive sampling through harvesting, drying and weighting the living biomass, hereby assuming a carbon content of dry biomass from 50% (Goetz et al. 2009; Malhi et al. 2004). While this method is very precise, it is cost- and time-consuming and in tropical forests often impractical. Forest inventories are usually accomplished to collect in-situ biomass data. Allometric equations of ground-based measurements, such as diameter at breast height (DBH) and total tree height are used to extrapolate plot values to forest stands (Chave et al. 2005; FAO 1997; IPCC 2006). Forest inventories are also expensive and time-consuming, especially in remote and inaccessible tropical forests, but extrapolation of the results is reasonably accurate. The simplest but least precise method to derive AGB maps is the biome approach whereby forest type specific biomass values are linked to land cover map classes (Goetz et al. 2009). Land cover maps can be generated by remote sensing technology, and biomass values are available in the published literature (for example: Lasco 2002; Waldes et al. 2001).

Observations and measurements by satellites have nowadays become the primary source for estimating AGB in tropical forests (Lu 2006). Since no remote sensing instrument can directly measure either biomass or carbon content, additional in-situ data is required for establishing a relationship between the remote sensing signal and the biomass (Rosenqvist et al. 2003). Various optical remote sensors have bands in the infrared, which allow the discrimination between different forest types and other land covers. However, frequent cloud coverage in the inner tropics often hampers the acquisition of high-quality data. Another major disadvantage is the low saturation level

of the spectral bands and the derived spectral indices regarding the biomass estimation (Gibbs et al. 2007).

LiDAR (light detection and ranging) instruments mounted on airplanes send out active laser pulses and measure various echoes of the signal. This determines the three-dimensional vertical structure of vegetation in great detail (Goetz et al. 2009). LiDAR has been proven to allow accurate estimates of tree height, canopy closure and AGB (Duncanson et al. 2010; Kronseder et al. 2012; Zhao et al. 2009). The disadvantage is that the acquisition of airborne LiDAR data requires sophisticated technical equipment, is very expensive especially in remote areas and has, therefore, not often been used in tropical forests (Gibbs et al. 2007).

Spaceborne synthetic aperture radar (SAR) sensors such as the L-band ALOS PALSAR, the C-band ERS/SAR, RADARSAT/SAR or ENVISAT/ASAR and the X-band TerraSAR-X instrument are also active systems, transmitting microwave energy at wavelengths from 3.0 cm (X-band) to 23.6 cm (L-band). The major advantage of all SAR systems is their weather- and daylight-independency. Their penetration depth and therefore their ability to measure biomass mainly depend on the wavelength: the longer the wavelength, the deeper the penetration (Henderson et al. 1998; Le Toan et al. 2001). The ability to measure biomass is additionally affected by other sensor properties such as the polarization and the incidence angle, but also by the land cover and terrain properties, i.e. roughness and dielectric constant (Lu 2006).

Various studies have analyzed the retrieval of AGB using radar data in tropical regions (Gama et al. 2010; Kuplich et al. 2005; Mitchard et al. 2009; Pandey et al. 2010; Santos et al. 2006). Longer wavelengths have proven to be more useful because of an increasing backscatter range with changing biomass (Castro et al. 2003; Dobson et al. 1992; Lu 2006; Luckman et al. 1997). These biomass estimations are valid up to a certain threshold where saturation occurs, i.e. where the slope of the biomass/backscatter coefficient curve approaches zero (Lucas et al. 2007; Mitchard et al. 2009).

The X- and C-band backscatter saturate at low biomass levels (30 - 50 t/ha). Pandey et al. (2010) found high r^2 values for a C-band backscatter/biomass relationship up to 250 t/ha. For L-band backscatter published saturation levels range from 40 t/ha (Imhoff 1995; Luckman et al. 1997) to 150 t/ha (Kuplich et al. 2005; Lucas et al. 2007; Mitchard

et al. 2009). Austin et al. (2003) stated that the L-band saturation level is possibly up to 600 t/ha.

Three different methods of calculating the saturation threshold are found in published literature. Luckman et al. (1997) established the saturation of an asymptotic backscatter/biomass relationship at 90% and 95% of the asymptotic intensity values. Rauste (2005) determined the saturation at regression analyses in a series of steps leaving a part of the stem volume range out. Watanabe et al. (2006) chose an arbitrary slope threshold of the backscatter/biomass curve of 0.01 dB ha/t.

In general, the saturation level not only depends on the SAR frequency but also on the amount of reference data. In the above mentioned SAR studies the correlation between AGB and SAR backscatter signal was often assessed using only a very limited set of in-situ data. Kuplich et al. (2005), Watanabe et al. (2006), Santos et al. (2006) and Lucas et al. (2007) made AGB predictions in the tropics on the basis of SAR imagery in combination with approximately 51 in-situ reference data, whereas Pandey et al. (2010) and Mitchard et al. (2009) analyzed up to 191 field inventory data. The latter found a limitation of biomass/backscatter correlation at 400 t/ha. Only Solberg et al. (2010) used upscaled biomass reference data from airborne LiDAR measurements, calibrated to in-situ data, resulting in estimations valid up to 250 t/ha with interferometric X-band data for pine and spruce forests.

In this study we investigated the capability of two different SAR sensors, TerraSAR-X (X-band) and ALOS PALSAR (L-band) in single and combined use as well as the use of mono- and multi-temporal data to retrieve AGB in tropical forest ecosystems in Kalimantan, Indonesia. The main focus is hereby on the impact of the different frequencies in regard to the biomass estimation capabilities for intact (high biomass) and degraded (low biomass) tropical forests using a novel approach. The upscaling approach included field inventory data and LiDAR based AGB estimations.

3. Materials and Methods

3.1. Study area

The principal study area of 280,062 ha is located in the Indonesian province Central Kalimantan on the island of Borneo and encompasses parts of the Mega Rice Project (MRP) (Block C) near Palangka Raya and the upper catchment of the river Sebangau

(Figure III-1). It includes two types of peat swamp forests, regrown peat swamp forest on fire scars and heavily degraded forests after recurrent fire episodes (shrubs), as well as riparian forest and seasonally flooded wetlands. The Sebangau catchment was designated as a National Park in 2004 because of its conservation value and importance of natural resource functions. The forests of Block C have been drained several times and recurrent fires destroyed approximately 50% of the forest cover in the past decade. A second study area (34,652 ha) was used to analyze the spatial transferability of biomass regression models, meaning if the established model can be applied other areas. This site is located in the floodplain of Borneo's largest river, the Kapuas River, in West Kalimantan (Figure III-1). The vegetation cover is very similar to the Central Kalimantan site and comprises peat swamp, heath and riparian forest, shrubs and seasonally flooded wetlands. Forest inventory data was available for comparison for this site.

Both areas are located in alluvial plains with extensive peatlands. The topography is extremely flat, which is advantageous for SAR analysis, avoiding shadow and layover effects. The ombrogenous (rain-fed) peat swamps are covered by peat swamp forests and are extremely deficient in mineral nutrients and acidic, fostering many endemic species. The peat deposits are between 0.5 m and 20 m thick and contain up to 10 times more biomass per ha than the forests growing on top of them (Jaenicke et al. 2008; MacKinnon et al. 1996; Rieley et al. 2005). Under undisturbed conditions, peatlands make a significant contribution to the global terrestrial carbon storage, both in terms of their forest AGB and belowground peat deposits (Page et al. 2009a).

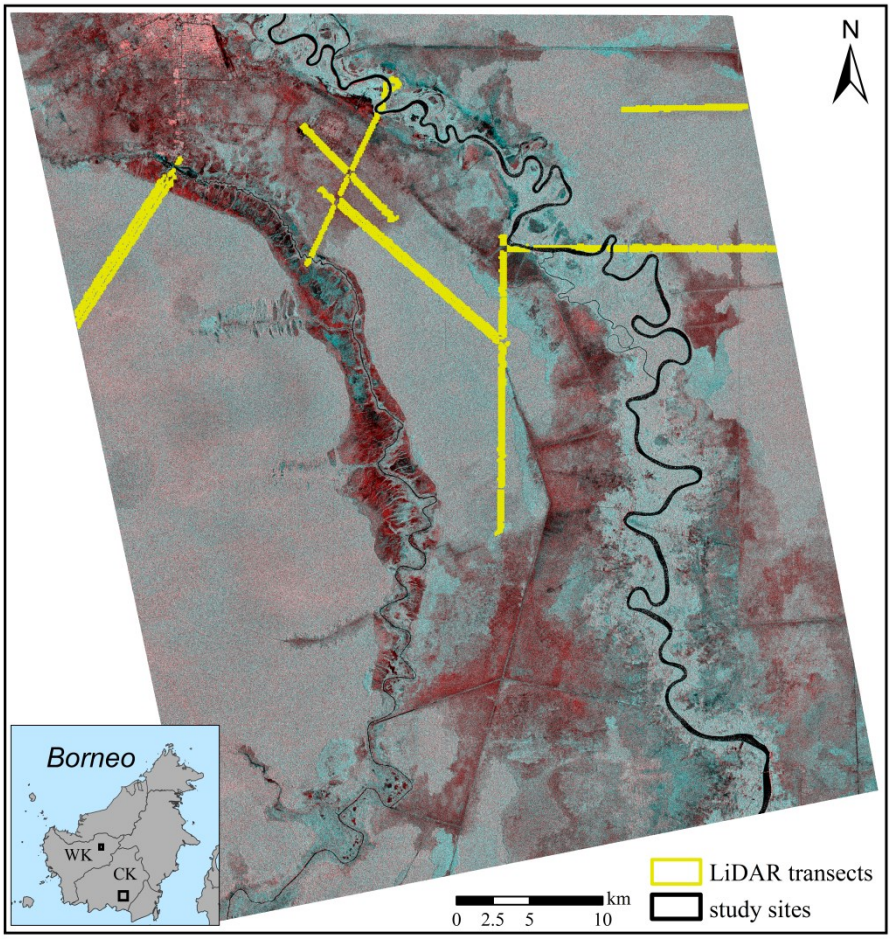

Figure III-1: Multi-sensor image combining TerraSAR-X ScanSAR VV (30/08/2008, R) and ALOS PALSAR HV polarized (26/08/2008, GB) scenes featuring the study area located in Central Kalimantan (CK), Indonesia. The location of the study area in West Kalimantan (WK) is indicated in the outline map. Available LiDAR transects used for AGB calculations are illustrated in yellow.

3.2. Aboveground biomass data

Field inventory data was collected in 2007 and 2008 representing different forest and sub forest types and forests degraded by logging and fire. Data for more than 140 forest plots was collected using the angle count sampling method which estimates aboveground biomass within 1ha plots. Diameter at breast height (DBH), basal area, number of stems and tree species were gathered and used to calculate AGB based on allometric equations (Chave et al. 2005). The AGB sample plots were then related to airborne LiDAR measurements (Kronseder et al. 2012).

The small-footprint, full-waveform LiDAR dataset was acquired during a flight campaign conducted in August 2007. Altogether, 8,090 ha were used to analyze different biomass estimation models. The LiDAR data were differentiated into ground and vegetation echoes to obtain vegetation heights. The following point cloud statistics of the absolute vegetation heights within 1 ha plots were calculated and used as predictors: mean h_{mean}, measures of dispersion including the standard error of the mean (*SEM*) h_{SEM}, standard deviation (σ) h_{σ}, variance h_{var}, range h_{range} and maximum h_{max}, and the quantiles corresponding to the 5, 10, ..., 95 percentiles of the distributions ($h_{5,...,95}$). As a further potential predictor, canopy cover (*CC*) was determined. Multiple linear regression analysis using the stepwise forward method was conducted relating all above mentioned variables to corresponding AGB values per ha:

$$AGB = b_0 + b_1 * h_5 + b_2 * h_{10} + ... + b_{20} * h_{95} + b_{21} * h_{mean} + b_{22} * h_{\sigma} + b_{23} * h_{SEM} + b_{25} * h_{Var} + b_{26} * h_{Range} + b_{27} * CC \quad (5)$$

The model with the best regression result for peat swamp forests was selected for further analysis. The applied model depends on the 50 percentile, provides AGB estimations ranging from 1.5 t/ha to 369 t/ha and its independent validation results were r^2=0.32 with an *RMSE* of 94.77 t/ha. Although the independent validation is weak, this biomass estimation model performed best for estimations over the whole biomass range. Using continuous spatial datasets, as opposite to several point-based field inventories, provided an enormous amount of reference data featuring the spatial variability of the forest within the area of the SAR image. Thus, 3,970 data points (coming from the LiDAR estimates) within the study area, covering the entire biomass range and thereby characterizing the spatial distribution of biomass, were used. As the plots within the LiDAR transects are clustered (Figure III-1), the biomass reference data are not randomly distributed which is also represented by a Moran's Index of 0.88 indicating some spatial autocorrelation. However, plots were generated from 15 different LiDAR transects which were randomly distributed in the study area.

This enormous set of biomass reference data for a tropical forest ecosystem is very valuable, since field inventories are very time-consuming and expensive to conduct. The huge number of samples enhances the accuracy of the biomass regression models.

3.3. Remote Sensing

Various additional remote sensing datasets of the study area were available, leading to a better understanding of the landscape features. Land cover maps and land cover change maps based on optical imagery such as Landsat ETM+ (Enhanced Thematic Mapper Plus) and high resolution RapidEye images (6.5 meters spatial resolution) were available as additional data sources. The TerraSAR-X satellite was launched on 15 June 2007 by the German Aerospace Center (DLR). It provides different acquisition modes with varying spatial resolution at X-band wavelength (3 cm) with a frequency of 9.65 GHz. Six images acquired in 2008 and 2009 were available in the ScanSAR mode at VV polarization, with incidence angles between 29.9° and 36.2° and a pixel spacing of 8.25 m (Table III-1). The different incidence angles are supposed to have no effect on the radar signal of forests as the angular dependence between 20° and 40° of X-band VV polarized backscatter signals was proved to be less than 1 dB in an Aspen forest (Henderson et al. 1998; Sun et al. 1991; Wang et al. 1993).

The Phased Array type L-band Synthetic Aperture Radar (PALSAR), on-board the Advanced Land Observing Satellite (ALOS), was launched on 24 January 2006 by the Japan Aerospace Exploration Agency (JAXA). It records data at a frequency of 1.27 GHz (23.6 cm wavelength). In total, 9 images from 2007 to 2009 in dual mode at HH and HV polarization, with an incidence angle of 38.8° and a pixel spacing of 12.5 m were examined within this study (Table III-1). Preliminary analyses showed that HH polarized images were not sensitive to AGB and were therefore not included in the analysis.

The preprocessing included radiometric calibration, georeferencing and Lee-Sigma speckle reduction, whereby the radiometric calibration was done on the basis of following equations:

(6) $\sigma^0\,[dB] = 10\log_{10}((k_s * |DN_i|^2 - NEBN) * \sin\theta_i)$

TerraSAR-X (Fritz 2009)

(7) $\sigma^0\,[dB] = 10\log_{10}|DN_i|^2 + K_{dB}$

ALOS PALSAR (Shimada et al. 2009)

where σ^0 = backscattering coefficient, DN_i = digital number of each pixel, k_s/K_{dB} = calibration coefficients, *NEBN* = noise equivalent beta naught and θ_i = local incidence angle.

Table III-1: Properties of radar imagery available for the study areas in Central and West Kalimantan.

Sensor	date (dd/mm/yyyy)	polarization	pixel spacing (m)	incidence angle
Central Kalimantan, Block C				
ALOS PALSAR	07/09/2007	HV	12.5	38.8°
fine resolution	24/08/2007	HV	12.5	38.8°
	10/09/2007	HV	12.5	38.8°
	26/05/2008	HV	12.5	38.8°
	26/08/2008	HV	12.5	38.8°
	11/10/2008	HV	12.5	38.8°
TerraSAR-X	14/06/2008	VV	8.25	32.1°
ScanSAR	08/08/2008	VV	8.25	29.9°
	30/08/2008	VV	8.25	32.1°
West Kalimantan, Kapuas Hulu				
ALOS PALSAR	02/07/2009	HV	12.5	38.8°
fine resolution	17/08/2009	HV	12.5	38.8°
	02/10/2009	HV	12.5	38.8°
TerraSAR-X	07/06/2009	VV	8.25	34.1°
ScanSAR	23/08/2009	VV	8.25	36.2°
	03/09/2009	VV	8.25	34.2°

The calibration coefficient of TerraSAR-X (k_s) depends on the incidence angle θ_i, whereas the one of ALOS PALSAR (K_{dB}) is a constant of -80.2 or -83.0 at dual mode HV polarized images, depending on the processing date. The digital number of each pixel DN_i was transformed into a backscattering coefficient sigma naught (σ^0) in decibels (dB).

Additionally, ALOS PALSAR images were co-registered with a Landsat ETM+ master scene and speckle noise in ALOS PALSAR and TerraSAR-X scenes was reduced by applying Lee-Sigma filters with moving-windows of 5x5 and 9x9 pixels.

It is essential to consider the climatic conditions during image acquisition when analyzing radar data because rain can change physical and dielectric properties of the surface soil and vegetation, thus affecting backscatter. Daily precipitation data from the Global Precipitation Climatology Project (GPCP) of both study areas were analyzed for this purpose. GPCP data incorporates infrared and microwave satellite retrievals and rain gauge observations. It is freely available since 1997 with a spatial resolution of 1° latitude and longitude.

In order to minimize any impact by rainfall, surface water and soil moisture, only radar imagery acquired during the dry season (May to October) were used in this study. The precipitation pattern of the two study areas and their similarities was analyzed by examining the daily GPCP data from January 2007 until April 2009 (only available for this period) and by relating the total monthly values of both study areas to each other.

3.4. Biomass regression modeling

The relationship between radar signals and AGB was analyzed using spatially averaged backscattering coefficients over a grid with a cell size of 100 m (1 ha). Different grid sizes were previously tested, but the chosen size of 100 m contained the best trade-off between radiometric accuracy and loss of spatial information and is similar to the one used for the LiDAR estimations. The radiometric accuracy was calculated according to Laur et al. (1998) and varies as a function of the size of the sampling window (Baup et al. 2007). It constitutes 0.52 dB, 0.27 dB and 0.18 dB in TerraSAR-X ScanSAR scenes and 0.79 dB, 0.41 dB and 0.28 dB in ALOS PALSAR dual polarized images for a cell size of 50 m, 100 m and 150 m, respectively.

For mono-temporal analyses, a single image acquired in August was used. Multi-temporal analyses included temporally averaged radar backscatter signals from three scenes acquired during the dry season of either 2007 or 2008 (May to October) and thus extreme conditions which might affect the radar signal are compensated. Surface moisture resulting from heavy rainfall, occurring especially in the tropics, can have an effect on the radar signal. In general, longer wavelengths are less affected by surface moisture (Henderson et al. 1998) but increases in the backscatter are reported (Dobson et al. 1991). The multi-temporal approach compensates possible extreme conditions and is supposed to be more feasible for biomass modeling.

The mono- and multi-temporal ALOS PALSAR models of 2007 and 2008 can be

compared as the preprocessing of the imagery was the same. Furthermore, it was investigated if there is any systematic change in the backscatter signal of 2007 to 2008 analyzing the descriptive statistics but no systematic change could be detected.

As AGB reference data, a total of 3,970 points featuring the whole biomass range, were available, randomly 10% of the LiDAR-derived biomass reference data were left out of the modeling process for the subsequent independent validation. The preliminary modeling step was to investigate single frequency biomass models of X- or L-band SAR data. Both mono- and multi-temporal radar signals were related to AGB values examining these relationships. The combined biomass regression models included two frequencies, the X-band TerraSAR-X and L-band ALOS PALSAR, and multivariate regression analyses on the basis of mono- and multi-temporal backscattering values were conducted. The coefficient of determination r^2 for the linearized models were calculated for no-intercept models, as within the later analysis this type of model proved to be the most sufficient. The following formula was used as described by (Kvalseth 1985):

$$(8)\quad r^2 = 1 - \sum (y - \hat{y})^2 / \sum y^2$$

where $\hat{y}$ is fitted (calculated) value and y is the actual value of the dependent variable (aboveground biomass).

Subsequently the independent validation was used to evaluate the predictive accuracy of the model, comparing estimated to actual AGB values, whereby the coefficient of determination (r^2) and root mean square error (*RMSE*) were calculated. The coefficient of determination r^2 of the independent validation was calculated as the square of Pearson's correlation coefficient r for a linear transformation of the model.

Additionally, the mean error (*ME*) was determined, of which the algebraic is relevant. If the mean error is positive, the predicted values are underestimated and if it is negative, they are overestimated.

3.5. Saturation level estimation

Biomass analyses using radar imagery are limited by the saturation of the radar signal at high biomass values which occurs when the biomass/backscatter slope approaches zero. Similar to Watanabe et al. (2006), the saturation was determined on the basis of a

backscatter/biomass slope threshold which was calculated on the basis of the radiometric accuracy and a specific accuracy interval for the estimates. The radiometric accuracy of an area of 1 ha is, as above mentioned, 0.27 dB in TerraSAR-X ScanSAR images and 0.41 dB in ALOS PALSAR dual polarized scenes. The accuracy intervals of the estimates was set to 50 t/ha and 100 t/ha. Within the 50 t/ha accuracy interval the AGB estimations are supposed to be accurate whereas estimations within the 100 t/ha accuracy interval are only indicators for the spatial AGB distribution.
The slope *m* of the saturation threshold can be calculated as follows:

$$(9)\quad m = \frac{\Delta\partial^0}{\Delta AGB}$$

where $\Delta\partial^0$ is difference of the backscattering coefficient σ^0 (in this case: the radiometric accuracy of the respective sensor) and ΔAGB is the difference of the aboveground biomass (the accuracy interval of the estimates). Above the calculated saturation point, the biomass estimations cannot be differentiated within the determined biomass accuracy interval due to the radiometric accuracy. The slopes of the saturation threshold with the different accuracy intervals are depicted in Table III-2. The saturation point of the different established biomass models was determined on the basis of the derivative of the respective regression model. The combined model was differentiated with respect to either TerraSAR-X or ALOS PALSAR backscatter signal and identified with the slope threshold depicted in Table III-2.

Table III-2: Slopes of the biomass saturation threshold (in dB ha/t) for the respective sensors within two different accuracy intervals of the estimates calculated on the basis of equation (9).

sensor	accuracy interval of the estimates	
	50 t/ha	100 t/ha
TerraSAR-X	0.0054	0.0027
ALOS PALSAR	0.0082	0.0041

3.6. Spatial application of biomass estimation models

Finally, the biomass models were applied to the full extent of the study area in Central Kalimantan. The most accurate regression model was applied to the study area in Kapuas Hulu, West Kalimantan, testing the spatial transferability of the model. As TerraSAR-X data were only available for one year per study site, the temporal transferability was beforehand investigated by comparing mono- and multi-temporal ALOS PALSAR regression models covering a time period of two years (2007 and 2008).

As radar imagery was recorded only during the dry season and the multi-temporal approach compensates variable climatic conditions, the SAR backscatter is supposed to be constant. Romshoo (2004) has shown that the L-band (JERS-1 SAR) backscatter signal (of a scene recorded during the dry season) of peat swamp forests is very constant. This was confirmed by Jaenicke et al. (2011) who found the ALOS PALSAR HV polarized backscattering coefficient was very stable over a long time period. Both study areas comprise a very similar vegetation composition and forest structure. The preprocessing technique of the radar imagery of both study areas was the same and further potential errors were eliminated by using images recorded only during the dry season with the same incidence angles (Table III-1). These facts are very important preconditions as they increase the probability of the spatial transferability (Freitas et al. 2005). There was no LiDAR data available for Kapuas Hulu, and only a limited set of field inventory data to evaluate the spatial transferability. Instead, a detailed Landsat ETM+ land-use/land cover classification considering different forest types was available for 2009. The different forest classes were linked to AGB values derived from literature and/or forest inventory data and compared to the averaged biomass estimation result of the model and the potential of the spatial transferability was examined.

4. Results

4.1. Regression modeling

First, the relationship between AGB and backscattering coefficients was investigated for both X- and L-band data separately. By carefully examining the different curve progression of the correlation between biomass and radar signals, the optimal equation for mono- and multi-temporal single frequency regression models was found to be:

$$(10) \qquad y = a * \exp(\sigma^0)^b$$

where σ^0 = backscattering coefficient and *a, b* = coefficients depending on sensor and date.

Equation (10) was fitted after a logarithmic transformation and for a least squares linear regression. The coefficients of determination (r^2) are given for the logarithmic version of the models and were recalculated for no-intercept models. The results are summarized in Table III-3 and Table III-4 in which the exact date is listed for mono-temporal and the respective year for multi-temporal models. The independent validation of the models is given within the AGB range up to the saturation threshold with accuracy requirements of 50 t/ha and 100 t/ha. The multi-temporal relationships between AGB and TerraSAR-X or ALOS PALSAR radar signals in 2008 are depicted in scatterplots in Figure III-2.

Table III-3: Results of single frequency AGB regression modeling on the basis of equation (10) (n=3970; 90% were used for regression modeling and 10% for the independent validation). The date indicates mono-temporal models, all others specify multi-temporal models of the respective year..

Sensor	date	regression model $y = a * \exp(\sigma^0)^b$		
		r^2	*a*	*b*
TerraSAR-X	08/08/2008	0.462	$4.48*10^8$	2.04
	2008	0.462	$26.94*10^8$	2.30
ALOS	24/08/2007	0.651	$2.44*10^8$	1.02
PALSAR	2007	0.693	$1.02*10^8$	0.95
	26/08/2008	0.637	$3.97*10^8$	1.06
	2008	0.706	$1.14*10^8$	0.97

Table III-4: Results of the independent validation of equation (10) given within an accuracy requirement of 50 t/ha and 100 t/ha. The coefficients of determination (r^2), root mean square error (RMSE) and mean error (ME) of the independent validation are depicted for the single frequency mono- (exact date) and multi-temporal (year) regression models.

Sensor	date	saturation (t/ha)	validation			saturation (t/ha)	validation		
		accuracy 50 t/ha	*RMSE* (t/ha)	r^2	*ME* (t/ha)	*accuracy 100 t/ha*	*RMSE* (t/ha)	r^2	*ME* (t/ha)
Terra	08/08/08	91	439.56	0.01	-67	181	542.68	0.05	-135
SAR-X	2008	80	117.10	0.12	-28	161	257.45	0.18	-65
ALOS	24/08/07	119	158.54	0.27	-54	239	150.03	0.30	-47
PALSAR	2007	128	122.42	0.32	-42	256	109.43	0.39	-23
	26/08/08	115	151.42	0.23	-50	230	143.42	0.36	-54
	2008	126	105.20	0.35	-38	252	103.33	0.48	-35

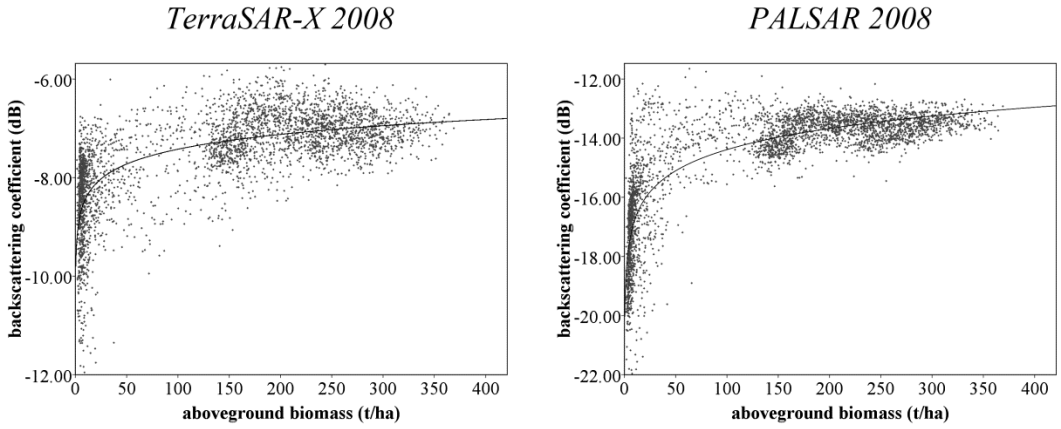

Figure III-2: Single frequency multi-temporal correlation between TerraSAR-X VV (left) or ALOS PALSAR HV polarized backscatter (right) of 2008 and AGB with corresponding curve progressions.

ALOS PALSAR backscatter is in general more sensitive to AGB than TerraSAR-X due to a higher backscatter range but the accuracies are lower in the low biomass range because of a higher variance. In detail, the independent validation of TerraSAR-X mono-temporal model features higher *RMSEs* and lower r^2 within the different accuracy requirements. These result from an extreme overestimation in the higher biomass range which is negatively influenced by extreme climatic conditions, such as moisture, which is not compensated in the mono-temporal model. However, the multi-temporal

TerraSAR-X model is considered to be useful in low biomass ranges. The ALOS PALSAR backscatter signal is in contrast sensitive to a wider biomass range which is indicated by higher saturation levels: 126 t/ha with an accuracy requirement of 50 t/ha and 252 t/ha with an accuracy requirement of 100 t/ha for the multi-temporal model of 2008 while TerraSAR-X models saturate at 80 t/ha and 161 t/ha, respectively. Therefore, ALOS PALSAR imagery is considered to be appropriate for AGB estimations in the higher range up to the saturation.

In a comparison of mono- to multi-temporal regression models from the same year, it was found that multi-temporal models are generally more accurate, as they are less influenced by any short-term variations. The mean error of all regression models is negative, indicating that the predicted biomass is overestimated. These results are comparable to previous studies that found longer wavelengths more adequate for AGB retrieval (Castro et al. 2003; Lu 2006).

ALOS PALSAR imagery was available for the years 2007 and 2008. The respective mono- and multi-temporal biomass models for both years, the curve progression results, the parameters, validation and saturation levels are very similar, indicating the temporal stability of the models as well as their transferability to subsequent years.

4.2. Combined X- and L-band regression models

In a next step we combined X-band and L-band backscatter in the analysis. The best biomass model is described by the following equation:

$$(11) \qquad y = a * 10^6 * \exp(\sigma^0_{PSR}) + b * 10^3 * \exp(\sigma^0_{TSX})$$

where σ^0_{PSR} = ALOS PALSAR backscatter, σ^0_{TSX} = TerraSAR-X backscatter and a,b = variables.

Again, the coefficients of determination (r^2) were calculated for no-intercept models. The results of the mono- and multi-temporal regression model are depicted in Table III-5 and Table III-6. The independent validation results are given up to the saturation thresholds at 307 t/ha with an accuracy requirement of 50 t/ha and at 614 t/ha with an accuracy requirement of 100 t/ha for both mono- and multi-temporal biomass models.

Figure III-3a shows ALOS PALSAR and TerraSAR-X signals in a 3D scatterplot and depicts the multi-temporal correlation with biomass values. The scattering of the

relationship in the low biomass range is less than for only using ALOS PALSAR, while a slight curve inclination is still visible in the high biomass range. Figure III-3b displays the corresponding scatterplot of estimated versus actual biomass values from the independent validation, also indicating the 1:1 line through the origin. Using the combined approach the low biomass range is slightly overestimated while the high biomass range (> 100 t/ha) is slightly underestimated and overall results in an underestimation which is indicated by the positive mean error.

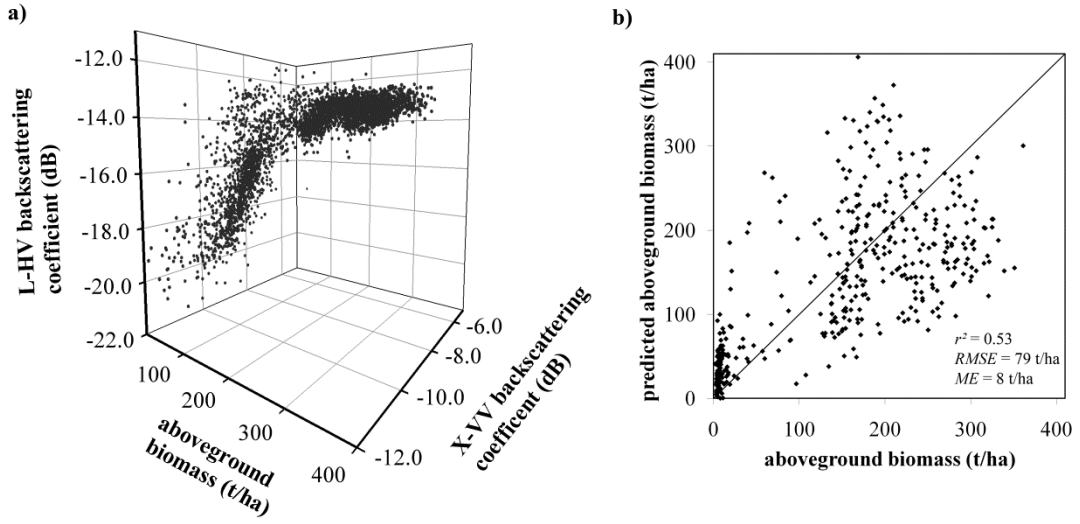

Figure III-3: a) Multi-temporal correlation between TerraSAR-X VV, ALOS PALSAR HV polarized backscatter and biomass. b) Corresponding actual versus predicted AGB values of the independent validation, shown with 1:1 line.

The multi-temporal biomass model is, similar to the results presented above, more accurate than the mono-temporal model as short-term variations are compensated. Both combined models tend to generally underestimate the AGB, which is indicated by positive mean errors. Nevertheless, the bias is much lower than with single frequency models.

To summarize, combined X- and L-band biomass regression models, both mono- and multi-temporal, achieved more significant results than the respective single frequency models, both in terms of regression analyses and model validation. They also have higher saturation thresholds demonstrating that they are applicable to a broader biomass

range. The most reliable biomass model is based on a multi-temporal combined X- and L-band dataset.

Table III-5: Results of biomass regression modeling using a combination of TerraSAR-X and ALOS PALSAR data based on equation (11)(10). The exact date depicts the mono-temporal and the year the multi-temporal model (n=3,970; 90% were used for regression modeling and 10% for the subsequent independent validation).

sensor	**date**	**regression model** $y = a*10^6 * \exp(\sigma^0_{PSR}) + b*10^3 * \exp(\sigma^0_{TSX})$		
		r^2	*a*	*b*
Combined	26/08/2008+ 08/08/2008	0.709	55.660	86.620
	2008	0.789	60.626	106.189

Table III-6: Results of the independent validation of equation (11) given with an accuracy requirement of 50 t/ha and 100 t/ha. The coefficients of determination (r^2), root mean square error (RMSE) and mean error (ME) are depicted for the X- and L-band combined SAR mono- (exact date) and multi-temporal (year) regression model.

sensor	**date**	**saturation (t/ha)**	**validation**			**saturation (t/ha)**	**validation**		
		accuracy 50 t/ha	*RMSE* (t/ha)	r^2	*ME* (t/ha)	*accuracy 100 t/ha*	*RMSE* (t/ha)	r^2	*ME* (t/ha)
Combined	26/08/08 + 08/08/08	307	82.71	0.43	19	614	86.97	0.43	23
	2008	307	75.72	0.53	4	614	78.77	0.53	8

4.3. Large scale model application

The validated multi-temporal regression models were applied to the 280,062 ha study area in Central Kalimantan. The spatial pattern of the biomass estimations indicating different vegetation types and degradation levels was compared to a multispectral satellite imagery showing these different vegetation types (Figure III-4). Biomass estimations are shown in aggregated classes from 0 t/ha (dark red) to 600 t/ha (dark green). Values exceeding 600 t/ha appear in grey and are assumed to overestimate the

actual biomass. The saturation levels for the two different accuracy levels (50 t/ha and 100t/ha) are indicated within the legend. As expected, the spatial pattern of biomass show low values in degraded, deforested or burnt areas and high values in peat swamp forests.

Subsets of deforested areas and peat swamp forest, whose locations are indicated in Figure III-4, are displayed in Figure III-5. TerraSAR-X estimated AGB is better in low biomass ranges (up to 100 t/ha where the saturation starts) while the performance is weaker at high biomass values above 150 t/ha which exceeds the saturation threshold of the 100 t/ha accuracy interval. ALOS PALSAR demonstrates opposite results: low biomass values were hardly resolved, while high biomass values show great detail up to 150 t/ha (saturation level for 50 t/ha accuracy interval) and allow discrimination between different forest types up to 300 t/ha (saturation level for 100 t/ha accuracy interval). The regression model combining X- and L-band data estimates values in low biomass ranges and up to 300 t/ha within the 50 t/ha accuracy interval while it represents the spatial pattern of the vegetation over the whole biomass range (up to 600 t/ha, saturation threshold for the 100 t/ha accuracy interval) which is also apparent in the Landsat image.

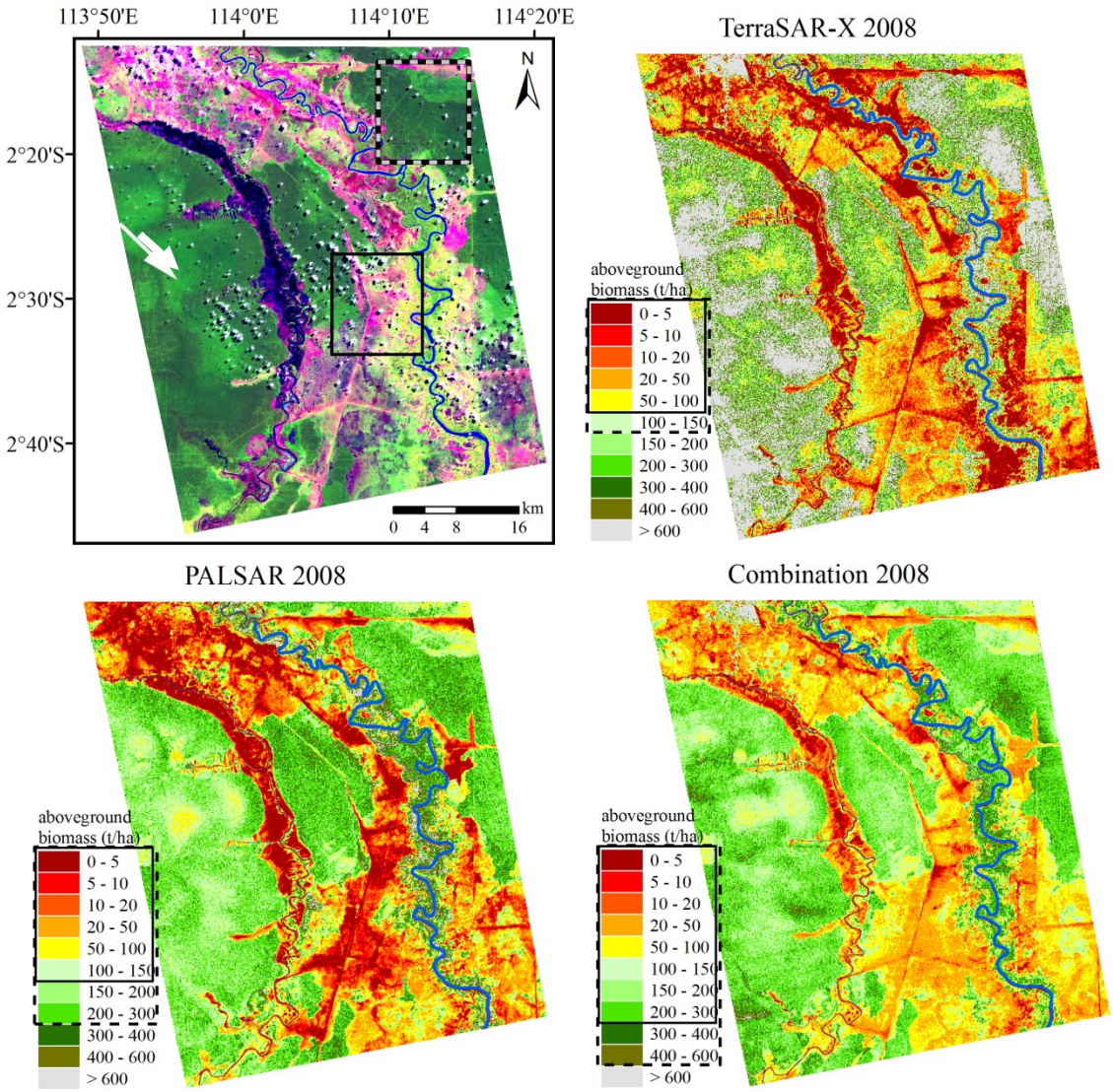

Figure III-4: Multi-temporal TerraSAR-X, ALOS PALSAR and combined regression models applied to the study area in Central Kalimantan in comparison to a Landsat scene from 19/05/2008 (RGB: bands 543). The saturation threshold is indicated in the respective biomass legends for an accuracy interval of 50 t/ha (solid line) and 100 t/ha (dashed line). The rectangles in the Landsat image indicate the extent of the subsets of a deforested area (solid line) and peat swamp forest (dashed line) shown in Figure III-5. Note the spatial variation in biomass in the large forest area to the left. The same pattern is visible as different shades of green in the Landsat image (white arrow). The pattern relates to different growth conditions due to various levels of flooding.

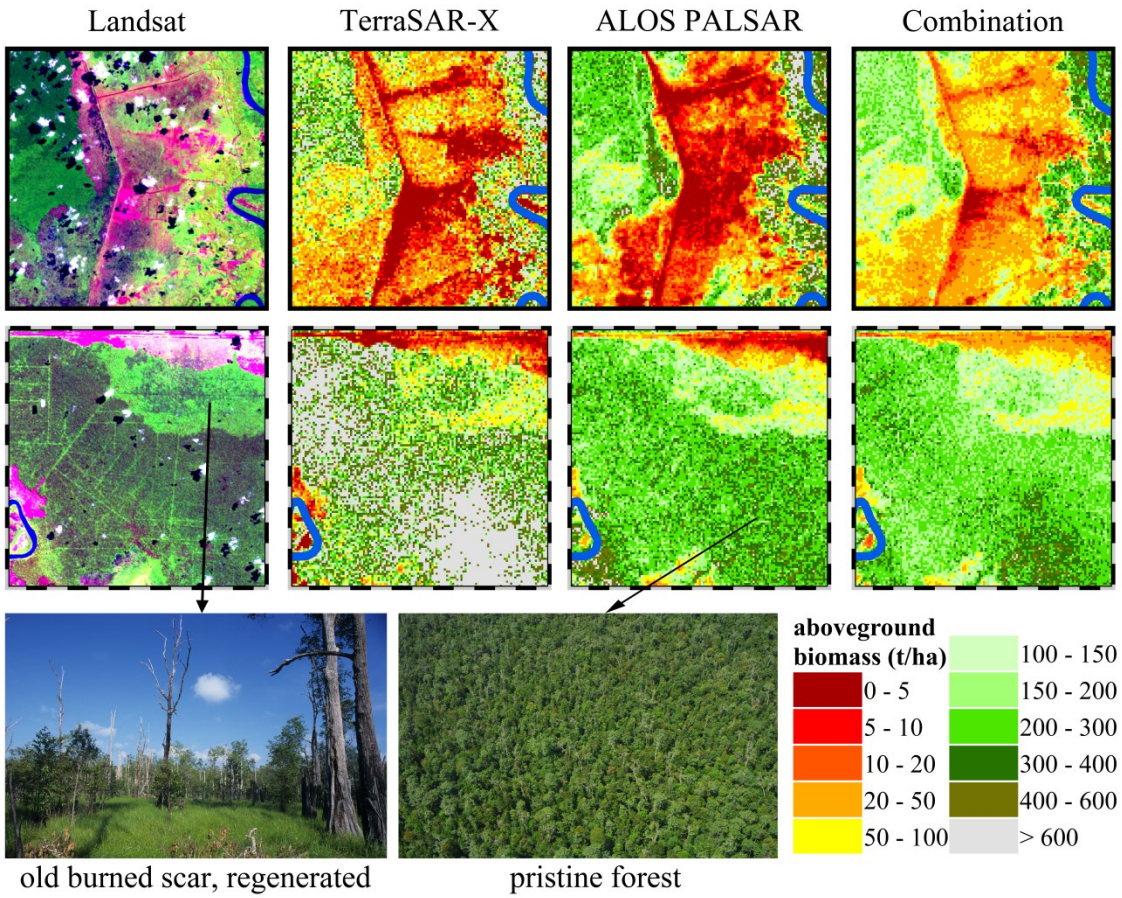

Figure III-5: Details of multi-temporal TerraSAR-X, ALOS PALSAR and combined biomass estimation models of deforested areas with low biomass (upper panels) and peat swamp forest areas with high biomass (lower panels). Left panels show a Landsat scene from 19/05/2008 (RGB: bands 543). Photographs show examples of different land covers indicated by arrows within the biomass maps (© F. Siegert).

Figure III-6 displays a comparison of biomass estimations using multi-frequency SAR and LiDAR data, superimposed on an ALOS PALSAR image. The diagram depicts the AGB along the marked 9.6 km long transect shown on the Landsat image. The transect covers the whole biomass range and thus features a rather complex biomass pattern. Low biomass predictions appear in red and high biomass values in green. The spatial pattern of degraded areas (dark in ALOS PALSAR image and bright green or pink in the Landsat scene) and forest areas (bright in the ALOS PALSAR scene and dark green in the Landsat image) are clearly visible in both biomass estimations. In this example, the majority of LiDAR biomass estimations are lower than X- and L-band combined SAR estimations, which are mostly below 300 t/ha (saturation within an accuracy

requirement of 50 t/ha). SAR biomass estimations do not exceed the saturation level of 600 t/ha (saturation with an accuracy requirement of 100 t/ha). However, the crucial point is that both estimation methods feature the same complex biomass variation pattern. This becomes obvious in a biomass transect with increasing biomass between km 3 and 4 when entering the peat swamp forest area and the rapid decrease in the fire scar at 6.7 km.

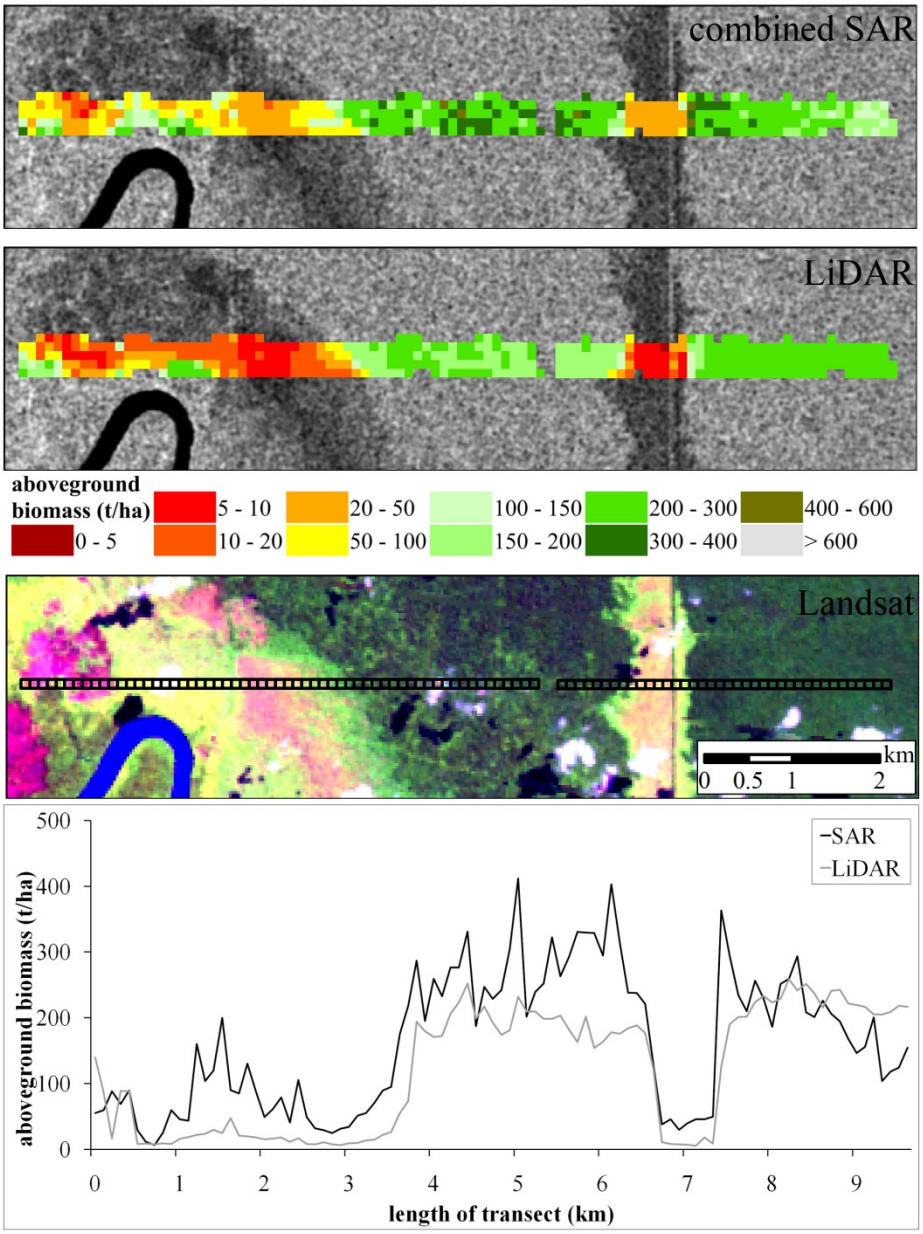

Figure III-6: Multi-temporal combined X- and L-band SAR biomass estimation in comparison to LiDAR estimation along the marked transect superimposed on the Landsat image (19/05/2008; RGB bands: 543). Both estimations are depicted on an ALOS PALSAR HV polarized scene from 26/08/2008.

In order to test the robustness and transferability of the multi-temporal combined biomass regression model, it was applied to the study area in West Kalimantan which represents a very similar ecosystem. In a preliminary step, the total monthly GPCP precipitation data from January 2007 to April 2009 of the two study areas were related to each other to test the climatic conditions. They result in a high correlation with a Pearson's coefficient of correlation of 0.6. This correlation demonstrates that both study areas feature similar climatic conditions during the time of image acquisition which is a very important precondition for analyzing the spatial transferability applying the same preprocessing algorithms on radar imagery and similar vegetation composition.

TerraSAR-X imagery of this study area was only available for 2009. Hence, the regression model based on combined X- and L-band SAR data from 2008 was applied to 2009 data, in order to not only test the spatial transferability, but also to demonstrate the temporal transferability. Figure III-7 displays the resulting biomass estimation map in comparison to a Landsat image and a Landsat-based forest classification. The spatial distribution of the different forest types, which is depicted in the classification, is also identifiable in the biomass estimation map. Forest types with lower biomass (e.g. low pole peat swamp or dwarf forest), which are below the saturation threshold of 50 t/ha accuracy, appear in yellow/bright green in the biomass estimation map, indicating aggregated biomass classes from 50 t/ha to 200 t/ha. Forest types comprising higher biomass stands, such as the riparian forest, appear in dark green in the biomass estimation map, indicating aggregated biomass classes from 200 t/ha to 600 t/ha which are below the saturation level of 100 t/ha accuracy. To examine the spatial transferability, the average estimated biomass was compared to either field derived values and to indirectly estimated biomass values for each forest type (Table III-7). The indirect values were calculated by linking the respective forest types of the classification result with average biomass values from either the literature and/or field inventory data. The comparison, which includes only biomass values between 80 t/ha and 300 t/ha (which is below any saturation), is more accurate than the independent model validation, using the LiDAR based biomass values, in Central Kalimantan. The estimations of the biomass model are in comparison to broad scaled forest type AGB slightly underestimated which is indicated by the positive mean error.

These results show that the multi-temporal combined regression model is transferable and still provides appropriate AGB estimations validated at a broad scale.

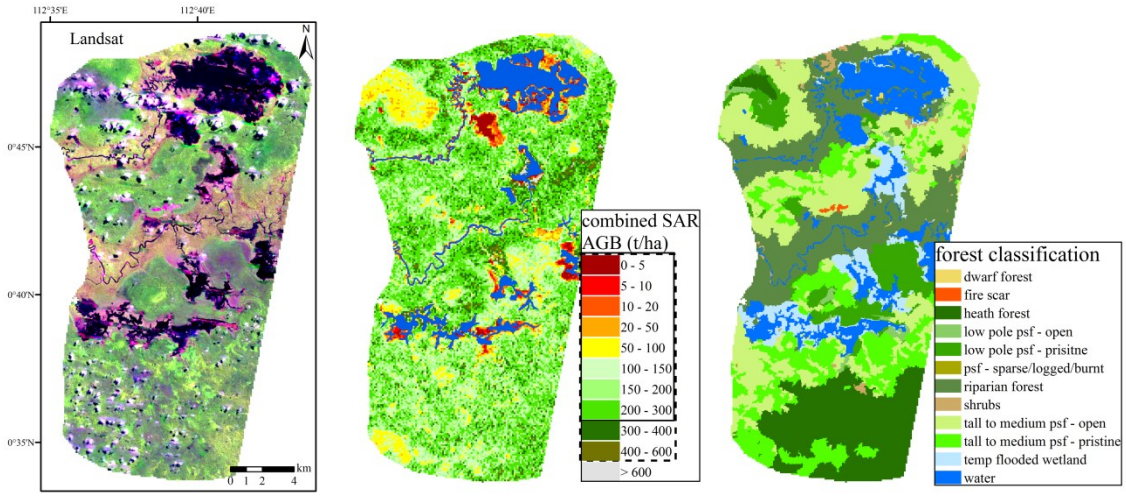

Figure III-7: Spatially and temporally transfer of the multi-temporal X- and L-band combined regression model to the study area in West Kalimantan in comparison to a Landsat image (13/05/2009, RGB: bands 543). The saturation threshold is indicated in the biomass legend for an accuracy requirement of 50 t/ha (solid line) and 100 t/ha (dashed line). A detailed forest classification of 2009 on the basis of Landsat is shown on the right.

Table III-7: AGB values of a forest type classification of 2009 in Kapuas Hulu, West Kalimantan, compared to average estimated values of the spatially and temporal transferred multi-temporal X- and L-band combined regression model (psf = peat swamp forest).

Average aboveground biomass (t/ha)	***Forest types***							
	tall to medium psf		low pole psf		psf	heath forest	dwarf forest	riparian forest
data base	*pristine*	*open*	*pristine*	*open*	*sparse*			
classification	210	217	249	209	101	235	82	294
X-/L-band synergy 2009	186	214	139	175	83	196	140	199

**RMSE*=59 t/ha, r^2= 0.49, *ME*= 33t/ha.

5. Discussion

The regression modeling of AGB based on TerraSAR-X and ALOS PALSAR imagery, alone and in combination, show that multi-temporal regression models are more accurate than mono-temporal models featuring higher coefficients of determination and lower root mean square errors. Mono-temporal regression models can be affected by extreme climatic conditions and the spatial and temporal transferability is therefore limited. Multi-temporal models compensate extreme conditions, e.g. heavy rainfall, and

are more feasible for temporal and spatial transfer.

The results also demonstrate that low biomass values can be better estimated with X-band and high biomass with L-band data while biomass estimation in the higher range are extremely overestimated by single-frequency TerraSAR-X models. Both radar signals have different vegetation penetration depths: the L-band has a deeper penetration than the X-band signal and is therefore influenced by ground and double-bounce interaction at low biomass levels. The X-band backscatter signal mainly interacts with leaves, twigs and small branches and the main scatter of the L-band are from primary and secondary branches (Henderson et al. 1998; Le Toan et al. 2001). The combined use of TerraSAR-X and ALOS PALSAR imagery achieves the most accurate estimation over the whole biomass range, combining both penetration depths (Figure III-4 and Figure III-5).

Biomass analyses using radar imagery are normally limited by the saturation of the radar signal at high biomass values which occurs when the biomass/backscatter slope approaches zero. The saturation threshold within the 50 t/ha accuracy interval is at 80 t/ha in multi-temporal TerraSAR-X and at 126 t/ha in multi-temporal ALOS PALSAR regression models of 2008 (Table III-4) and is clearly visible in the scatterplots in Figure III-2, while it is at 300 t/ha at the multi-temporal combined model (Table III-6 and Figure III-3). The saturation level within an accuracy requirement of 100 t/ha is much higher (161 t/ha at TerraSAR-X, 252 t/ha at ALOS PALSAR and 600 t/ha at the combined multi-temporal model of 2008) however it is not accurate enough for reliable AGB estimation but it can be used for indicating the spatial distribution of high biomass and different forest types.

Other studies also found valid biomass predictions based on radar data beyond the otherwise stated saturation. For example, Mitchard et al. (2009) used ALOS PALSAR imagery in tropical regions for biomass estimations up to 400 t/ha, indicating an increased capability in the use of SAR imagery for AGB retrieval than previously assumed, also in tropical regions with high biomass volumes.

The regression models were calibrated with numerous biomass reference data (n=3,970), of which 10% were left out for the independent validation. This enormous amount of data was generated through an upscaling approach, using airborne LiDAR measurements in connection with field inventory data. Such an upscaling approach of this kind (forest inventory → LiDAR AGB estimation → SAR AGB estimation) has, to

date, only been performed by Solberg et al. (2010). Other previous studies often used a very limited amount of in-situ data, ranging from 51 up to 191 samples in total (Kuplich et al. 2005; Lucas et al. 2007; Mitchard et al. 2009; Pandey et al. 2010; Santos et al. 2006; Watanabe et al. 2006). By using this upscaling approach the merit of only having a few in-situ data, which have to be divided into samples for the regression model training and the independent validation of the findings, is overcome. Additionally the independent validation, which utilized almost 400 data points excluded from the model calibration, provides a powerful basis for validating the regression models. Therefore, the results of the validation are very accurate. Due to the upscaling approach of biomass data, there were numerous data available covering the whole biomass range and representing the spatial variability of the complex tropical forest. This amount of data makes the biomass modeling more powerful.

The accuracy of the biomass models is denoted by coefficients of determination and root mean square errors at the independent validation, but there are several factors which influence the overall accuracy; the radiometric accuracy of radar images is, for example, an important element. The radiometric accuracy of an area of 1 ha is 0.27 dB in TerraSAR-X ScanSAR scenes and 0.41 dB in ALOS PALSAR dual polarized images. As the biomass/backscatter slope decreases in high biomass ranges, the model is influenced by the radiometric accuracy in high rather than in low biomass ranges. Time lag is another potential influence of overall accuracy, firstly between field inventory and LiDAR measurements, and secondly between LiDAR biomass estimations and radar analysis, assuming that new growth is not balanced by stem mortality, but this is supposed to have no effect. Significant land cover changes were monitored by optical remote sensing and if necessary considered. A further aspect that has an impact on the overall accuracy of the biomass model is the error propagation from the upscaling approach. Field inventory biomass data generally contain only a small uncertainty, whereas LiDAR biomass estimations imply a higher uncertainty. The utilization of these biomass estimations for radar biomass modeling leads to an error propagation. Nevertheless, using LiDAR biomass estimations instead of field inventory data is advantageous because they represent the spatial biomass distribution and provide ample reference data.

Finally, the temporal and spatial transferability of the multi-temporal X- and L-band combined biomass model was tested (Figure III-7). The model was proved to be

appropriate for AGB estimation of different broad scale forest classes in the study area in West Kalimantan which comprises the same ecosystem. Only radar imagery with the same preprocessing, same incidence angles and which were recorded during the dry season were used. These constraints are very important for the spatial transferability of biomass regression models (Freitas et al. 2005). Previous studies also found potential in the spatial transfer of biomass regression models. Mitchard et al. (2009) found a widely applicable general relationship between AGB and ALSO PALSAR HV polarized backscatter with expected errors of 20-30%. Chen et al. (2009) proved the spatial transferability of a biomass regression model from one study area to another, both comprising the same dominant land cover types. The validation result was $r^2 = 0.81$.

In the current study, additional in-situ biomass data would be preferable for an exact model calibration and validation. The standard approach of linking one specific biomass value to different land cover classes implies a high uncertainty, as variability within a land cover class is disregarded and the definitions of the land cover classes are often ambiguous. The multi-temporal combined regression model can differentiate between biomass variations within different stages of forest (e.g. regeneration on burned scars, degraded forests due to logging or fire events or intact peat swamp forests) (Figure III-5 and Figure III-6). The spatial distribution over the whole biomass range is displayed with the current approach but only validated for a broad scale. However, it implies crucial information for carbon stock assessment.

Considering the needs of REDD, in the context of accuracy and the trade-off between feasibility and costs, the presented approach for estimating aboveground biomass in tropical inaccessible forests is a superior possibility for AGB values up to 300 t/ha and is furthermore able to indicate the spatial variability of the forest over the whole biomass range (up to 600 t/ha).

6. Acknowledgements

The authors would like to thank the Japan Aerospace Agency (JAXA) for supplying ALOS PALSAR data within the PI project No. 211 as well as Infoterra GmbH and German Space Agency (DLR) for providing TerraSAR-X data and their cooperation within the For-X Project (50 E705, PI: LAN0236). We gratefully acknowledge FFI (Fauna and Flora International) for making field data on biomass available and the National Aeronautics and Space Administration (NASA) for providing GPCP precipitation data free of charge. Special thanks to Peter Navratil, Julia Jaenicke, Uwe Ballhorn, Karin Kronseder, Jonas Franke and Keith Peterson for their help and support.

IV. Modeling aboveground biomass in tropical forests using multi-frequency SAR data - a comparison of methods

S. Englhart [a], V. Keuck [b], F. Siegert [a,b]

IEEE Journal of Selected Topics in Applied Earth Observation and Remote Sensing 5 (2012) 298 - 306

[a] *Biology Department II, GeoBio Center, Ludwig-Maximilians-University, Großhadener Str. 2, D-82152 Planegg-Martinsried, Germany*

[b] *Remote Sensing Solutions GmbH, Isarstr. 3, D-82065 Baierbrunn, Germany*

1. Abstract

In the context of climate change mitigation mechanisms for avoiding deforestation, i.e. reducing emissions from deforestation and forest degradation (REDD+), comprehensive forest monitoring, especially in tropical regions, is of high relevance. A precise determination of forest carbon stocks or aboveground biomass (AGB) for large areas is of special importance.

This study analyzes and compares three different methods for retrieving AGB in Indonesia's peat swamp forests from multi-frequency SAR backscatter data. Field inventory AGB data were related to LiDAR measurements allowing plentiful accurate AGB estimations. These estimated AGB data provided a powerful basis for SAR based AGB model calibration and validation. Multivariate linear regression (MLR), artificial neural network (ANN) and support vector regression (SVR) were examined for their performance to retrieve AGB on the basis of multi-temporal TerraSAR-X and ALOS PALSAR imagery.

The MLR model resulted in lower coefficients of determination and higher error measures than the other two approaches and showed significant overestimations in the high biomass range. SVR modeled AGB was more accurate than ANN in terms of

independent validation, but showed less variation in the spatial distribution of AGB and saturated at approximately 260 t/ha. The ANN model showed a superior performance for modeling AGB up to 650 t/ha without a saturation in the lower biomass ranges.
For the needs of REDD+, it is very important to know the possibilities, constraints and uncertainties of AGB retrieval based on satellite imagery.

Keywords: ALOS PALSAR, artificial neural networks (ANN), biomass, forest, Indonesia, REDD+, regression, support vector regression (SVR).

2. Introduction

Tropical forests are known as a major carbon sink (Hooijer et al. 2010). In general, 78% of their living biomass is stored aboveground and 22% belowground in roots (Saatchi et al. 2011a). In contrast, tropical forested peatlands accumulate most of the carbon in thick belowground peat deposits which are sustained by intact forests on top of it. In Indonesia, forested peatlands cover approximately 11% of the land surface and comprise approximately 55 - 58 Gt of carbon (Jaenicke et al. 2008; Page et al. 2011). Due to strong economic and social pressure for timber as well as land for agriculture and oil palm or pulp tree plantations, these areas are being drained, deforested and often burned (Hooijer et al. 2010; Koh et al. 2009). Approximately half (47.6%) of the peatland areas in Southeast Asia had been deforested and mostly drained by 2006 (Hooijer et al. 2010).
Emissions from Southeast Asia, caused by deforestation, forest degradation and peatland fires, were estimated to be 12% of the global anthropogenic CO_2 emissions in 2008 and were therefore the second largest anthropogenic source of CO_2 behind fossil fuel combustion (Le Quere et al. 2009; van der Werf et al. 2009). In 2006, peat fires in Indonesia released approximately 0.25 Gt of carbon which is equivalent to 16% of all global emissions by land use change in that year (Ballhorn et al. 2009). At present, Indonesia is the largest emitter of CO_2 from ongoing peat decomposition (excluding fires), responsible for 82% of Southeast Asian emissions in 2006 (Hooijer et al. 2010).
Due to the high emissions from land conversion, the implementation of environmental projects which aim at avoiding deforestation bear good prospects in Indonesia. One example for such a climate change mitigation mechanism is REDD+ (reducing

emissions from deforestation and forest degradation and the role of conservation, sustainable management of forests and enhancement of forest carbon stocks), which was accepted at the United Nations Climate Change Conference in December 2010. Forest activities which have been identified within the REDD+ context require a forest monitoring system to precisely assess the total amount of carbon stored within the vegetation and its spatial distribution, assuming a carbon content of dry biomass of 50% (Gibbs et al. 2007; Goetz et al. 2009).

The most accurate way of AGB retrieval are forest inventories which use field based measurements (e.g. tree height, diameter at breast height) to extrapolate the biomass on the basis of allometric equations (Chave et al. 2005; Lu 2006). Although this method provides very precise AGB values, it is time consuming, laborious, difficult to implement in remote areas and lacks information on the spatial distribution (Lu 2006).

Methods based on the use of satellite observations and measurements are less accurate. However, the major advantage is the ability to cover large and remote areas. Therefore, the technique has become the primary source of AGB estimation (Gibbs et al. 2007; Lu 2006). Different approaches have been developed to assess AGB with remote sensing techniques. The simplest method is the 'indirect approach', which links a biomass value determined for a specific vegetation type to a remote sensing based land cover map (Goetz et al. 2009). A more accurate method is the 'direct approach', for which radiometric satellite measurements are calibrated to field based AGB values (Goetz et al. 2009). Regression analyses (Chen et al. 2009; Mitchard et al. 2009; Watanabe et al. 2006) and different machine learning techniques, such as artificial neural networks (ANN) (Amini et al. 2009; Del Frate et al. 2004; Wijaya et al. 2010), are used to train an algorithm for estimating AGB. Support vector machines (SVM) are a promising alternative to ANN models and their implementation for regression and function approximation, the support vector regression (SVR), was successfully applied for the estimation of biophysical parameters from satellite imagery. Nevertheless, a SVR has, till now, rarely been used for estimating AGB from SAR data (Camps-Valls et al. 2006; Camps-Valls et al. 2009; Monnet et al. 2011).

Airborne LiDAR (light detection and ranging) systems can directly measure components of the vegetation in great detail (e.g. canopy height) and has been proven to result in very accurate AGB estimations (Kronseder et al. 2012; Zhao et al. 2009). Unfortunately, LiDAR measurements are very expensive and are therefore often limited

to small areas (Gibbs et al. 2007). Optical remote sensing based AGB estimation in tropical regions is often restrained by clouds, but is considered to be appropriate using spectral signatures, vegetation indices or image texture (Sarker et al. 2011; Soenen et al. 2010; Wijaya et al. 2010). SAR (synthetic aperture radar) systems have the ability to record data irrespective of weather or light conditions and have been extensively used in tropical regions to retrieve AGB (Englhart et al. 2011; Mitchard et al. 2009; Santos et al. 2006). Estimations of AGB using SAR imagery are limited by the saturation of the radar signal at high biomass values. The saturation level not only depends on the SAR wavelength but also on the amount and quality of AGB reference data (Englhart et al. 2011).

This work builds upon a detailed investigation on the relationship between AGB and X- and L-band SAR backscatter considering single-frequency and multi-frequency relationships and saturation levels (Englhart et al. 2011). Numerous AGB reference data were generated by relating forest inventory data to airborne LiDAR point cloud signals resulting in accurate AGB estimations representing the whole biomass range, from low growing bushes to mature tropical rainforest. This upscaling approach provided a powerful basis leading to a stronger biomass/backscatter relationship and higher saturation levels.

The scope of this paper is to provide a comparison of methods for AGB estimation from multi-temporal combined TerraSAR-X and ALOS PALSAR data. Multivariate linear regression (MLR), ANN and SVR models were analyzed in detail and quantitatively compared to each other for their performance to retrieve AGB in tropical peat swamp forests. The different models were also examined for their ability to predict AGB over large areas, which is crucial for REDD+ projects.

3. Materials and Methods

3.1. Study area

The study area, approximately 280,000 ha in size, is located in the Indonesian province of Central Kalimantan on the island of Borneo (Figure IV-1). The land cover is comprised by peat swamp forests, riparian forests, forest areas heavily degraded by fire (shrubs/regrowing forest) and seasonally flooded wetlands. The forests have been drained and deforested (mainly for agricultural development and plantations (Hooijer et

al. 2010) and recurrent fire events destroyed approximately 50% of the forest cover in the past decade. The belowground peat deposits store huge amounts of carbon (up to ten times more biomass per ha than the forests growing on top of them) as they were formed from plant debris under waterlogged conditions over thousands of years (MacKinnon et al. 1996; Posa et al. 2011). To protect these huge carbon stores, an intact forest cover is of high relevance, as the probability of recurrent fires increases dramatically in degraded forests (Langner et al. 2009).

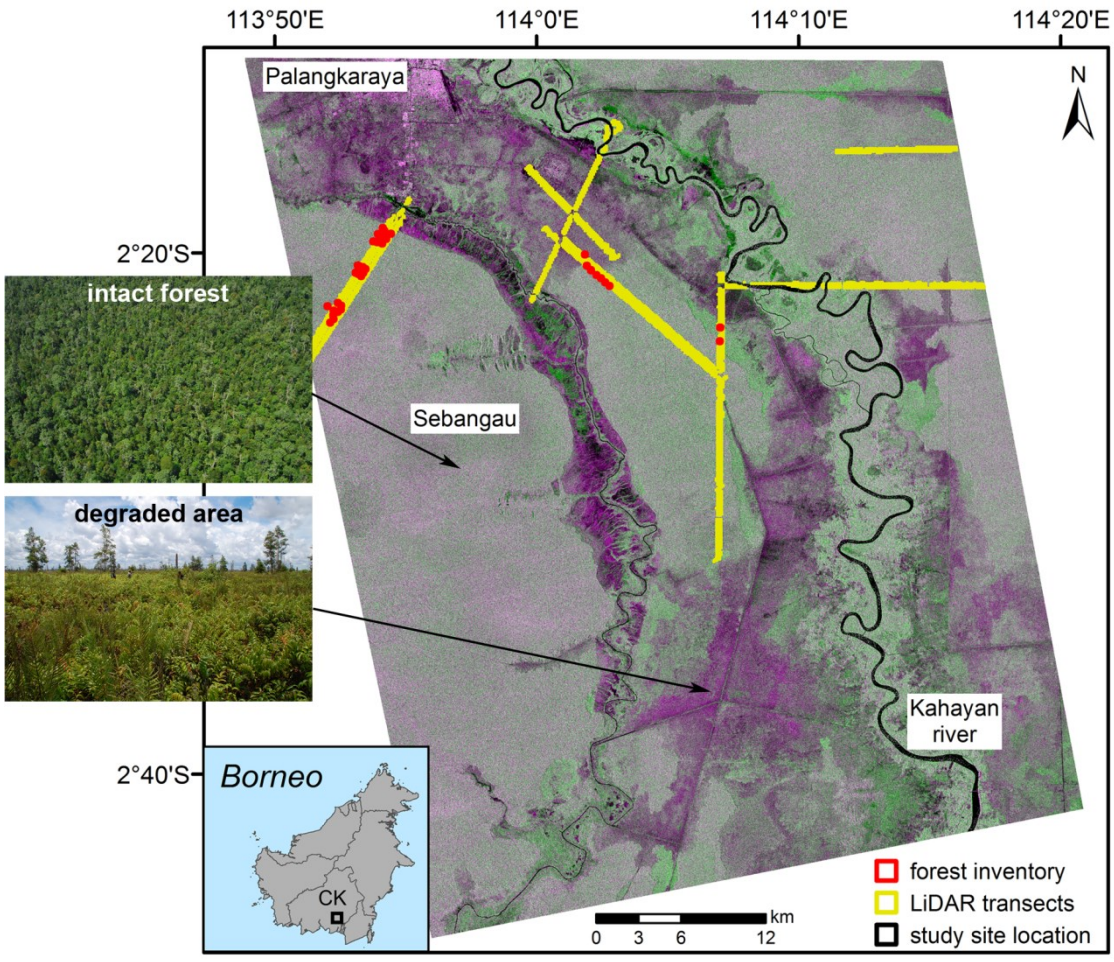

Figure IV-1: Multi-sensor TerraSAR-X ScanSAR VV (30/08/2008, RB) and ALOS PALSAR HV (26/08/2008, G) image showing the study area with a dynamic range of approximately 20 dB (TerraSAR-X [-24.779;-4.548], ALOS PALSAR [-29.038;-10.226]) . The location of the forest inventory plots and of the LiDAR transects are depicted in red and yellow, respectively. Photos show examples of an intact forest and a degraded, regrowing area (© F. Siegert, S. Englhart). The outline map indicates the study site in Central Kalimantan (CK) on Borneo, Indonesia.

3.2. Aboveground biomass data

The AGB reference data were generated by relating forest inventory AGB data to LiDAR measurements, taking advantage of LiDAR's ability to create accurate biomass predictions for an area within the SAR images. This upscaling from point data (field inventory) to transects (LiDAR) was chosen to provide a more powerful basis for AGB model calibration and validation from SAR backscatter data. As peat swamp forests are very difficult to access on the ground, this approach is the only possibility for getting comprehensive AGB data.

Altogether, 140 forest plots were surveyed in 2007 and 2008 with the angle count method (Bitterlich 1951). The AGB was calculated for 1 ha using allometric equations (Chave et al. 2005) (some of them are located within the study area and are shown in Figure IV-1). The ground based AGB values were related to LiDAR transects acquired in 2007 in order to estimate biomass reference data using a previously established regression model. The model depends on the 50th percentile of the LiDAR point cloud within 1 ha and was calibrated with AGB field inventory values ranging from 1.5 t/ha to 567.8 t/ha. Altogether, 3,790 AGB reference data were provided within the study area ranging from 1.5 t/ha to 369 t/ha. The independent validation resulted in a coefficient of determination of r^2=0.32 and a root mean square error *(RMSE)* of *RMSE*=94.77 t/ha. The details of this method are described by Kronseder et al. (2012) and Englhart et al. (2011). Although the independent validation is weak, this AGB estimation model performed best over the whole biomass range, even showing variations in the low biomass range.

3.3. SAR data

TerraSAR-X ScanSAR VV and ALOS PALSAR fine beam HV polarized images were analyzed in combination for AGB retrieval. Three scenes from each sensor, acquired during the dry season (May to October) in 2008, were selected to minimize any influence of varying rainfall and soil moisture. Table IV-1 lists the properties of all investigated SAR scenes in detail. The preprocessing of the SAR images included the standard radiometric calibration, speckle filtering and co-registration and is described in detail by Englhart et al. (2011).

Table IV-1:Main characteristics of analyzed SAR imagery.

Sensor	date (dd/mm/yyyy)	polarization	pixel spacing [m]	incidence angle
TerraSAR-X	14/06/2008	VV	8.25	32.1°
ScanSAR	08/08/2008	VV	8.25	29.9°
	30/08/2008	VV	8.25	32.1°
ALOS PALSAR	26/05/2008	HV	12.50	38.8°
fine resolution	26/08/2008	HV	12.50	38.8°
	11/10/2008	HV	12.50	38.8°

3.4. Aboveground biomass estimation

Three different methods were analyzed and compared for their ability to retrieve AGB from multi-frequency, multi-temporal TerraSAR-X and ALOS PALSAR imagery: MLR, ANN and SVR models. Spatially averaged backscatter values over 1 ha plots were used and related to the LiDAR derived AGB estimates. To produce the multi-temporal SAR images, both the TerraSAR-X and ALOS PALSAR backscatter coefficients were temporally averaged. The multi-temporal backscatter signals of the dry season are very stable and show little influence by climatic conditions (Englhart et al. 2011).

The AGB reference dataset (n=3,790) was randomly split up to be used for training (90% of all data) and validating (10%) the AGB models. To allow a comparison of methods, the same training and validation data were used for each method.

The regression modeling was conducted on the basis of a least-square MLR (Englhart et al. 2011). Based on our previous study (Englhart et al. 2011), exponential backscatter values of TerraSAR-X and ALOS PALSAR imagery were used to test their sensitivity to AGB in a MLR model. The backscatter signals were entered in a single step and r^2 was calculated.

ANN models have the ability to learn patterns or relationships from training data and to generalize or extract results. An ANN consists of an input layer with multiple inputs (e.g. radar signals), a single or multiple hidden layer(s) with a certain number of processing nodes and a single output layer with the predicted variable(s). The inputs are usually linked to the neurons in the hidden layer, which are in turn fully connected to

the output node. The hidden layer consists of an optimal number of neurons, of which each multiplies the input signal *I* with a specific weight (Rumelhart et al. 1986):

$$(12) \qquad I = \sum_{i=1}^{n} w_i S_i + b$$

where *I* is the total input signal to a node, *n* is number of input signals S_i, w_i is the weight of an input signal and *b* is the bias associated with the node. The weights and bias term for each node are unique to that node and optimized by the network activation function. These optimal weights and biases minimize the error between the desired and actual output for all training patterns. A detailed description of ANN models is beyond the scope of this paper and are provided by Del Frate et al. (2004) and Mas et al. (2008). In this study a feed-forward multi-layer perceptron ANN was analyzed, which means that all input signals go directly through one hidden layer to the output node. The multi-temporal spatially averaged TerraSAR-X and ALOS PALSAR backscatter values were used as input signals to estimate AGB. For training the ANN, 79.3% of the training dataset were used to train the network and the remaining 20.7% were used for testing the ANN which avoids over-fitting. The subsequent independent validation was executed with the validation dataset.

SVM is also a supervised nonparametric statistical learning technique and is considered as a promising alternative to ANN models (Mountrakis et al. 2011; Smola et al. 2004). SVR, a special form of SVM, is a kernel method for regression and function approximation and has the ability to model complex, non-linear dependencies in high dimensional feature space (Smola et al. 2004).

The SVR function $f(x)$ is defined as (Chang et al. 2001):

$$(13) \qquad f(x) = \sum_{i=1}^{l} (-\alpha_i + \alpha_i^*) k(x_i; x) + b$$

where α_i and α_i^* are Lagrange multipliers (which have to satisfy positivity constraints), $k(x_i; x)$ is a kernel function with the training vector x_i, and *b* is the bias term in the regression which is calculated during the SVR training (please refer to Smola et al. (2004) and Chang et al. (2001) for a detailed description).

The regression implementation of imageSVM 2.0 was used for estimating AGB with the SVR approach (Rabe et al. 2009a). The SVR was trained using a radial basis function kernel:

$$k(x_i; x_j) = \exp(-g\|x_i - x_j\|^2) \quad (14)$$

where *g* is the kernel function parameter.

The regularization parameter *C,* which is also determined during the SVR modeling (Smola et al. 2004), specifies the tradeoff between flatness of *f(x)* and the amount up to which deviations larger than *ε* (the parameter of Vapnik's ε-insensitive loss function) are tolerated (Chang et al. 2001). Although *ε* is in the same domain as the target, no explicit relationship between the chosen ε-loss and performance of the SVR exists (Rabe et al. 2009b).

Optimal values for the kernel parameter *g* and regularization parameter *C* were selected via a 2-dimensional grid search inside an interval of [0.1; 819.2] using a multiplier value of 2 and an optimization criteria of cross-validated mean absolute error (*MAE).* The loss function parameter was fixed to *ε*=0 and could not be changed. Hence, every training vector became a support vector but over-fitting was prevented by the grid search (Rabe et al. 2009b).

3.5. Independent validation of AGB models

For the subsequent independent validation, previously 10% (n=396) of the AGB reference data were randomly chosen to compare the performance of the different AGB estimation methods. The accuracy statistics included the *RMSE*, *MAE*, the mean error (*ME*) and the relative errors to the mean value of AGB. The value of the *RMSE* is affected by large errors which give disproportionately large weights because of the squaring process. Therefore, the *MAE* may be a more relevant criterion, as the true cost of the error is roughly proportional to the size of the error. The *MAE* is usually similar in magnitude to, but slightly smaller than the *RMSE.* In cases where outliers may seriously overstate the error, the *MAE* is a better summary measure of error than the *RMSE* (Chen et al. 2009). The *ME* is a signed measure of error which indicates whether the predicted AGB is biased. The predicted AGB is underestimated with a negative *ME* and overestimated with a positive *ME.* Additionally, the coefficient of determination (r^2)

was calculated as the square of Pearson's correlation coefficient (*r)* for a linear transformation of the model.

A supplementary independent validation was conducted by estimating AGB using the different approaches for a LiDAR transect not included in the AGB data generated previously. Thereby it is possible to analyze the modeling performances not only for point based, but also for wall-to-wall AGB estimations.

4. Results

The most accurate MLR model, in terms of r^2, for predicting AGB from SAR data resulted in an equation of the form:

$$y = 106{,}189 * \exp(\sigma^0_{TSX}) + 60{,}626 * 10^3 * \exp(\sigma^0_{PSR}) \quad (15)$$

where σ^0 is the multi-temporal backscattering coefficient of TerraSAR-X (TSX) or ALOS PALSAR (PSR). R^2 was calculated for no-intercept models (Kvalseth 1985) and is r^2=0.789. A detailed evaluation of the relationship between TerraSAR-X, ALOS PALSAR and AGB and its saturation is given in Englhart et al. (2011).

AGB retrieval with ANN modeling resulted in a network with one hidden layer containing five processing nodes which have a hyperbolic tangent activation function of the form:

$$\gamma(c) = \frac{e^c - e^{-c}}{e^c + e^{-c}} \quad (16)$$

where c is a threshold value. That means that the multi-temporal TerraSAR-X and ALOS PALSAR backscatter signals from the input layer were transferred to the processing nodes and transformed to the range [-1;1] by the activation function. The activation form of the output layer was identity which means that the incoming signal was processed unchanged. The architecture of the retrieved ANN is depicted in Figure IV-2.

The optimal SVR for predicting AGB has a kernel function parameter of g=1.6 and a regularization parameter of C=51.2. The bias term was estimated to be b=-63.61. As

ε=0, every training vector became a support vector, so the SVR had 3,571 support vectors.

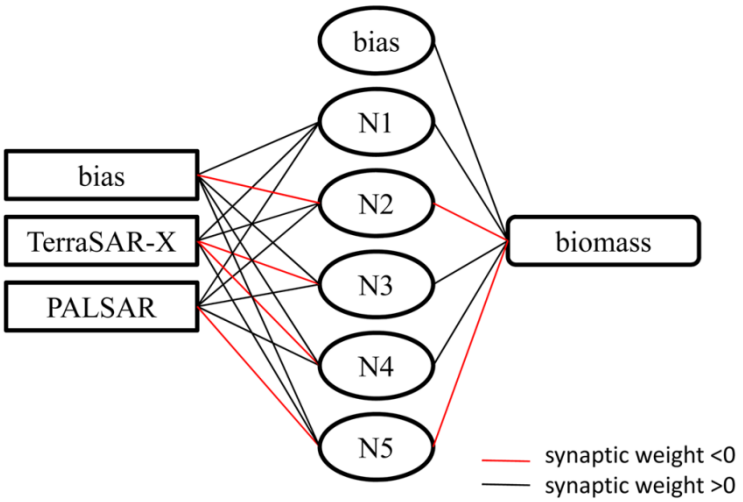

Figure IV-2: Schematic architecture of the retrieved multilayer perceptron ANN with one hidden layer containing five nodes (N1-N5). AGB was predicted using multi-temporal TerraSAR-X ScanSAR VV and ALOS PALSAR HV imagery.

The results of the independent validation of the different AGB models are depicted in Table IV-2. The SVR model featured the highest r^2 (r^2=0.68) and the lowest error measures ($RMSE_{rel}$=41.0%, MAE_{rel}=28.5% and ME_{rel}=1.0%). No AGB value predicted by the SVR approach was higher than 262 t/ha which indicates a saturation effect. Altogether, the independent validation of the ANN is less accurate than of the SVR, but more precise in terms of error measures than of the MLR model. The MLR model resulted in the lowest r^2 (r^2=0.47) and the highest errors ($RMSE_{rel}$=54.5%, MAE_{rel}=42.6% and ME_{rel}=-6.0%).

As the algebraic sign of the *ME* indicates the bias, the MLR modeling underestimates the real AGB, while it is slightly overestimated by the ANN and SVR approach.

Table IV-2: Results of the independent validation using identical 10% of the AGB reference dataset (n=396) for three different approaches to estimate AGB from multi-temporal TerraSAR-X and ALOS PALSAR data. The coefficient of determination (r^2), root mean square error (RMSE), mean absolute error (MAE) and mean error (ME) are depicted.

estimation approach	r^2	*RMSE* [t/ha]	$RMSE_{rel}$ [%]	*MAE* [t/ha]	MAE_{rel} [%]	*ME* [t/ha]	ME_{rel} [%]
MLR	0.47	79.84	54.5	62.42	42.6	-8.81	-6.0
ANN	0.63	64.84	44.3	52.07	35.6	4.85	3.3
SVR	0.68	60.06	41.0	41.66	28.5	1.52	1.0

Figure IV-3 depicts scatterplots of observed (LiDAR derived) versus predicted AGB as well as the respective histograms of the residuals. The scatterplots show a high scattering over the whole biomass range for the MLR and SVR model while there is less scattering for the ANN approach. A remarkable scattering occurs between 0 t/ha to 20 t/ha for all three approaches which may result from ground signal interference or soil moisture, which is of great importance in peat swamp areas. The distribution of the residuals' frequencies depicts a high peak near zero in the SVR model, indicating a very accurate model in terms of validation. The distribution of the residuals of the MLR model is broader, showing a peak in the negative spectrum, but altogether there are more values in the positive interval, indicating an underestimation of AGB which is also denoted by the negative *ME*. The residuals of the ANN are distributed more consistently, featuring more values in the negative spectrum which indicates an overestimation of AGB.

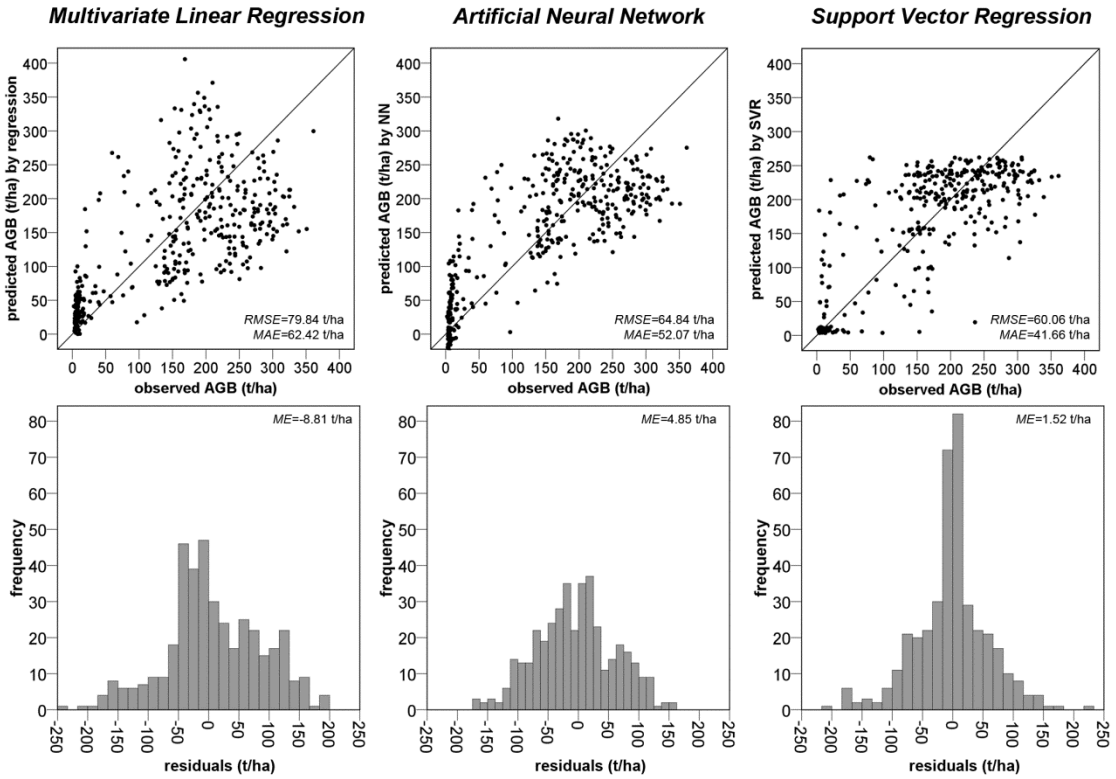

Figure IV-3: Results of the independent validation for estimating AGB with MLR (left), ANN (middle) and SVR (right) models (n=396). Scatterplots showing observed vs. predicted AGB values are depicted in the upper panels and histograms featuring the frequency of the residuals in the lower panels.

Figure IV-4 displays the spatial application of the different AGB estimation methods to the entire study area and the histograms of the respective AGB values up to a maximum of 600 t/ha. AGB values higher than 600 t/ha are assumed to overestimate the real biomass range in this area and were therefore excluded. Especially the MLR model predicts AGB values which are much higher than 600 t/ha (maximum: 3.21 Mt/ha). These values are beyond the saturation threshold of 600 t/ha which was evaluated in Englhart et al. (2011).

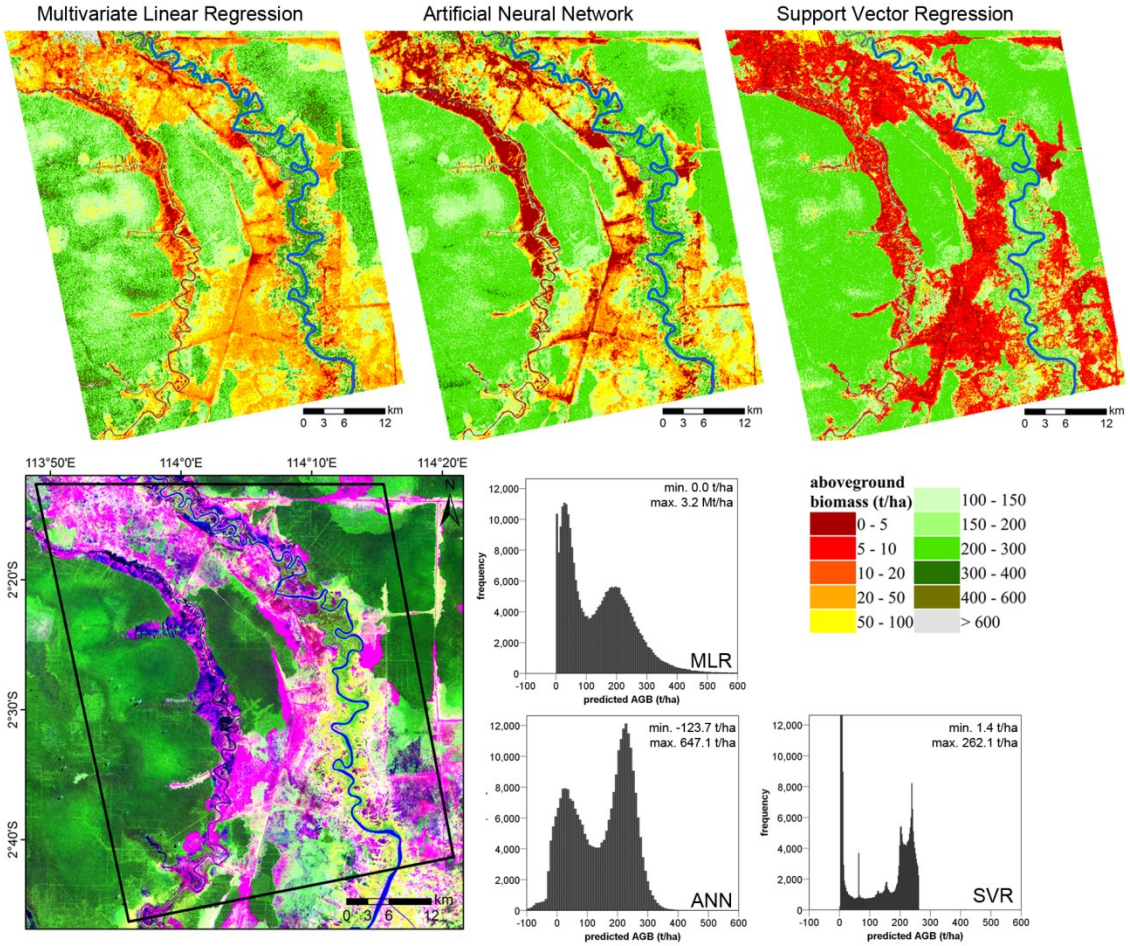

Figure IV-4: AGB maps showing the spatial application of the different AGB modeling approaches to 1 ha plots in comparison to a Landsat scene of 05/08/2007 (RGB: bands 543) indicating the study area. The histograms depict the frequencies of predicted AGB values within the biomass range lower than 600 t/ha.

The AGB map modeled by the ANN seems more homogenous and there are only very few overestimations up to 650 t/ha, but there are several underestimations up to -125 t/ha. AGB values lower than 0 t/ha are unrealistic and were assumed to be equal to 0 t/ha. The spatial application of the SVR model barely depicts any variation in the low (0 - 50 t/ha) or in the high biomass range (150 - 600 t/ha), whereby the maximum estimated AGB value of 262 t/ha is certainly a constraint, clearly indicating a saturation of the SVR. The spatial distribution of different degradation levels or forest types are hardly visible. In addition to the independent validation, AGB was estimated by the different approaches for an independent LiDAR transect (Table IV-3). Figure IV-5 shows the different AGB estimation in comparison to the LiDAR derived values along a

part of the transect. The transect is located over a burnt and degraded area and the biomass is therefore lower than in a pristine forest (only up to 170 t/ha). The area of the transect partly burnt in the years 2004, 2006 and 2009. The end of the transect (from kilometer 2.6 on) burnt in 2009 and the biomass is therefore very low.

Table IV-3: Validation results of a LiDAR transect which was not used for model calibration for estimating AGB from multi-temporal TerraSAR-X and ALOS PALSAR data (n=71). The coefficient of determination (r^2), root mean square error (RMSE), mean absolute error (MAE) and mean error (ME) are depicted.

estimation approach	r^2	*RMSE* [t/ha]	$RMSE_{rel}$ [%]	*MAE* [t/ha]	MAE_{rel} [%]	*ME* [t/ha]	ME_{rel} [%]
MLR	0.87	28.34	48.5	20.31	52.6	-6.30	-10.8
ANN	0.93	19.58	33.5	13.53	35.1	3.13	5.4
SVR	0.91	32.18	55.1	17.14	44.4	13.31	22.8

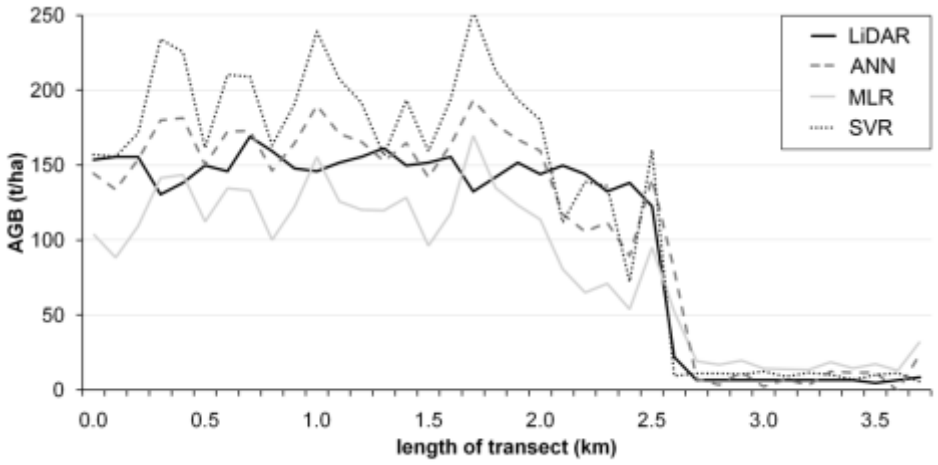

Figure IV-5: AGB comparison of different estimation approaches of a LiDAR transect which was not used for calibrating the models.

The validation errors indicate that the ANN outperforms the MLR and SVR model. Overall, one can state that the independent validation results are very good.

In the high biomass range, AGB is clearly overestimated by the SVR approach and underestimated by the MLR model (Figure IV-5). This is also indicated by a positive *ME* of the SVR and by a negative *ME* of the MLR model (Table IV-3).

AGB predicted by the ANN is the best approximation, as under- and overestimation is mostly balanced (Figure IV-5). The positive *ME* specifies a minor overall overestimation.

The low biomass range is clearly overestimated by the MLR and slightly overestimated by the SVR (Figure IV-5). Values modeled by the ANN are, again, the best approximation in the low biomass spectrum.

5. Discussion

This study compares the ability of MLR, ANN and SVR for modeling AGB from multi-temporal TerraSAR-X and ALOS PALSAR data.

The upscaling from field based AGB values using LiDAR measurements provided numerous AGB reference data. This approach presents not only a powerful basis for the modeling process but also leads to error propagation. An opportunity to reduce the source of error would be to collect enough in-situ AGB data within the study area distributed evenly over the whole biomass range which is very expensive, time-consuming and difficult to implement in remote tropical forests.

The independent validation results of the MLR model featured the lowest r^2 and the highest errors. The *ME* indicates that the real biomass is underestimated, while the spatial application to the entire study area partly results in extreme overestimations. When using MLR models to estimate AGB from SAR data, a saturation level is often specified. The calculation of the saturation threshold was conducted on the basis of the radiometric accuracy and a specific accuracy requirement. The saturation of the presented MLR model was determined at 600 t/ha for an accuracy requirement of 100 t/ha and at 300 t/ha for an accuracy requirement of 50 t/ha (Englhart et al. 2011). AGB values within an accuracy requirement of 50 t/ha are supposed to be accurate enough for the needs of REDD+, while AGB predictions within the 100 t/ha interval show the spatial distribution in the high biomass spectrum (Englhart et al. 2011).

The independent validation of the SVR model concludes that this is a superior method for calculating AGB featuring the lowest errors and highest r^2. In contrast, the spatial application resulted in mostly low (0 - 50 t/ha) and medium (150 - 250 t/ha) biomass values were estimated. The range in-between (50 - 150 t/ha) and the spatial variation is almost not represented. Potentially, this biomass range is not sufficiently incorporated within the training data for the needs of SVR models. The maximum estimated biomass

value (262 t/ha) denotes a saturation effect, which means that AGB estimations higher than this value cannot be differentiated. This saturation also affects the error measures; the error values are lower due to the low maximum AGB value. However, in total there is a larger difference between predicted and observed values.

The ANN method was the most appropriate for the estimation of AGB from multi-temporal SAR data. The different ranges of low and high biomass are clearly visible and there is no effect of saturation (predicted AGB values range from -124 t/ha to 647 t/ha). The estimations below zero clearly underestimate the real biomass, thus they are considered to be equal to 0 t/ha. The underestimation occurs in regions which are flooded or very wet. Despite the possible biomass range is supposed up to 600 t/ha, the estimation of 647 t/ha is considered to be feasible. The comparison with multispectral optical imagery (Landsat, RapidEye) and video material acquired during flight surveys suggests that the spatial distribution of AGB represents a good estimate of the real AGB (Figure IV-5). Biomass values of the entire area are mostly in the low biomass range (up to 50 t/ha) in deforested or burnt areas and in the high biomass range (150 - 600 t/ha) in previously logged and pristine forested areas. The transition between the low and high biomass range (50 - 150 t/ha, predominantly forest regrowth after fire impact) makes up only a small fraction of the total. A limitation of the ANN model is that it does not reveal the mathematical relationship between the SAR signals and AGB.

A comparison of methods is very valuable, as most studies assess only one method, making it difficult to compare various approaches using different data in diverse ecological environments (Lu 2006). Some previous studies already compared different methods to retrieve ecological parameters from remotely sensed data. ANN models were superior to regression models (Foody et al. 2003; Wijaya et al. 2010; Xie et al. 2009) or achieved similar results (Muukkonen et al. 2005). Other studies stated that SVR outperformed ANN (Camps-Valls et al. 2006) or also obtained similar results with a regression model (Monnet et al. 2011).

These findings are comparable to the results of this study, stating that the ANN outperformed the MLR model. In contrast to Camps-Valls et al. (2006), we found out that ANN performed better for large scale AGB estimations than SVR, even if the independent validation of the SVR model was more accurate. Unlike Monnet et al. (2011), this study reveals a better performance of the SVR compared to the MLR model.

Despite the constraints, the ANN approach is considered a superior method to retrieve AGB from multi-temporal TerraSAR-X and ALOS PALSAR data in tropical peat swamp forests in Indonesia and to be accurate enough to meet the requirements of REDD+ projects. An area-wide AGB estimation in that area is very important, as tropical peat swamp forests are difficult to assess on the ground and contain huge carbon stores which must be preserved. In general, estimating AGB with the 'direct' instead of the 'indirect' remote sensing approach provides information on the spatial distribution of the biomass and its variation. This information is very important, especially for the needs of REDD+, as AGB can vary extremely within one land cover class, making an indirect AGB estimation using single biomass values per calls rather vague.

6. Acknowledgements

The authors would like to thank the Japan Aerospace Agency (JAXA) for supplying ALOS PALSAR data within the PI project No. 211 as well as Infoterra GmbH and the German Space Agency (DLR) for providing TerraSAR-X data and their cooperation within the For-X Project (50 E705, PI: LAN0236). We gratefully acknowledge Andreas Rabe, Humboldt University of Berlin, for helping with the imageSVM tool.

V. Carbon stock monitoring of tropical forests on Borneo, Indonesia, and related REDD+ requirements

S. Englhart [a], J. Franke [b], V. Keuck [b], F. Siegert [a,b]

EARSeL-Springer Book "Land use and land cover mapping in Europe", submitted.

[a] *Biology Department II, GeoBio Center, Ludwig-Maximilians-University, Großhadener Str. 2, D-82152 Planegg-Martinsried, Germany*

[b] *Remote Sensing Solutions GmbH, Isarstr. 3, D-82065 Baierbrunn, Germany*

1. Introduction

Tropical forests store huge amounts of carbon, the majority (78%) in aboveground trunks, branches, and leaves as well as in belowground roots (22%) (Saatchi et al. 2011a). In addition, forested tropical peatlands accumulate carbon in belowground peat deposits which are sustained by intact forests. In Indonesia, approximately 55-58 Gt of carbon is stored belowground in peatlands and 18.6 Gt aboveground in forests (Baccini et al. 2012; Jaenicke et al. 2008; Koh et al. 2009). Peatlands are often drained, deforested or burned for industrial agricultural development such as the establishment of oil palm and pulp wood plantations, which causes massive carbon emissions that are released to the atmosphere (Hooijer et al. 2010).

Emissions from deforestation and forest degradation in Southeast Asia, including tropical peatland burning and oxidation amounted to 23% of total anthropogenic CO_2 emissions worldwide between 1997 and 2006 (van der Werf et al. 2009). Hooijer et al. (2012) estimated the carbon loss from converting peat swamp forests into agriculture to be on average 100 tCO_2 per hectare per year annualized over 25 years. Through these processes, Indonesia became one of the largest producers of CO_2 worldwide.

Considering these high emission rates, projects aiming at forest conservation offer good prospects for climate change mitigation in developing countries. One example is REDD+ which aims at reducing emissions from deforestation and forest degradation,

conservation of forest carbon stocks, sustainable management of forest land and enhancement of forest carbon stocks (Campbell 2009). REDD+ was approved at the United Nations Climate Change Conferences in 2009 and 2010, the year 2011 was the starting point for the development of a worldwide forest monitoring system. The system considers current technical capabilities to monitor greenhouse gas emissions and removals from deforestation, reforestation and degradation activities in forest land remaining forest land (GOFC-GOLD 2011). REDD+ intends for conditional payments to countries reducing emissions, and conditional payments from national levels to forest stewards reducing emissions (Campbell 2009). Implementation of REDD+ policies depends on accurate and precise estimates of emissions avoided at national scale. A nationwide monitoring is needed to prevent leakage within a country, where reduced deforestation or forest degradation could occur in one part of the country but increase in another through displaced activities (DeFries et al. 2007).

In May 2010, a contract between the Indonesian and Norwegian government was signed providing 1 billion USD for a cooperation on REDD+. A major component is a moratorium on new agricultural and logging licenses which aims to support Indonesia's goal of reducing national emissions by 26% until 2020 and to prepare Indonesia to draw payments from industrial nations via the REDD+ scheme (Sloan et al. 2012).

A crucial element for REDD+ is the estimation of current carbon emissions. The Intergovernmental Panel on Climate Change (IPCC) provides Guidelines for National Greenhouse Gas Inventories which refer to two basic inputs for calculating greenhouse gas inventories: activity data, which specifies the extent of deforestation, reforestation and forest degradation/enhancements in unit area, and emission factors, which describe emissions/removals of greenhouse gases per unit area (IPCC 2006). Uncertainties of both activity data and emission factors are an important element of greenhouse gas inventories to identify the contributions to the overall accuracy (Grassi et al. 2008). The guidelines include three different tiers which represent the level of methodological complexity: Tier 1 uses IPCC default values to estimate emissions, Tier 2 requires country specific carbon data, and Tier 3 is based on a detailed national inventory.

The most accurate way of aboveground biomass (AGB) and carbon stock retrieval using Tier 3 are forest inventories which use field based measurements (e.g. diameter at breast height (DBH), tree height, tree species specific wood density) to extrapolate the biomass on the basis of allometric equations (Brown 1997; Chave et al. 2005). The

carbon stock is generally derived from AGB estimates by assuming a carbon content of dry biomass of 50% (Goetz et al. 2009). Albeit this method provides very precise AGB values, it is time consuming, laborious, difficult to implement in remote areas and most importantly lacks information on the spatial variability (Lu 2006). Monitoring AGB by remote sensing is less accurate but the major advantage is the ability to generate spatially explicit and potentially 'wall-to-wall' carbon stock estimations in large and remote areas. Most approaches are based on an assessment of historic, current and future deforestation rates based on detectable changes in forest area using satellite or airborne data (Boettcher et al. 2009). The accuracy of AGB estimations depends on the size of the area and the quality of the remote sensing data. Moderate to coarse resolution data (e.g. MODIS) is normally used for global carbon stock estimation (Baccini et al. 2012) and medium resolution data (e.g. ALOS PALSAR) is usually selected for AGB estimations at national or regional scales (Englhart et al. 2012; Ryan et al. 2012). Monitoring systems that allow for credible measurements, reporting and verification (MRV) of forest carbon stocks and their changes in REDD+ project sites are among the most crucial elements for a successful implementation of REDD+.

Different approaches have been developed to assess AGB by remote sensing using additional forest inventory AGB data. The indirect approach is a simple way to retrieve a carbon stock map by linking a single AGB value (or a defined range, ideally derived from field inventories) determined for a specific vegetation type to a remote sensing based land cover map (Goetz et al. 2009). A major disadvantage of the indirect approach is the lack of information on the spatial variance of AGB within one land cover class.

A more sophisticated technique is the direct approach at which radiometric satellite measurements are calibrated to field based AGB measurements to derive a wall-to-wall AGB estimation map also indicating the spatial distribution of the carbon stock (Goetz et al. 2009). Examples using LiDAR, optical and SAR data for a direct estimation of AGB are described in the following paragraph.

LiDAR has the potential to assess the three-dimensional vertical structure of the vegetation in great detail and its use has increased for retrieving AGB (Koch 2010). Airborne sensors provide highly accurate AGB estimates in tropical forests (Asner et al. 2012; Kronseder et al. 2012; Treuhaft et al. 2010), but the associated large data volume and high costs usually limit a repetitive application. As an alternative, the first

spaceborne LiDAR system, the GeoScience Laser Altimeter System (GLAS) onboard NASA's Ice, Cloud and land Elevation Satellite (ICESat), has also proven to be valuable for AGB assessment in tropical forests (Baccini et al. 2012; Ballhorn et al. 2011; Helmer et al. 2009). However, with a footprint of about 65 m, the ICESat/GLAS sensor does not allow spatially continuous AGB maps.

Optical satellite images have been widely used to derive AGB in tropical regions using vegetation indices (Li et al. 2010; Zhang et al. 2009), spectral signatures (Avitabile et al. 2012; Baccini et al. 2008; Li et al. 2010; Tangki et al. 2008), image texture (Lu 2005; Nichol et al. 2011; Sarker et al. 2011; Wijaya et al. 2010), and spectral mixture analysis (SMA) (Soenen et al. 2010). Major constraints of using optical data for AGB estimation are the saturation of the signal in the high biomass ranges, the dependence on daylight, and the obstruction by clouds, which is a crucial point in tropical regions.

Active SAR systems can operate day and night while penetrating through haze, smoke, and clouds. The correlation of backscatter signal and biomass is mainly dependent on wavelength, polarization, and incidence angle. Longer wavelengths have been proven to be more useful for AGB estimation because of an increasing backscatter range with changing biomass (Lu 2006; Luckman et al. 1997) and a higher saturation level in regard to the biomass range (Englhart et al. 2011; Saatchi et al. 2011b).

In order to compare the performance of SAR and optical satellite data in their ability to directly estimate AGB, a case study was established in a tropical peat swamp forest area in Central Kalimantan, Indonesia. The potential of different approaches and data sources are demonstrated in the context of REDD+ requirements. The objectives of this case study are therefore (i) an evaluation of either different SAR frequencies and polarizations or spectral mixture analysis of multispectral RapidEye data to estimate AGB directly and (ii) a comparison of the direct and indirect AGB estimation method using the example of RapidEye data.

2. Methodology

2.1. Study area

The study area is located east of Palangka Raya, the capital of the province Central Kalimantan, on the island of Borneo, Indonesia (Figure V-1).

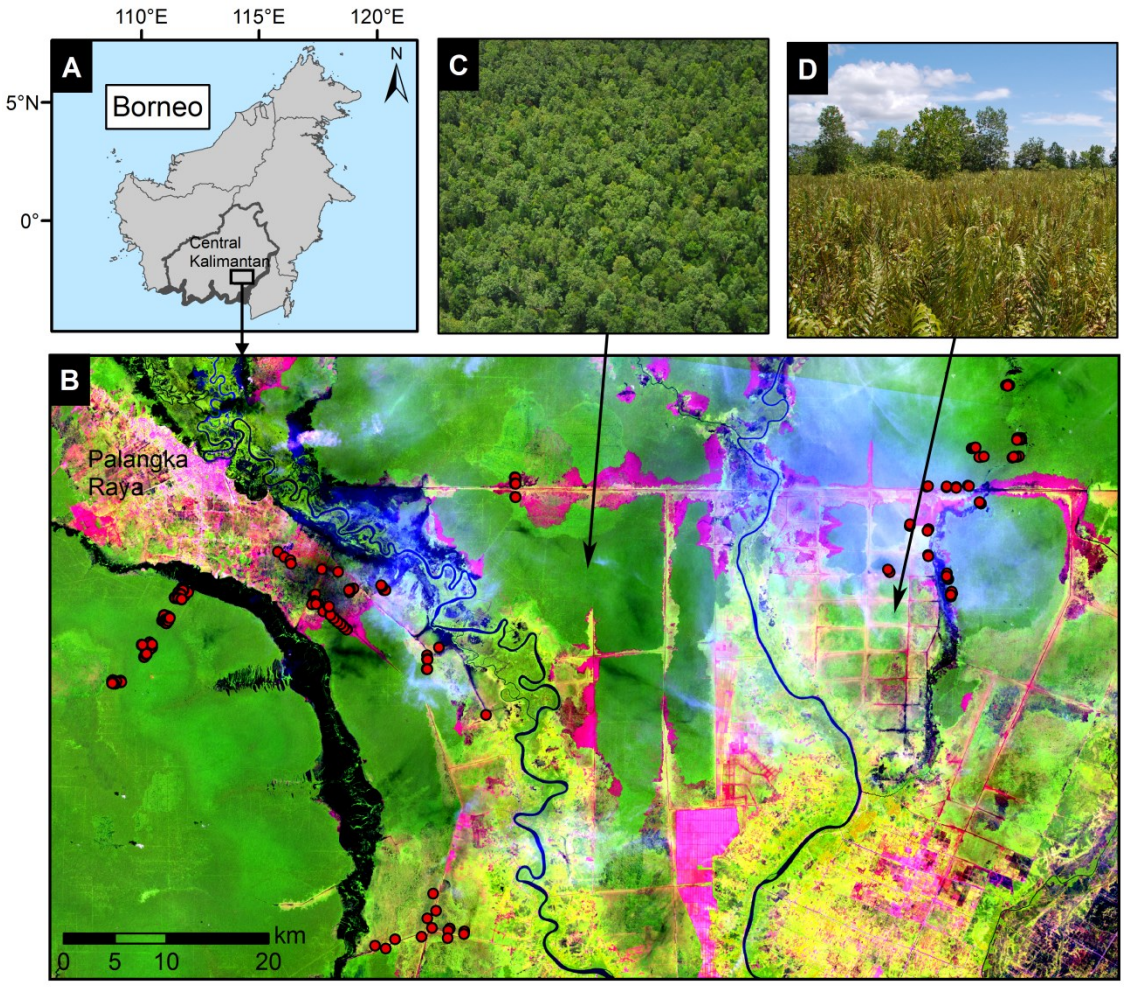

*Figure V-1: (**A**) Overview map of the study area in Central Kalimantan on Borneo. (**B**) Landsat ETM+ satellite image from 10/02/2010 (bands R:5, G:4, B:3) showing the study area. Field inventory locations are depicted in red. (**C**) shows an aerial photo of an intact forest and (**D**) depicts a degraded regrowing area (© F .Siegert, S. Englhart); typically locations are indicated by arrows.*

Peat swamp forest is the predominant vegetation type besides riparian forest, forest areas heavily degraded by fire (shrubs and regrowing forest) and seasonally flooded wetlands. The peatlands have been drained and deforested, mainly for agricultural development and plantations (Hooijer et al. 2010) and recurrent fire events destroyed approximately 50% of the forest cover in the past decade. The most severe impact was caused by the Mega Rice Project (MRP), conceptualized by the Indonesian government in 1995 in order to convert an area of one million hectare for rice cultivation through the construction of about 4,000 km of drainage and irrigation channels in peatlands (Boehm et al. 2004; Page et al. 2002).

2.2. Data

2.2.1. Field inventory data

Field inventory data was collected in the years 2008, 2010 and 2011. Forest inventory plots with different plot sizes were established in forested and regrowing areas (Figure V-1B depicts the plot locations).

For regrowing forests, a 20 m x 50 m rectangular plot was chosen and all trees within this area were recorded. For forests, three circular nested plots with radii of 4 m, 14 m, and 20 m were sampled. In each nest, trees of a certain DBH were measured depending on degradation intensity: 2 cm to 10 cm or 5 cm to 20 cm (within the 4 m radius), 10 cm to 20 cm or 20 cm to 50 cm (within 14 m radium), and greater than 20 cm or 50 cm (within 20 m radius).

Within the regrowing and forested plots, the following parameters were recorded: DBH, tree height, and species of all trees in order to estimate their wood density. Tree specific wood densities were derived from databases provided by Chudnoff (1984), World Agroforestry Centre (2011), and IPCC (2006). If the tree species could not be identified, an average specific wood density for Asian tropical trees of 0.57 Mg m^{-3}, was applied (Brown 1997).

AGB was calculated using a combination of allometric models from Hughes et al. (1999) for saplings (if DBH < 5 cm and height ≤ 1.3 m) or trees (if DBH < 5 cm and height > 1.3 m) and Chave et al. (2005) for moist tropical forest stands including DBH and tree height (if DBH ≥ 5 cm and height > 1.3 m).

Altogether 107 plots were sampled, 48 plots in regrowing vegetation ranging from 0.0 t/ha to 19.6 t/ha and 59 plots in forested areas ranging from 8.7 t/ha to 458.4 t/ha.

2.2.2. SAR data

X-, C- and L-band data in HH and HV polarizations were investigated for their ability to estimate AGB. Four TerraSAR-X ScanSAR HH polarized images with a pixel spacing of 8.25 m and an incidence angle of 34.2° (acquired on: 11/07/2011, 22/07/2011, 13/08/2011, and 24/08/2011) and three RADARSAT-2 standard mode HH and HV polarized images with a pixel spacing of 8.00 m and an incidence angle of 36.6° (22/07/2011, 15/08/2011, and 08/09/2011) were analyzed. In addition, six ALOS PALSAR fine beam HH and HV polarized images with a pixel spacing of 12.5 m and an incidence angle of 38.8° were evaluated, as two different paths were necessary to

cover the whole study area (path 421: 30/06/2010, 15/08/2010, 30/09/2010; path 422; 17/07/2010, 01/09/2010, 17/10/2010). It is important to note that all images were acquired during the dry season (May to October) to minimize any impact of rainfall and soil moisture.

The preprocessing of the SAR images included standard radiometric calibration for sigma naught (Englhart et al. 2011; Fritz 2009; Luscombe 2009; Richter 1997; Shimada et al. 2009), frost speckle filtering with a moving window of 7x7 pixel, and co-registration.

Multi-temporal backscatter coefficients were used because averaging backscatter in time reduces speckle without losing spatial resolution. And in a previous study we found that multi-temporal backscatter values were superior to mono-temporal values for estimating AGB (Asner et al. 2009; GOFC-GOLD 2011; Souza et al. 2005).

2.2.3. Multispectral RapidEye imagery

A RapidEye scene was used to analyze the potential of estimating AGB using spectral mixture analyses (SMA). RapidEye data has a pixel resolution of 5 m and contains five spectral bands. An image recorded on 21/06/2010 was preprocessed including an geometric and atmospheric correction (Adams et al. 1986; GOFC-GOLD 2011). SMA have a high potential to derive forest parameters from remote sensing data (Mundt et al. 2007; Williams et al. 2002). Forests degraded by logging or fire are characterized by mixed pixels due to the reflectance from green vegetation (GV), non-photosynthetic vegetation (NPV), soil, shade etc., within the area of on image element (pixel). The advantage of SMA is that sub-pixel components can be detected, whereby continuous values of sub-pixel abundances of components are derived. A special type of SMA, the Mixture Tuned Matched Filtering (MTMF) was applied. A detailed description of SMA and MTMF is provided by Adams et al. (1986), Williams et al. (2002), and Mundt et al. (2007). The result of the MTMF is a grey-scale matched filtering (MF) fraction image representing the estimated relative degree to which each pixel matches the reference spectrum (Williams et al. 2002). The matched fractions derived from the RapidEye image were scaled to values between 0 and 1, where 1 indicated a perfect match of the pixel spectrum to the reference spectrum.

2.3. AGB estimation

2.3.1. Direct AGB estimation using SAR and multispectral data

The relationship between SAR backscatter or RapidEye matched fractions and AGB was analyzed using spatially averaged signals over a grid with a cell size of 40 m x 40 m. This size was chosen as it is similar to the size of the biggest nested field plot (radius 20 m). Due to the saturation in high biomass ranges, only field data smaller than 300 t/ha were used for the regression modeling. The AGB field data was randomly split up to be used for training (85% of all data) and validating (15%) the AGB models. For the SAR images, all 98 AGB reference samples were applicable, while for RapidEye only 53 AGB samples were available due to clouds and area coverage. In a first step, the relationship of each single input signal and AGB was analyzed. Based on the resultant dependencies, a combined regression model was tested. Therefore, a least-square multivariate linear regression was conducted using exponential values of either SAR backscattering coefficients or RapidEye derived matched fractions of GV, soil and NPV.

2.3.2. Comparison direct vs. indirect AGB estimation using multispectral imagery

A comparison of direct and indirect AGB estimation was conducted on the basis of RapidEye. The direct AGB estimation is based on the SMA fractions and the indirect AGB is determined by a land cover classification linking a single AGB value derived from field inventory data to each land cover class. The RapidEye land cover classification is based on the scene from 21/06/2010 and a object based classification approach was used. A hierarchical rule set defining the different classes was applied using spectral, spatial, geometric, thematic or topologic criteria.

In total, eleven land cover classes were defined whereby only six are relevant for carbon stock comparison (primary and secondary peat swamp forest, riparian forest/agroforestry, bush/shrubs/regrowth, grassland/fern/agriculture, recently burned/sparse regrowth). For a quantitative accuracy assessment of the land cover classification, 75 sample plots, mapped according to the LCCS (land cover classification system) standard and recorded with differential GPS, were evaluated.

3. Results

3.1. Direct AGB estimation using SAR and multispectral data

The relationship between SAR backscattering coefficients of X-, C- and L-band data or RapidEye spectral unmixed fractions was investigated separately. The relationships between SAR backscatter signals and RapidEye fractions are depicted in scatter plots in Figure V-2. A correlation between SAR backscatter and AGB was only found with TerraSAR-X HH and ALOS PALSAR HV polarized data (Figure V-2). Two of the field inventory plots were located in a freshly burned area and are visible in the ALOS PALSAR HV polarized scatter plot (Figure V-2, ALOS PALSAR HV circle). Trunks of dead trees scattered on the ground cause double bounce backscatter and thus high backscatter signals. RADARSAT-2 HH and HV and ALOS PALSAR HH polarized backscatter showed no correlation to AGB. All investigated RapidEye fractions show a correlation to AGB. Different curve progressions were examined, but the exponential one yielded in all cases the best results. The exponential dependency is also linked to saturation in higher biomass ranges as the slope flattens in higher biomass ranges. The saturation effect is visible in the scatter plots depicted in Figure V-2, showing similar backscatter or fraction values from approximately 100 t/ha.

On the basis of the exponential dependencies, a multivariate linear regression using exponential values from either the SAR signals or the RapidEye matched fractions was also analyzed. Table V-1 depicts the regression and independent validation results of all investigated relationships. The multivariate regression using either SAR backscatter coefficients or RapidEye matched fractions turned out to be more accurate for AGB estimation than using only a single variable (Table V-1). A regression model which combed SAR backscatter and RapidEye fractions was also evaluated but the achieved accuracy was not higher than the multivariate RapidEye regression model and was therefore not further analyzed. The independent validation demonstrates that AGB derived from RapidEye SMA fractions is more accurate, resulting in higher coefficients of determination (r^2) and lower root mean square errors (*RMSE*). The multivariate SAR AGB model was more accurate than the single variable TerraSAR-X or ALOS PALSAR model in terms of the independent validation. The multivariate RapidEye model achieved a higher r^2 during the regression modeling, but the results of the independent validation resulted in slightly lower r^2 and slightly higher *RMSE* than the

GV and soil fraction model. The NPV model is the least accurate model of the RapidEye matched fractions with a remarkably high *RMSE*.

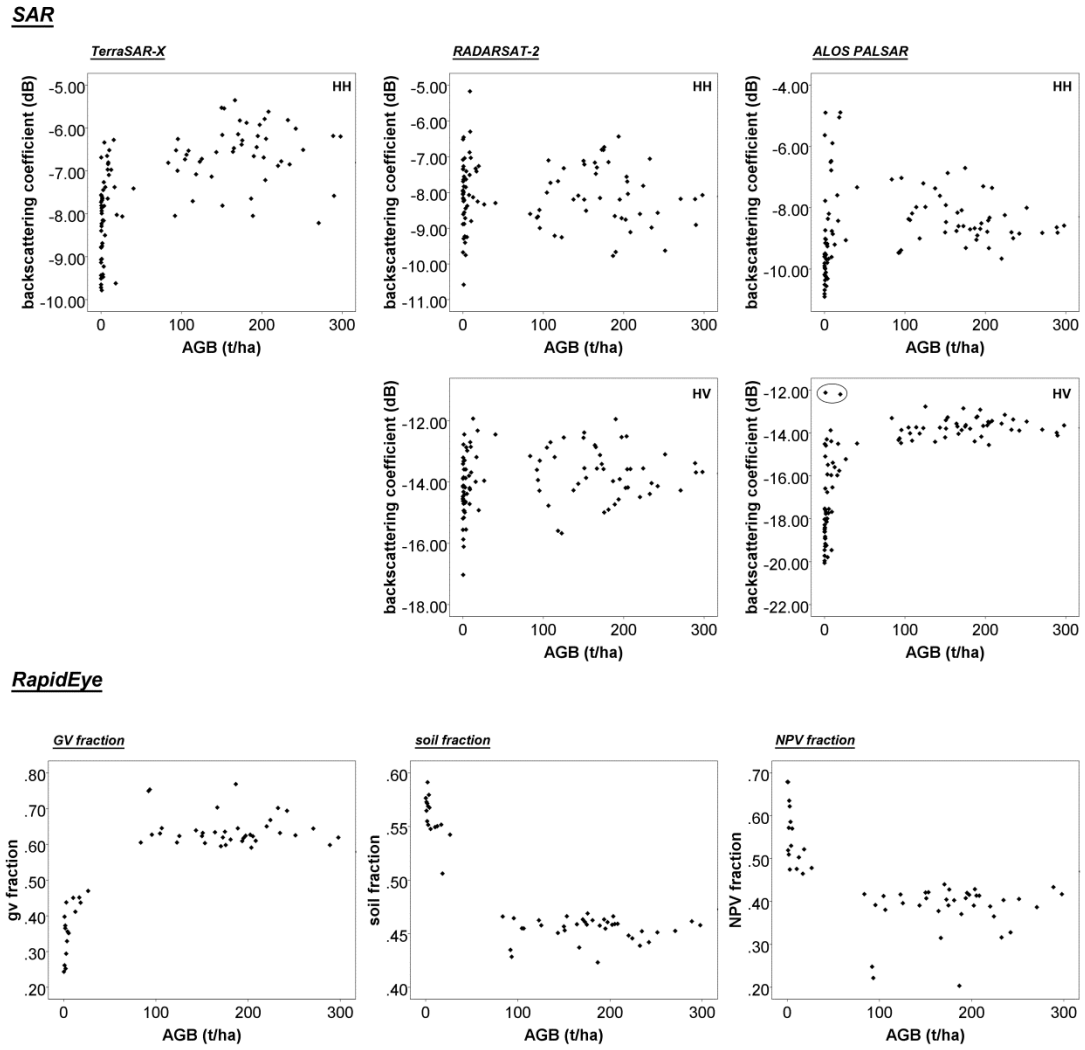

Figure V-2: Scatter plots showing AGB versus SAR backscatter signal of TerraSAR-X, RADARSAT-2 and ALOS PALSAR (upper panel: HH polarization, middle panel: HV polarization; n=98) or RapidEye GV, soil, and NPV fraction (lower panel; n=53).

Table V-1: Results of regression modeling (reg.) and subsequent independent validation (val.) on the basis of TerraSAR-X HH and ALOS PALSAR HV polarized data (n=98) or RapidEye GV, soil, and NPV fractions (n=53).

Input data	r^2 **(reg.)**	r^2 **(val.)**	***RMSE*** **[t/ha]**	***RMSE*** **[%]**
TerraSAR-X	0.51	0.30	81.71	110%
ALOS PALSAR	0.68	0.69	63.77	86%
TerraSAR-X & ALOS PALSAR	0.68	0.50	60.92	82%
RapidEye GV	0.86	0.86	37.11	37%
RapidEye soil	0.89	0.82	38.11	38%
RapidEye NPV	0.70	0.87	67.87	67%
RapidEye GV & soil & NPV	0.92	0.83	44.17	44%

The validated regression models were applied to a 1.893 ha test area (Figure V-3). Biomass estimations are shown in aggregated classes from 0 t/ha (dark red) to 300 t/ha (dark green). Estimations exceeding 300 t/ha appear in dark green and are assumed to be equal to 300 t/ha due to the saturation effect. TerraSAR-X performed better in low biomass ranges and worse in high biomass ranges and ALOS PALSAR showed opposite results. Due to double bounce on fresh burned scars, ALOS PALSAR derived AGB clearly overestimates biomass in these areas (see Figure V-3 arrow). AGB estimations derived from the combined TerraSAR-X and ALOS PALSAR regression model are higher in the low biomass range than derived from either TerraSAR-X or ALOS PALSAR. AGB of burned areas is also overestimated by the combined TerraSAR-X and ALOS PALSAR model due to the double bounce of the ALOS PALSAR HV polarized signal.

AGB estimated by RapidEye data is clearly affected by clouds which cover 12.8% of the study area. AGB estimations based on GV and NPV fractions are very similar. AGB predicted by soil fractions is overestimated in burned areas, but apart from that, similar to GV and NPV estimated AGB. AGB derived from the multivariate RapidEye model is predicted to be higher in the low biomass ranges than estimated by the single variable fractions model. In burned areas, AGB is again overestimated.

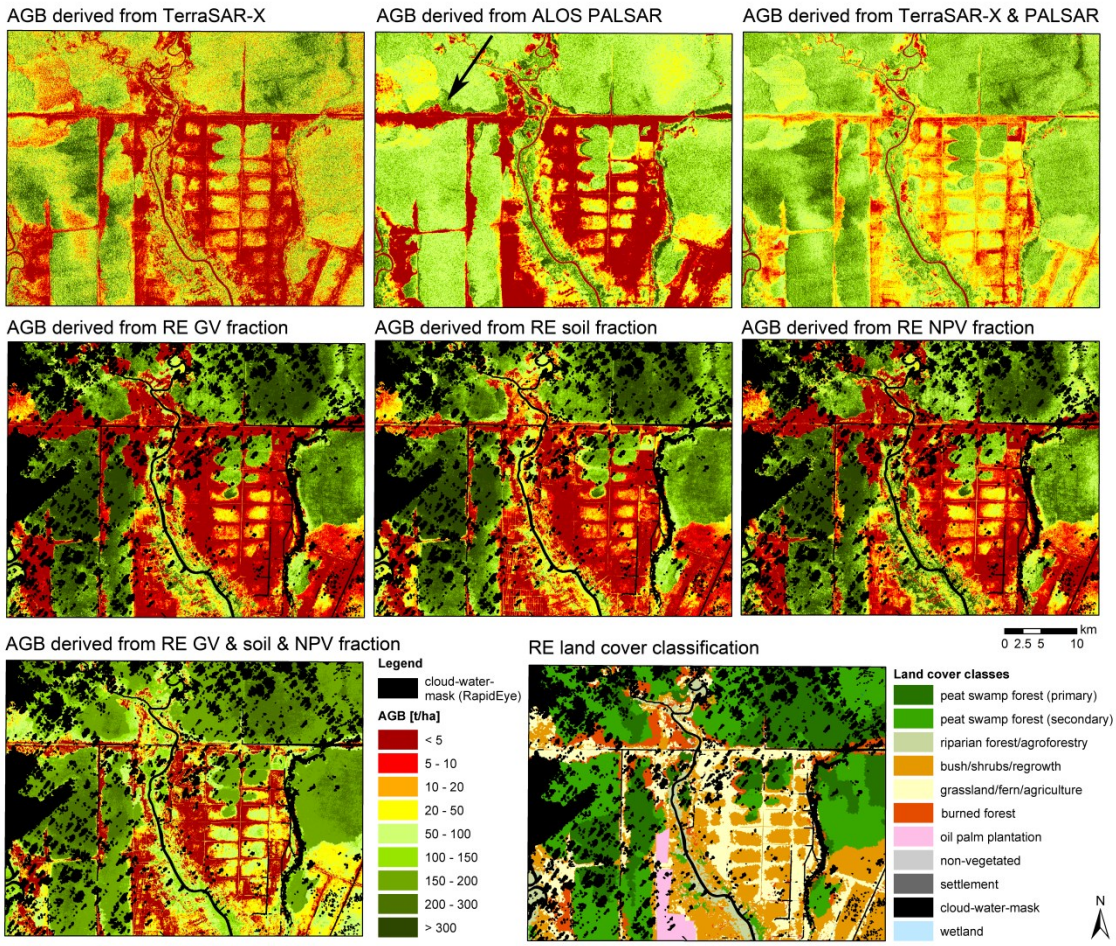

Figure V-3: Direct estimated AGB maps of the different regression models. A detailed RapidEye (RE) land cover classification of 21/06/2010 is shown for a comparison to the indirect AGB estimation method for which this map was used (example given in Figure V-4).

3.2. Comparison direct vs. indirect AGB estimation using multispectral data

The AGB directly estimated by the multivariate RapidEye model was compared to the indirectly estimated AGB using a detailed RapidEye land cover classification (Figure V-3) with an overall accuracy of 87.8%. AGB was either estimated by the multivariate RapidEye model (direct approach) or each land cover class was linked with a single value derived from field inventory data (indirect approach). Table V-2 depicts the median and the standard deviation AGB value for each land cover class. The number of 40 m x 40 m grid cells used for averaging of estimated AGB values (direct approach) or used field inventory data (indirect approach) is given in brackets. Every predicted AGB value within one land cover class was used for the calculation of the direct AGB mean

value. The mean AGB value of the indirect approach was calculated on the basis of all available field inventory data within each class. Two additional field inventory plots of riparian forest which were located outside of the study area were used because no field inventory plot was located inside the study area. The directly estimated AGB of primary and secondary peat swamp forest is similar (196.7 t/ha and 183.1 t/ha, respectively) with a relatively low standard deviation (25.2 t/ha and 26.7 t/ha) whereas the indirectly estimated AGB values have a higher difference (220.2 t/ha and 178.4 t/ha) with a higher standard deviation (73 t/ha and 73.3 t/ha) although the number of field inventories is much lower than the number of direct AGB estimations. The field inventory values indicate a high biomass variability within these two classes. AGB of riparian forest/agroforestry is difficult to compare, as only two field inventory plots were available which were both located in riparian forest outside of the study area. Agroforestry is not included in the field data. Agroforestry and riparian forest cannot be differentiated in this region using RapidEye for the land cover classification and were therefore combined. These facts may explain the high difference between directly and indirectly estimated AGB (110.7 t/ha and 294.2 t/ha) of riparian forest/agroforestry. The class bush/shrubs/regrowth shows higher AGB values with a higher variability (indicated by a higher standard deviation) in the direct method (37.7 t/ha, std dev: 33.1 t/ha) compared to the indirect approach (12.6 t/ha, std dev: 8.3 t/ha). It is assumed that the biomass variability of this class is not correctly represented by three field inventory plots. AGB of the class grassland/fern/agriculture was estimated very similar by the direct and indirect method (3.8 t/ha and 3.3 t/ha) but there is a higher standard deviation in the direct AGB estimations. AGB on recently burned/sparse regrowth areas is extremely overestimated by the direct approach which is also indicated in Figure V-3. Figure V-4 depicts an area of active logging showing the direct and indirect AGB estimation, the land cover classification used for the indirect AGB estimation and the true colored RapidEye image. The narrow logging tracks (2 m to 4 m wide) are clearly visible within the RapidEye scene (purple color) and the biomass loss from logging is indicated in the direct AGB map. The land cover classification does not differentiate different levels of degradation.

Table V-2: Comparison of directly and indirectly estimated AGB median and standard deviations (std) for different land cover classes. AGB values are either derived from a direct approach using SMA fractions or from an indirect approach by linking average field biomass values to each land cover class. The number of 40 m x 40 m grid cells used for averaging AGB estimations (direct approach) or field inventory data (indirect approach) are given in brackets.

AGB (t/ha) *Std (t/ha)*	peat swamp forest (primary)	peat swamp forest (secondary)	riparian forest/ agro-forestry	bush/ shrubs/ regrowth	grassland/ fern/ agriculture	recently burned/ sparse regrowth
direct	**196.7**	**183.1**	**110.7**	**37.7**	**3.8**	**87.7**
	25.2	*26.7*	*27.6*	*33.1*	*30.7*	*35.2*
	(n=183,435)	(n=255,159)	(n=25,371)	(n=187,209)	(n=143,331)	(n=45,238)
indirect	**220.2**	**178.4**	**294.2**	**12.6**	**3.3**	**0.7**
	73.0	*73.3*	*36.7*	*8.3*	*10.4*	*8.4*
	(n=15)	(n=24)	(n=2)	(n=3)	(n=5)	(n=6)

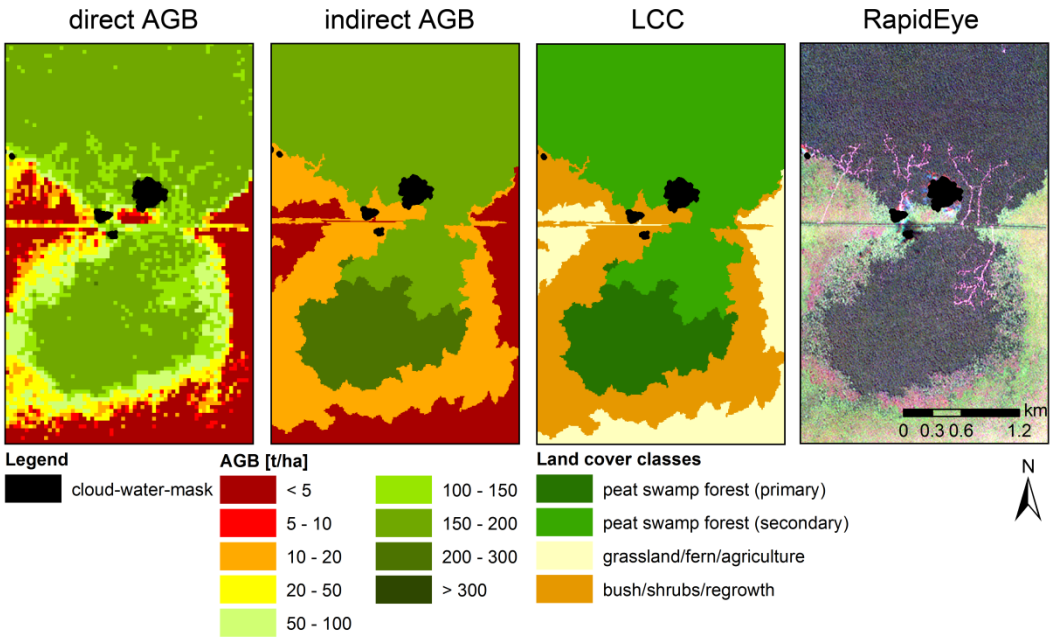

Figure V-4: Example of a logging area showing direct and indirect AGB estimations, RapidEye land cover classification (LCC) used for the indirect AGB estimation and the true color RapidEye scene from 21/06/2010.

4. Discussion

Different SAR frequencies and polarizations and RapidEye fractions were analyzed for their ability to predict AGB. The most accurate SAR AGB regression model is based on a multivariate TerraSAR-X HH and ALOS PALSAR HV model. The combined RapidEye matched fraction model achieved a higher accuracy. Combining RapidEye matched fractions and SAR backscatter was not found to be useful for AGB estimation, because a higher accuracy than the multivariate RapidEye fraction model could not be achieved. Both multivariate SAR and RapidEye AGB models overestimate AGB in recently burned areas (three years and less after the fire event). The combined TerraSAR-X and ALOS PALSAR AGB model is negatively influenced by double bounce from the ALOS PALSAR signal occurring in fresh burned areas (see Figure V-2 circle and Figure V-3 arrow). The RapidEye fraction model is affected by high AGB estimations of the soil fractions in burned areas (Figure V-3). The soil fraction is relatively low in these areas due to the large amount of NPV (dead trees and trunks, standing and lying) and GV (rapid regrowth of young trees, fern and bushes). The acquisition of RapidEye imagery is hampered by frequent cloud cover occurring in this part of the humid tropics. For this reason it is very difficult to produce repetitive AGB maps and ensure area coverage, which can only be overcome by very short repetition cycles of acquisitions. The combined SAR model is not as accurate as the RapidEye AGB estimation, but SAR is able to penetrate clouds, smoke and haze and repetitive area coverage can be achieved. Since the SAR signal is influenced by water, it is very important to use multi-temporal SAR data acquired during the dry season to minimize any impact of precipitation or soil moisture.

A further crucial point is the AGB field reference dataset. The range between 20 t/ha and 100 t/ha is underrepresented in the reference dataset (Figure V-2) as it is difficult to access these areas on the ground in the study area. On the one hand, regrowing areas contain mostly AGB values lower than 20 t/ha due to recurrent fire events. If a forest area has burned once, the risk of a repeated fire increases dramatically (Langner et al. 2009). On the other hand, logged over or degraded forest areas mostly contain AGB higher than 100 t/ha. To improve the AGB estimation models, it is necessary to expand the AGB reference dataset representing the whole biomass range.

The most accurate direct AGB model, based on multivariate RapidEye fractions, was compared to indirect estimated AGB using a detailed RapidEye land cover classification. Due to our long-term experience in the study area, it is assumed that the real biomass variability of primary peat swamp forest is not correctly described by the direct approach which results from the saturation effect in high biomass ranges. AGB loss caused by severe degradation, e.g. intense selective logging, is visible in the direct estimated AGB map (Figure V-4). AGB of bush/shrubs/regrowth and grassland/fern/agriculture is estimated very accurate. The AGB of recently burned/sparse regrowth areas was extremely overestimated, due to low soil fractions caused by rapid regrowth and large quantities of dead wood debris. Considering these results, a combination of direct and indirect estimated AGB appears to be the most promising approach. Forest areas with high AGB values, such as primary peat swamp forest and recently burned/sparse regrowth areas, are suggested to be estimated indirectly, whereas areas with low AGB values such as secondary peat swamp forest, riparian forest/agriculture, bush/shrubs/regrowth and grassland/fern/agriculture via a direct approach.

Using a combination of direct and indirect AGB estimations based on remote sensing and detailed field inventory data meets the Tier 3 definition of the IPCC guidelines, which describes the most complex methodological level of AGB estimation (IPCC 2006). The combined approach of direct and indirect AGB estimation overcomes the problem of saturation in higher biomass ranges. It has still to be proven if the AGB of areas that experienced low impact degradation can be differentiated from secondary forest despite the saturation occurring in high biomass ranges.

In general, LiDAR provides the most accurate AGB estimation due to the information that can be obtained on the vertical structure and height of the vegetation, but LiDAR measurements are mostly spatially limited. In contrast, the presented approach based on SAR and multispectral is very suitable for large scale sub national and national AGB carbon stock monitoring.

Nevertheless, due to the challenge to monitor carbon stocks and its changes without gaps, with low uncertainties and defined time intervals within REDD+ requirements, it is advantageous to use all available data and to combine different approaches.

5. Acknowledgements

The authors would like to thank the German Space Agency (DLR) and Canadian Space Agency (CSA) for providing TerraSAR-X and RADARSAT-2 data within the SOAR-DLR initiative (ID 5035) as well as the Japan Aerospace Agency (JAXA) for supplying ALOS PALSAR data (PI project No. 211). RapidEye data was provided by the German Aerospace Center (DLR) via the RESA - RapidEye Science Archive with funds from the Federal Ministry of Economics and Technology, (proposal no 267). Special thanks to Suwido Limin and his team from the Centre for International Co-operation in Management of Tropical Peatland (CIMTROP) in Palangka Raya for the logistical support during the field surveys. Furthermore, we acknowledge FAUNA & FLORA International (FFI) for providing aboveground biomass data of riparian forests.

VI. Quantifying dynamics in tropical peat swamp forest biomass with multi-temporal LiDAR datasets

S. Englhart [a], J. Jubanski [b], F. Siegert [a,b]

Manuscript in preparation for Remote Sensing.

[a] *Biology Department II, GeoBio Center, Ludwig-Maximilians-University, Großhadener Str. 2, D-82152 Planegg-Martinsried, Germany*

[b] *Remote Sensing Solutions GmbH, Isarstr. 3, D-82065 Baierbrunn, Germany*

1. Abstract

Tropical peat swamp forests in Indonesia store huge amounts of carbon and are responsible for a large proportion of carbon emissions every year due to forest degradation and deforestation. These forest areas are in the focus of REDD+ projects which require an accurate monitoring of their carbon stocks or aboveground biomass (AGB). Our study objective was therefore to evaluate multi-temporal LiDAR measurements of a tropical forested peatland area in Central Kalimantan on Borneo for quantifying canopy height and AGB dynamics with a special focus on unaffected, selective logged and burned forests. More than 11,000 ha were surveyed with airborne LiDAR in 2007 and 2011. The comparability of these datasets was examined and canopy height models were created. AGB regression models were developed on the basis of field inventory measurements and LiDAR derived height histograms for 2007 (r^2=0.77, n=79) and 2011 (r^2=0.81, n=53), taking the different point densities into account. High resolution multispectral imagery was used to identify changes in the peat swamp forests. Unaffected forests accumulated on average 20 t/ha AGB with a canopy height increase of 2.3 m over the four year time period. Selective logged forests experienced an average AGB loss of 55 t/ha within 30 m and 42 t/ha within 50 m of detected logging trails, although the canopy height increased by 0.5 m and 1.0 m, respectively. Burned forests lost 92% of the initial biomass. These results demonstrate

the great potential of airborne LiDAR surveys to precisely quantify even small scale AGB and canopy height dynamics in remote tropical forests, thereby featuring the needs of REDD+.

Keywords: aboveground biomass (AGB), Borneo, canopy height, carbon, change, LiDAR, multi-temporal, REDD+ (reducing emissions from deforestation and forest degradation), tropical peat swamp forest.

2. Introduction

Considering the global climate change, efforts are being made to reduce global greenhouse gas emissions. One example of such a climate change mitigation mechanism is REDD+ which aims at reducing emissions from deforestation, forest degradation and the role of conservation, sustainable management of forests and enhancement of forest carbon stocks (Campbell 2009). In the focus of REDD+ projects are tropical forests which are huge carbon reservoirs comprising 40% of the terrestrial carbon (FAO 2009; Page et al. 2009a). Tropical peatlands accumulate additional carbon in thick belowground peat deposits which are sustained by intact forests on top of it. The largest known tropical peat deposits occur in Southeast Asia, especially in Indonesia where 55 - 58 Gt of carbon is stored belowground and 18.6 Gt aboveground in forests (Baccini et al. 2012; Jaenicke et al. 2008; Page et al. 2011). Deforestation, forest degradation and peatland degradation in Southeast Asia produce considerable carbon emissions (Hooijer et al. 2012; Murdiyarso et al. 2010). Between 1997 and 2006, these activities were responsible for 23% of the total anthropogenic CO_2 emissions worldwide (van der Werf et al. 2009). Particularly, Indonesia became one of the largest carbon emitters worldwide, largely caused by degradation and deforestation of its peatland areas and forests due to large-scale agricultural development and exploitation of forest timber resources (Miettinen et al. 2012). Once the forest is degraded, e.g. through logging activities, the fire vulnerability increases (Miettinen et al. 2012; Siegert et al. 2001). As a result of these activities and the resulting emission rates, Indonesia became a prime target for REDD+ projects. Norway and Indonesia concluded a landmark deal which includes a payment to Indonesia up to one billion USD for forest conservation and slowing down deforestation and greenhouse gas emission rates.

Although, Indonesia agreed to halt the license of new logging concessions (on peatlands), large parts of selective logged forests are excluded from this moratorium which means that logged forests are highly vulnerable to re-logging and conversion to plantations (Edwards et al. 2012).

It is important to distinguish between managed or legal and unplanned or illegal selective logging. Managed logging constructs extensive infrastructure, for example substantial logging roads, railways along which the logs are being transported, and landing facilities. In contrast, illegal logging operations have no budget and equipment to establish regular roads or railways and their access tracks into the forest are limited. Illegal logging trails rather follow natural features, such as streams, drainage channels or abandoned logging tracks, and their spatial pattern is clearly different to that of straight extensive infrastructure of legal logging operations (Boehm et al. 2004). In Central Kalimantan, authorized and illegal logging increased in the 1990s as a direct result of the Mega Rice Project (MRP) which was initiated by the Indonesian government in 1995. The objective was to convert one million hectare of forest for rice cultivation. For this purpose, about 4,000 km of drainage and irrigation channels were excavated into the peatlands which allowed access into previously highly inaccessible peat swamp forests. Active illegal logging, which causes vast forest degradation, still takes place in Central Kalimantan's forests, even if no new logging concessions are granted. The level of degradation is dependent on the forest type and its accessibility. On Borneo, dipterocarp forests provide easy access due to the firm ground and are therefore often affected by logging using bulldozers (Berry et al. 2010; Pinard et al. 1996). In contrast, the access for heavy machinery is restricted to peat swamp forests due to the soft ground (Whitmore 1984). Hence, peat swamp forests which often contain high densities of valuable timer are logged by human power and the logs are mainly transported on nearby water courses. This way of logging is much less destructive than mechanized logging occurring in dipterocarp forests (Felton et al. 2003).

Monitoring forest degradation and deforestation is a crucial component of REDD+ projects. In general, forest carbon stocks are derived from aboveground biomass (AGB) by assuming a carbon content of 50% (Goetz et al. 2011). The most effective monitoring is based on satellite or airborne observations due to the high inaccessibility of the forests (Gibbs et al. 2007). As no remote sensing instrument can directly measure AGB, field inventory measurements are mandatory for both calibrating and validating

spatial estimations of AGB (Goetz et al. 2011). Especially the use of LiDAR (light detection and ranging) measurements has rapidly evolved in the last years due to the ability to precisely quantify the vertical structure of the vegetation and forest attributes such as canopy height distribution, tree height, and crown diameter (Duncanson et al. 2010; Gleason et al. 2011; Jung et al. 2012; Vincent et al. 2012). Particularly forest carbon stocks can be monitored with high accuracy (r^2=0.75, *RMSE*=20 t/ha and r^2= 0.83, *RMSE*=21%) without the constraint of saturation in high biomass ranges (Ballhorn et al. 2011; Kronseder et al. 2012). Multi-temporal LiDAR measurements offer tremendous potential for REDD+ projects. It is possible to detect small scale changes in the canopy height or AGB because height and intensity metrics have been proven to be reproducible (Bater et al. 2011; Vepakomma et al. 2008). For example, Dubayah et al. (2010) conducted a multi-temporal LiDAR study in Costa Rica and proved that old growth forests have a slower height growth rate (-0.33 m ± 4.09 m) compared to secondary forests (2.08 m ± 3.71 m) and accumulate therefore less biomass per hectare per year (0.3 t/ha y^{-1} compared to 3.6 t/ha y^{-1}).

The primary objective of this study was to utilize multi-temporal LiDAR and field inventory data to predict AGB dynamics in tropical peat swamp forests in Central Kalimantan on Borneo, Indonesia. The study site was surveyed in 2007 and 2011 and the comparability of both acquisitions was examined. Canopy height models (CHMs) were created and AGB regression models were developed on the basis of field inventory measurements. Changes in canopy height and AGB accumulation or loss during this four year interval were quantified with a special focus on undisturbed, selective logged and burned peat swamp forests.

3. Materials and Method

3.1. Study site

The study area is located east of Palangka Raya, the capital of the province Central Kalimantan, on the island of Borneo, Indonesia (Figure VI-1). The predominant vegetation type is peat swamp forest which has been under severe anthropogenic pressure for the last three decades, mainly through timber extraction and agricultural conversion (Boehm et al. 2004; Hooijer et al. 2010). The most severe impact was

caused by the MRP and the resulting degradation lead to recurrent fires which destroyed approximately 50% of the forest cover in the past two decades (Miettinen et al. 2012).

Another driver of forest degradation is illegal selective logging which causes small scale impacts in the forest canopy. Valuable trees are felled, cut into appropriate lengths and then dragged along narrow skid trails to the nearest river or canal where they are transported away.

The study area was legally logged during the 1980s and 1990s, thereby creating extensive infrastructure. Railways were built to grant access to the highly inaccessible peat swamp forests (Figure VI-2).

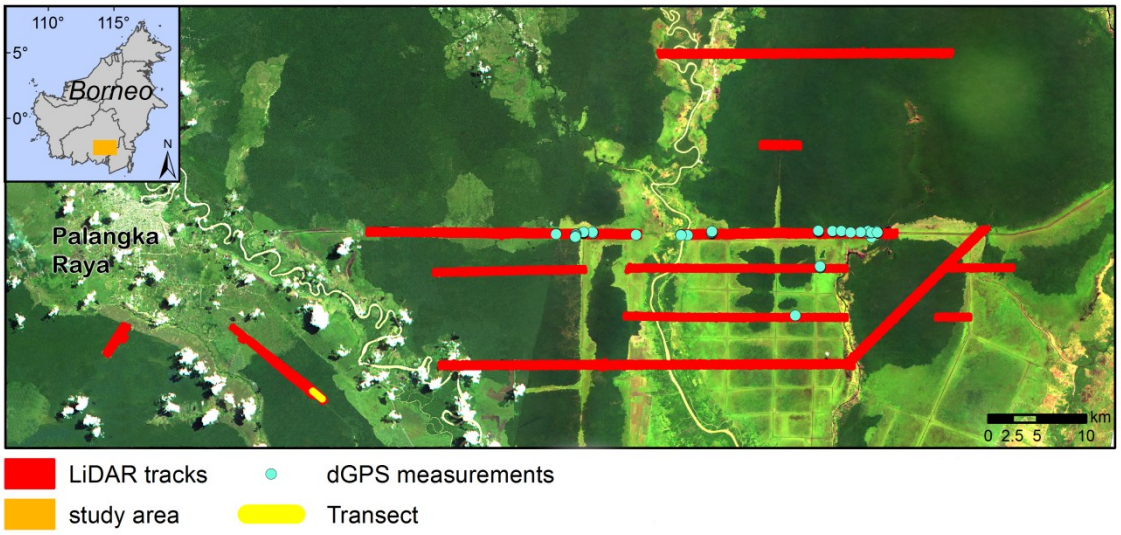

Figure VI-1: True color RapidEye mosaic from 28 July 2009 and 29 July 2012 showing the study area with the overlapping LiDAR tracks of 2007 and 2011 (depicted in red). The location of the study area is indicated in orange in the outline map of Borneo. The location of field derived dGPS measurements used for assessing the accuracy of DTMs and the location of the transect shown in Figure VI-9 are also depicted.

3.2. Data

3.2.1. Field inventory data

Field inventory campaigns were conducted in the years 2008, 2010 and 2011. Inventory plots with different plot sizes were established in forested and regrowing areas. The sample plot design of the field inventory was based on the guidelines provided by Pearson et al. (2005).

In forested areas, three circular nested plots with radii of 4 m, 14 m, and 20 m were recorded. Inside each nest, trees of a certain DBH (diameter at breast height) were measured depending on degradation intensity: 2 cm to 10 cm or 5 cm to 20 cm (within the 4 m radius), 10 cm to 20 cm or 20 cm to 50 cm (within 14 m radium), and greater than 20 cm or 50 cm (within 20 m radius). In regrowing areas, rectangular plots of 20 m x 50 m were used and all trees within this area were recorded.

Within both plot types, the following parameters were recorded: DBH, tree height, and tree species in order to estimate their wood density. Tree specific wood densities were derived from databases provided by Chudnoff (1984), World Agroforestry Centre (2011), and IPCC (2006). If the tree species could not be identified, an average specific wood density for Asian tropical trees of 0.57 Mg m^{-3}, was applied (Brown 1997).

AGB was calculated using a combination of allometric models from Hughes et al. (1999) for saplings (if DBH < 5 cm and height ≤ 1.3 m) or trees (if DBH < 5 cm and height > 1.3 m) and Chave et al. (2005) for moist tropical forest stands including DBH and tree height (if DBH ≥ 5 cm and height > 1.3 m).

Altogether, 26 plots were sampled in 2008 which were located within the LiDAR tracks of 2007, ranging from 8.7 t/ha to 458.5 t/ha, and 53 plots were sampled in 2010 and 2011 which were inside the LiDAR tracks of 2011 and ranged from 0.0 t/ha to 375 t/ha.

3.2.2. LiDAR data

LiDAR measurements were collected during the dry seasons (May to October) in 2007 and 2011, respectively, thereby avoiding any influence of water during the DTM generation. The 2007 acquisition was conducted in August with a Riegl LMS-Q560 flown 500 m aboveground. Full-waveform LiDAR data was recorded with a half scan angle of ±30°. Each LiDAR transect was generated by a single flight line, thus no strip matching was applied. In 2011, an Optech Orion M200 was used and data were acquired between August and October at a height of 800 m. Full-waveform LiDAR data were recorded with a half scan angle of ±11°. A strip adjustment procedure was applied resulting in an average vertical accuracy of a root mean square error (*RMSE*) of 0.036 m. Further data specifications and acquisition details are provided in Table VI-1. The specifications of both LiDAR instruments differed in some aspects, e.g. flight height and wavelength, but the most important difference was in terms of point density. Figure VI-4 illustrates the difference in LiDAR survey point density between 2007

(1.5 points/m²) and 2011 (10.7 points/m²) within an undisturbed peat swamp forest. During the 2011 LiDAR acquisition, photos were taken from the aircraft and were processed to orthophotos with a spatial resolution of 0.25 m. The two LiDAR campaigns resulted in a total overlapping area of 11,726 ha and the land cover comprised peat swamp forests, partly affected by former and recent selective logging, old burned scars, fern, grassland, bushes, and agricultural land.

Table VI-1: Specifications of LiDAR acquisitions.

Specification	2007	2011
LiDAR system	Riegl LMS-Q560	Optech Orion M200
Acquisition date	5 - 10 August	15 August - 14 October
Power	100Khz	100Khz
Nominal Altitude	500 m	800 m
Wavelength	1.5 µm	1.064 µm
Half Scan angle	±30°	±11°
Average point density	1.5 points/m²	10.7 points/m²

3.2.3. Multispectral imagery

High-resolution RapidEye imagery has proven to detect small scale logging in peat swamp forests and was therefore chosen to monitor logging activities and fire impacts between both LiDAR acquisitions (Franke et al. 2012). The RapidEye satellite system is a constellation of five identical satellites, which were launched in August 2008, and the images have a pixel resolution of 5 m. Scenes used in this study were acquired on 22 May 2009, 28 July 2009, 10 February 2010, 11 February 2010, 21 June 2010, 18 August 2011, and 29 July 2012 and were atmospherically corrected and co-registrated.

Medium resolution Landsat imagery was used to analyze historical managed logging during the 1980s and early 1990s. Landsat satellites have acquired scenes since 1972, mostly with a spatial resolution of 30 m. Former managed logging was investigated on the basis of a Landsat scene from 30 June 1991 which was atmospherically corrected and co-registrated (Figure VI-2). All logging activities before that date were included in the analyses.

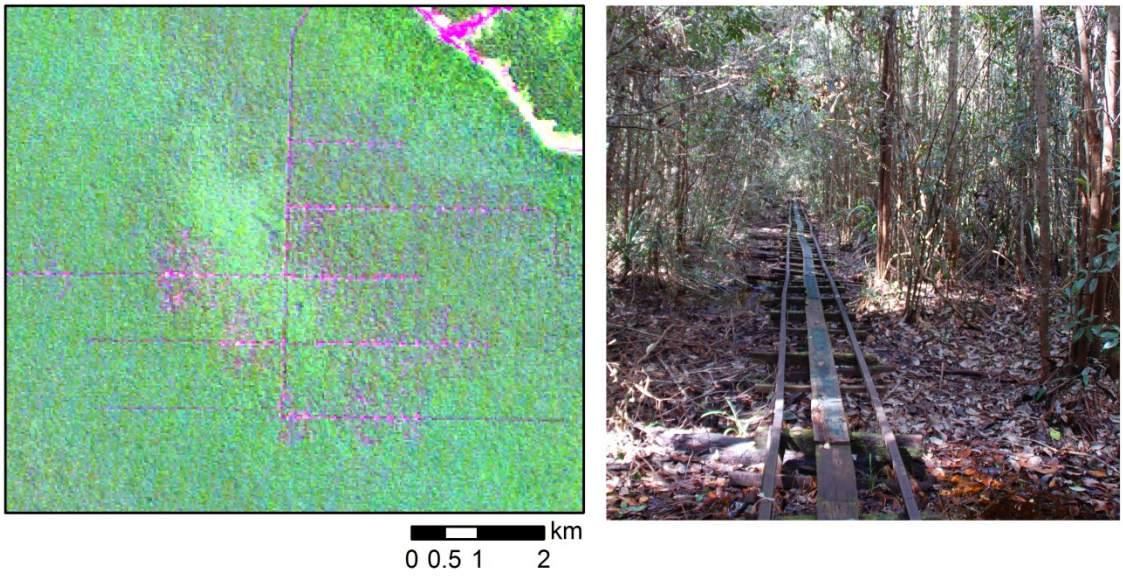

Figure VI-2: Landsat scene from 30 June 1991 (RGB: bands 543) showing a managed selective logged peat swamp forest area within the study area. An abandoned logging railway is depicted in the photograph (© S. Englhart).

3.3. Data analysis

In a first step, the LiDAR point clouds of 2007 and 2011 were compared to each other and the effect of different point densities was examined. The distribution of the LiDAR signal of different layers of the vegetation and the comparability of both acquisitions was investigated.

3.3.1. LiDAR filtering and DTM generation

A crucial step within the digital terrain model (DTM) generation is the LiDAR filtering. A hierarchic robust filter was applied to the LiDAR point clouds, separating the ground and non-ground (vegetation) points (Pfeifer et al. 2001). The linear adaptable prediction interpolation (kriging) was utilized to generate the DTMs with a resolution of 1 m. The accuracy of the DTMs was evaluated on the basis of field derived differential Global Positioning System (dGPS) measurements. Altogether, 93 dGPS measurements were available within both LiDAR tracks covering different land cover classes (peat swamp forest, open forest, burned scars, fern and shrubs) (Figure VI-1). The 2007 and 2011 DTM resulted in *RMSE*=0.41 m and *RMSE*=0.16 m, respectively. In comparison to each other, the DTM featured *RMSE*=0.37 m (Figure VI-3). The DTMs were further utilized

for the CHM creation and AGB estimation. Due to the difference of both DTMs, separated CHMs and AGB models for 2007 and 2011, which were based on the respective DTMs, were generated. Therefore, the difference of the DTMs does not influence the analyses as relative heights were used and are supposed to be stable (Hudak et al. 2012; Jenkins 2012).

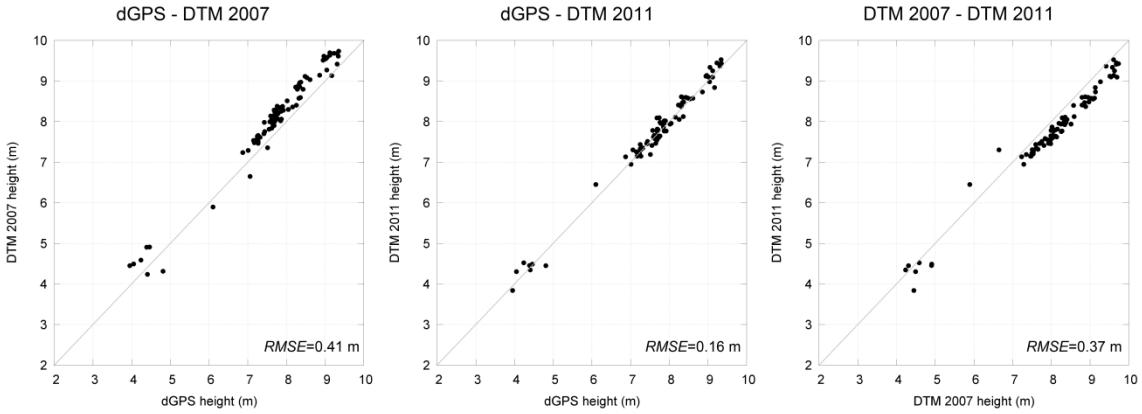

Figure VI-3: Scatterplots and accuracy of heights derived from generated DTMs of 2007 and 2011 and field derived dGPS measurements.

3.3.2. Canopy height models

CHMs of both years with a resolution of 1 m were produced by calculating the difference between the elevation of the digital surface model (DSM) and the underlying terrain of the DTM. The DSM was generated choosing the highest point within a grid of 1 m. Pixels containing no data were filled using the highest point of the neighborhood and a morphological operator. The changes of the CHMs between 2007 and 2011 were analyzed by calculating the difference of both models and subsequent median filtering.

3.3.3. Biomass estimation

Due to the differences of both LiDAR measurements, especially in point density, each acquisition was treated as an independent assessment and the biomass models were therefore developed separately. Similarly, Hudak et al. (2012) used LiDAR measurements with significant differences in point densities and found out that different point densities do not affect AGB estimations if LiDAR measurements were independently analyzed.

Only 26 field inventory plots were available for the 2007 LiDAR analysis and it was not sufficient data to develop an accurate regression model. Hence, the 2011 LiDAR point density of the 2011 field inventory plots was reduced and added to the 2007 analysis as reference data. The LiDAR point density of 2011 was reduced by taking the highest and lowest point within a square with a side length of 1 m. The 2011 plots within the reduced LiDAR data of 2011 resulted in a mean point density of 1.99 points/m² whereas the 2007 plots within the 2007 LiDAR data had an average point density of 1.52 points/m². In 2011, sufficient field inventory plots were available to develop an accurate AGB regression model.

LiDAR height histograms have found to be very useful for AGB estimation (Asner et al. 2010; Jubanski et al. 2012) and were calculated by normalizing all points within a grid of 35 m (similar to the size of the largest field inventory plot) to the ground using the DTMs as reference. A height interval of 0.5 m was defined and the number of points within this interval was stored in form of a histogram. The first height interval was considered as ground return and therefore excluded from the further processing. The centroid height (CH) of the height histogram was calculated by weighing each 0.5 m height interval with the relative number of LiDAR points stored within this interval (Jubanski et al. 2012). CH was related to field inventory derived AGB and regression models were developed. Jubanski et al. (2012) showed that the accuracy of AGB estimations derived from LiDAR height histograms increased with higher point density. For this reason, point density was also implemented in the regression in form of a weighting factor as already performed by Jubanski et al. (2012).

The commonly used power function resulted in significant overestimations in the higher biomass range. The optimal regression model to predict AGB was found to be a combination of a power function (in the lower biomass range up to a certain threshold CH_0) and a linear function (in the higher biomass range). The linear function is the tangent through CH_0 and was calculated on the basis of the first derivative of the power function:

$$(17) \qquad AGB = \begin{cases} a * CH^{b} & if\ CH \le CH_0 \\ \left(a * b * CH_0^{(b-1)}\right)(CH - CH_0) + a * CH_0^{b} & if\ CH > CH_0 \end{cases}$$

where CH is the centroid height, CH_0 is the threshold of function change and a, b are coefficients.

The threshold of CH_0 was determined by increasing the value of CH_0 in steps of 0.001 m by identifying the lowest *RMSE*.

The developed AGB regression models were independently validated by the Predictive Power of the Regression (*PPR*) as carried out by Asner et al. (2010). The *PPR* is the *RMSE* determined by running 1,000 iterations of the regression by randomly leaving out 10% of the reference field inventory plots.

The biomass models were applied to whole overlapping area of the LiDAR tracks. Changes in biomass were calculated over the four year time period by subtracting the 2007 AGB map from the one of 2011. Positive values thus indicate net biomass gain while negative values indicate loss.

3.3.4. Change analysis

Canopy height and AGB dynamics during 2007 and 2011 were analyzed over the whole study area. The vegetation within the study area is under strong anthropogenic pressure and thus experiences many changes. On the basis of RapidEye imagery, areas of peat swamp forest were identified that remained unaffected, were selective logged or burned within the four year time period. Canopy height change and AGB accumulation or loss was quantified within these areas. Logging trails could be easily identified due to the high spatial and temporal resolution of the RapidEye data. On the basis of field surveys, orthophotos and long term experience within the study area as well as lack of literature reference data, an area with a buffer of 30 m and 50 m, respectively, was chosen for the investigation of AGB loss caused by selective logging. It is assumed that loggers do not remove trees that are further away from the logging trail than 50 m because new trails would then be constructed.

Additionally, areas affected by former managed selective logging with extensive infrastructure were identified on the basis of a Landsat scene from 30 June 1991. All logging activities before that date were included in the analyses.

4. Results

First, the different point densities of 2007 and 2011 were investigated whether they have an influence on the analysis. As set out in Table VI-1, the mean point density

differed by factor 7. Figure VI-4 shows an orthophoto taken in 2011 and the corresponding LiDAR point clouds of 2007 and 2011 within an unaffected peat swamp forest. Although the point density differences are clearly visible, the relative distribution over the different vegetation layers is basically similar. In the 2007 data, the relative number of LiDAR returns from the ground and lower vegetation layer is less than in the 2011 data. Therefore, height histograms and consequently CH of both LiDAR measurements are slightly different. The point density also influences the accuracy of the generated DTMs which was assessed on the basis of 93 field derived dGPS measurements. The mean point densities on these locations were on average 0.41 points/m² for 2007 and 19.11 points/m² for 2011 and the accuracy resulted in *RMSE*=0.41 and *RMSE*=0.16, respectively (Figure VI-3). For this reason, it was reasonable to develop separate AGB regression models for 2007 and 2011.

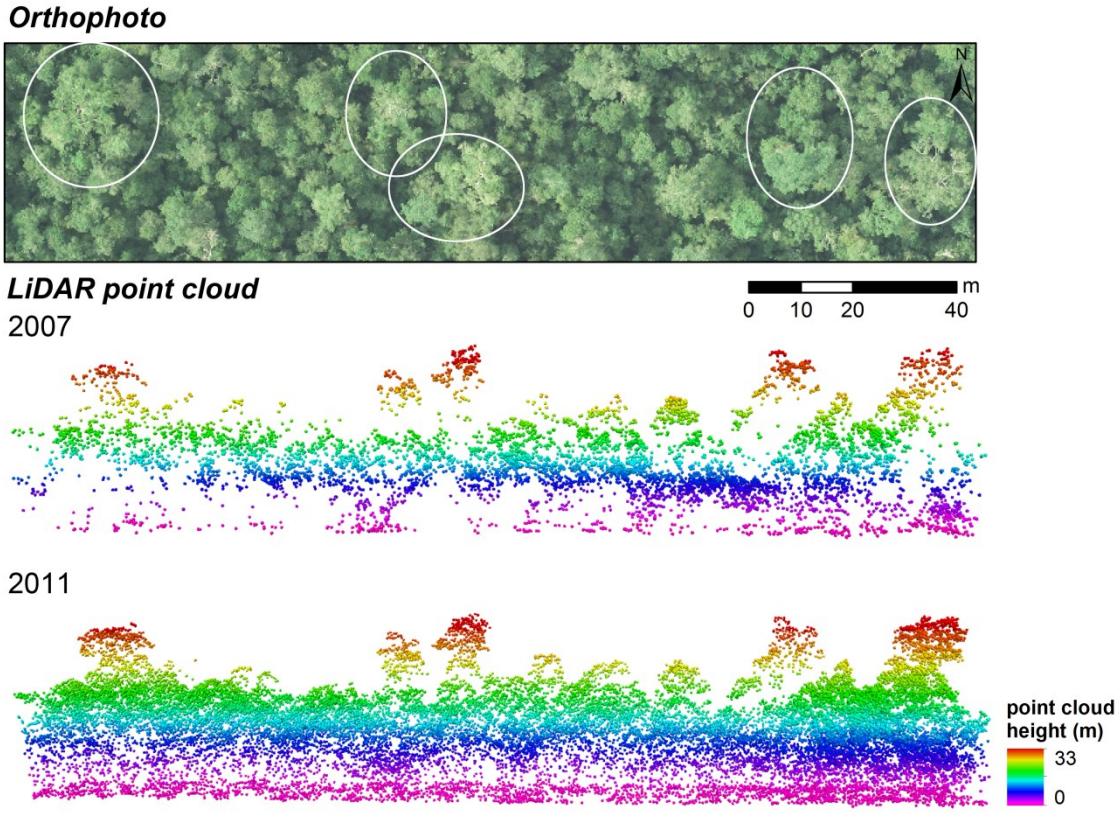

Figure VI-4: Orthophoto taken on 13 October 2011 and the corresponding LiDAR point clouds of 2007 and 2011 within an unaffected peat swamp forest. The locations of the higher tree crowns which are clearly visible within LiDAR point clouds are indicated by white circles in the orthophoto.

4.1. Canopy height models

Changes in canopy height were evaluated on the basis of CHMs. In unaffected forests, it was possible to identify crowns of single high trees and to quantify the growth rates. Figure VI-5A depicts the 2007 and 2011 CHM of such a tree crown. Tree height increased by 0.6 m within the four years, from 29.3 m to 29.9 m. An example of a degraded forest area is shown in Figure VI-5B. The degradation was most likely caused by felling the trees. The two examples demonstrate that changes in the CHM helped to identify areas of growth and disturbance.

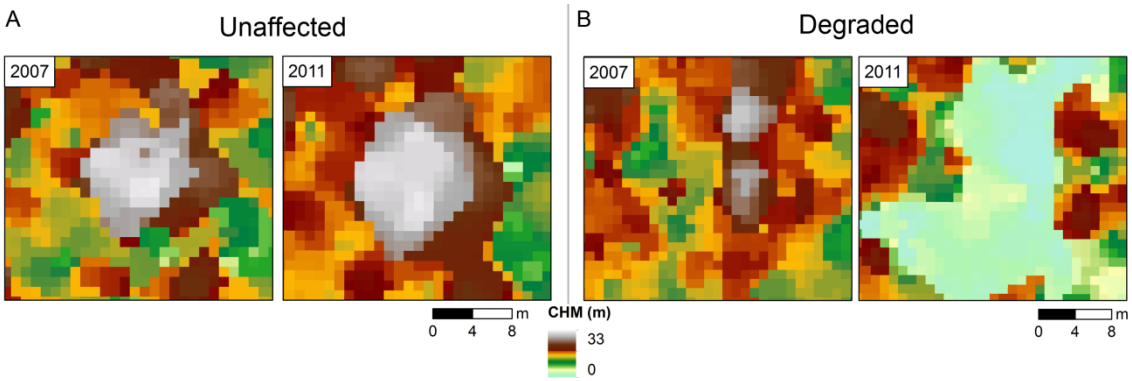

Figure VI-5: Canopy height models of 2007 and 2011 of (A) an unaffected and (B) degraded peat swamp forest.

4.2. AGB regression models

Due to different point densities of both LiDAR acquisitions, two separated AGB regression models were developed on the basis of a combined power and linear function (equation (17)). Figure VI-6A shows scatter plots of AGB and CH for 2007 and 2011 with the corresponding regressions. The part of the power function in the lower biomass range is depicted in turquoise and the linear part of the function in the higher biomass range in orange. The size of the reference field inventory plots depends on LiDAR point density, the higher the density, the bigger is the dot. Figure VI-6B displays the dependence of CH_0, the threshold of function change, and *RMSE* for the 2007 and 2011 AGB regression models. The lower the value of CH_0, the lower is the proportion of the power function and the higher the value of CH_0, the lower is the proportion of the linear function. The value with the lowest *RMSE* is marked and was chosen as CH_0. The 2007

AGB regression model was developed on the basis of 79 field inventory measurements resulting in a coefficient of determination r^2=0.77 with *PPR*=54.2 t/ha and CH_0=8.086 m. For the 2011 AGB regression model, 53 field inventory plots were available for calibration and validation and resulted in r^2=0.81, *PPR*=47.4 t/ha and CH_0=8.841 m.

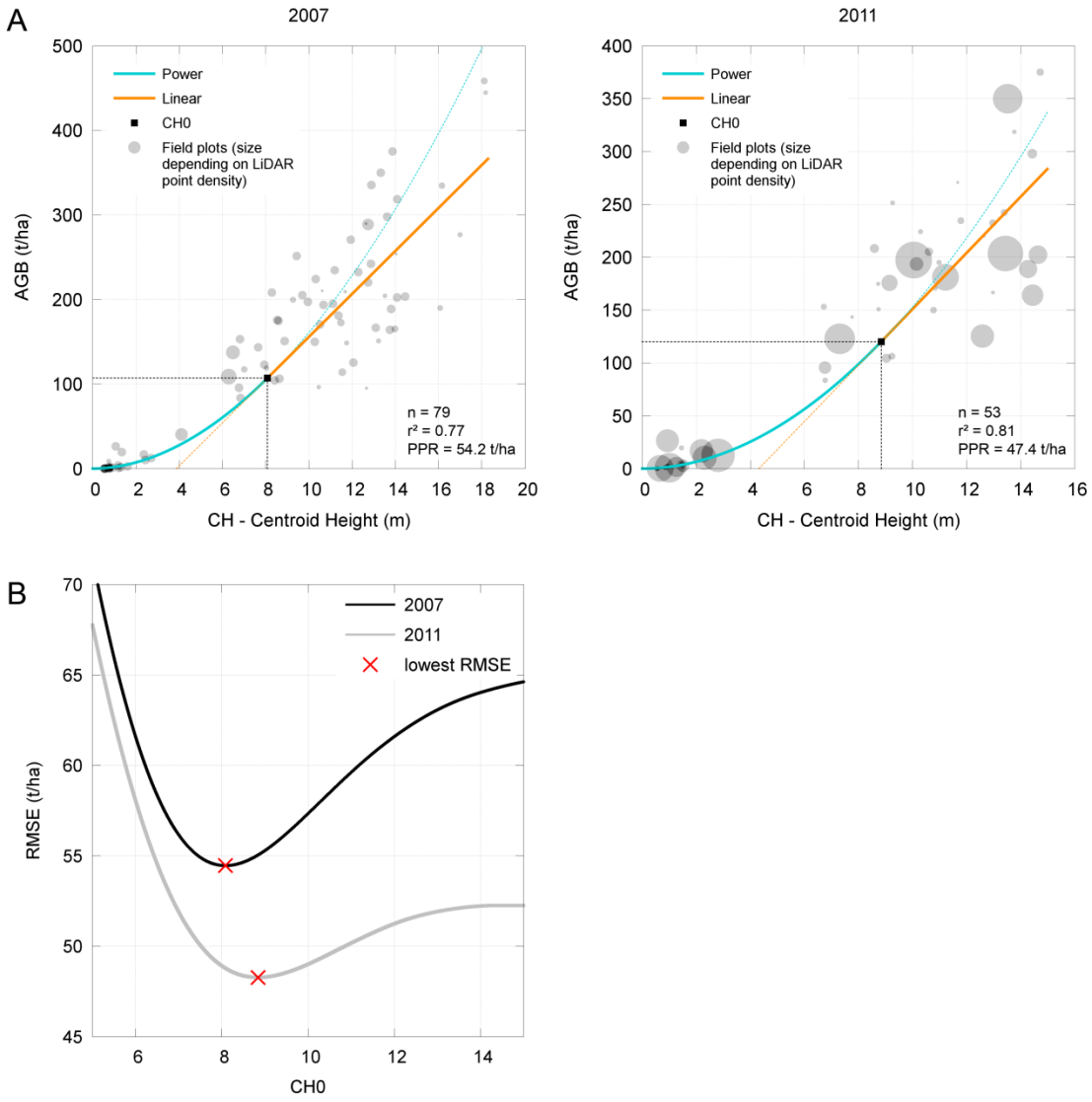

Figure VI-6: (A) Correlation between AGB and CH of 2007 (left) and 2011 (right) datasets. The optimal AGB regression models based on a combined power and linear function (equation (17)) are also displayed. (B) Dependence of CH0 and RMSE. The CH0 value with the lowest RMSE was chosen as threshold for function change.

4.3. Change analyses

The study area comprises several different land covers, such as peat swamp forest, former burned and regrowing areas containing fern, grassland, bushes, and agricultural areas. Due to the high variability, three main categories of change of initial peat swamp forests between both LiDAR acquisitions were evaluated on the basis of multi-temporal RapidEye images.

First, undisturbed forest areas of 3,393 ha were determined that had no or no visible impact between 2007 and 2011. Second, logging trails were identified on the basis of high temporal and spatial resolution RapidEye data. Figure VI-7 depicts four different RapidEye scenes showing the example of a selective logged area. The narrow skid trail infrastructure, which is clearly visible, was fast evolving and the rapid regrowth of the vegetation after the logging activities stopped hindered the detection of the full extent of logging in the RapidEye images. All skid trails that cloud be detected with available RapidEye data are also shown in Figure VI-7 ("detected logging trails"). On the basis of repetitive field observations, the area within 30 m and 50 m of the detected logging trails was analyzed which amounted to 67 ha and 113 ha, respectively. Third, forested areas that burned once between both LiDAR acquisitions were evaluated. This is important because recurrent fires further reduce AGB. Altogether, 555 ha of initial peat swamp forests within the study area burned.

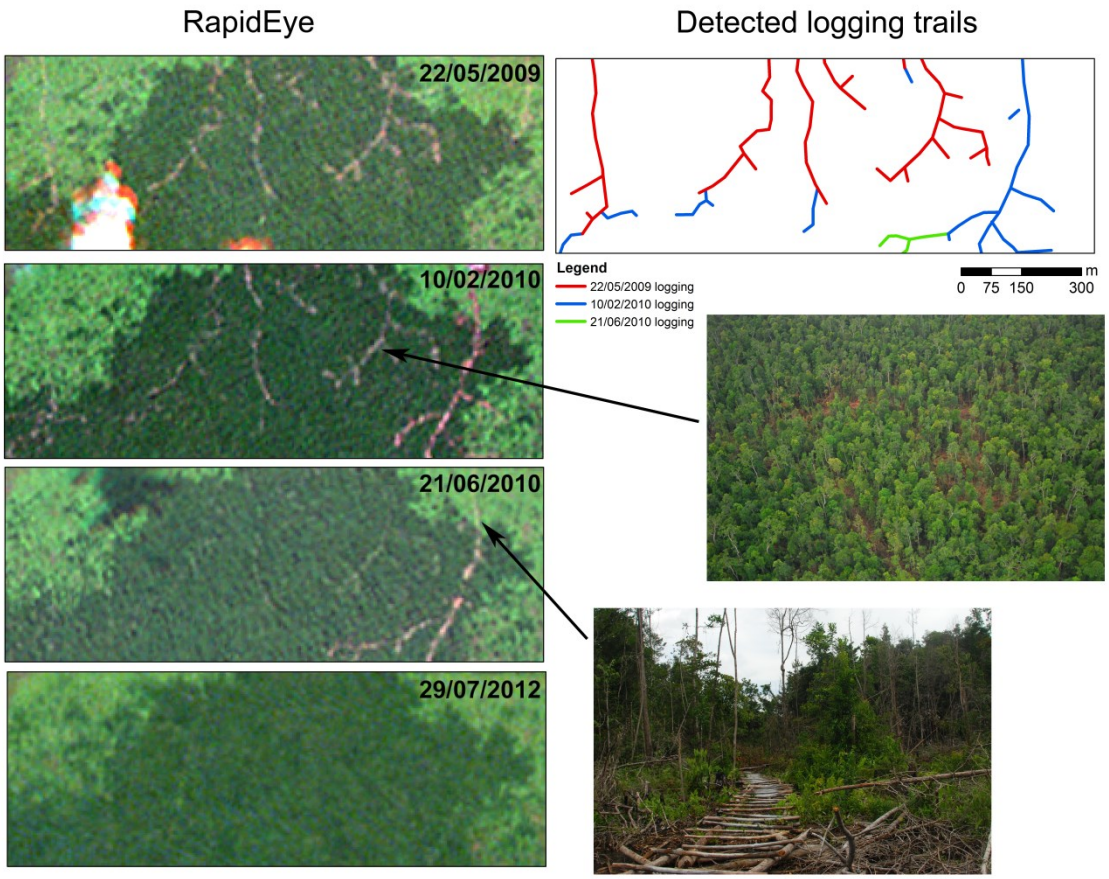

Figure VI-7: Multi-temporal RapidEye scenes of a selective logged peat swamp forest with the detected logging trails. Photos show an aerial image of a logged forest and an abandoned logging trail (© F. Siegert, P. Navratil).

Table VI-2 depicts canopy height and AGB dynamics within these areas. In undisturbed peat swamp forests, the canopy height increased on average by 2.3 m and accumulated 20 t/ha over this four year time period. In selective logged forests, the canopy height increased on average 0.5 m and mean AGB decreased by 55 t/ha within 30 m of the logging trails whereby a canopy height increase of 1.0 m and AGB loss of 42 t/ha was detected within 50 m of the logging trails. As expected, burned forests experienced an extensive loss in canopy height (9.4 m on average) and AGB (approximately 92%). The initial AGB of burned forests was on average 154 t/ha (compared to 203 t/ha of undisturbed peat swamp forest) which indicates that degraded forests are more vulnerable to fire.

Table VI-2: Quantification of changes in canopy height and AGB of unaffected, selective logged (within 30 m and 50 m of logging trails) or burned peat swamp forests. The mean values and standard deviations (std) are depicted.

forest condition	**unaffected**		**selective logged within**				**burned**	
			30 m		**50 m**			
	mean	*std*	mean	*std*	mean	*std*	mean	*std*
area [ha]	3,393		67		113		555	
CHM 2007 [m]	14.0	*5.8*	13.5	*6.0*	13.2	*6.0*	11.1	*6.7*
CHM 2011 [m]	16.3	*4.7*	13.9	*5.9*	14.2	*5.8*	1.7	*4.0*
CHM change [m]	+2.3	*1.9*	+0.5	*3.1*	+1.0	*3.0*	-9.4	*5.3*
AGB 2007 [t/ha]	203	*58*	215	*62*	209	*63*	154	*80*
AGB 2011 [t/ha]	223	*47*	160	*57*	167	*57*	12	*21*
AGB change [t/ha]	+20	*33*	-55	*41*	-42	*44*	-142	*77*

Figure VI-8 depicts AGB of 2007 and 2011 as well as its changes in the selective logged peat swamp forest area of Figure VI-7. The areas within 30 m and 50 m of the detected logging trails were analyzed and are also depicted. The forest area has already been degraded in 2007, but has further been exploited between both acquisitions which is not only evident from multispectral imagery (Figure VI-7) but also from AGB loss (Figure VI-8). The spatial pattern of AGB loss clearly follows the skid trails whereas AGB accumulated in remaining small forest patches.

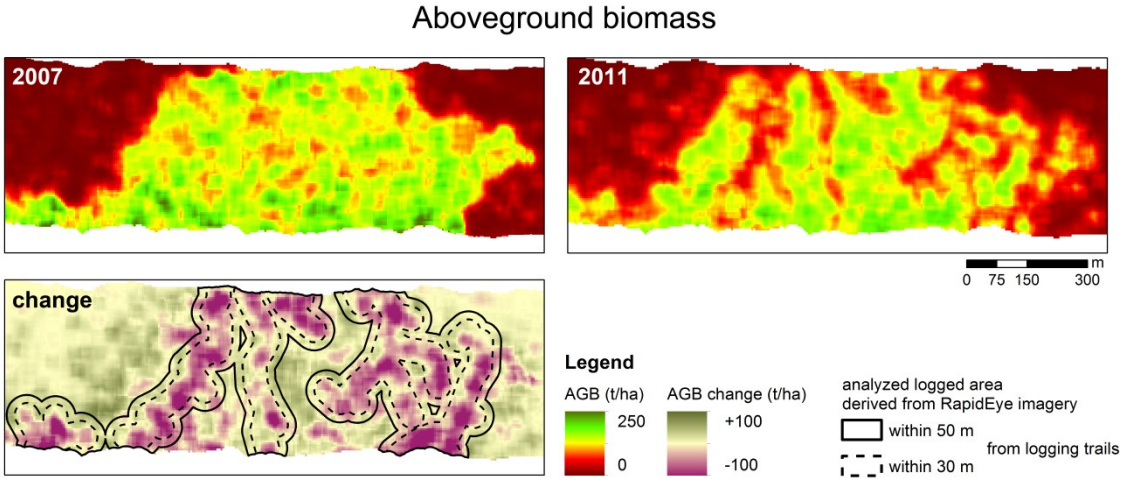

Figure VI-8: AGB of 2007 and 2011 as well as its spatial dynamic in a selective logged peat swamp forest. The analyzed area was within 30 m and 50 m of the detected logging trails (Figure VI-7).

Figure VI-9 depicts a transect through a burned and adjacent unaffected peat swamp forest with the changes in canopy height and AGB. The extensive loss of AGB and canopy height is clearly visible within the burned area (C) as well as growth of canopy height and accumulation of AGB in the unaffected area (E). The transitions area (D) between the burned and unaffected area is characterized by single remaining trees which increased in height over the four years. This effect is visible in the canopy height change diagram. Even if single remaining trees increased in height, AGB of this transition area was reduced due to the fire impact.

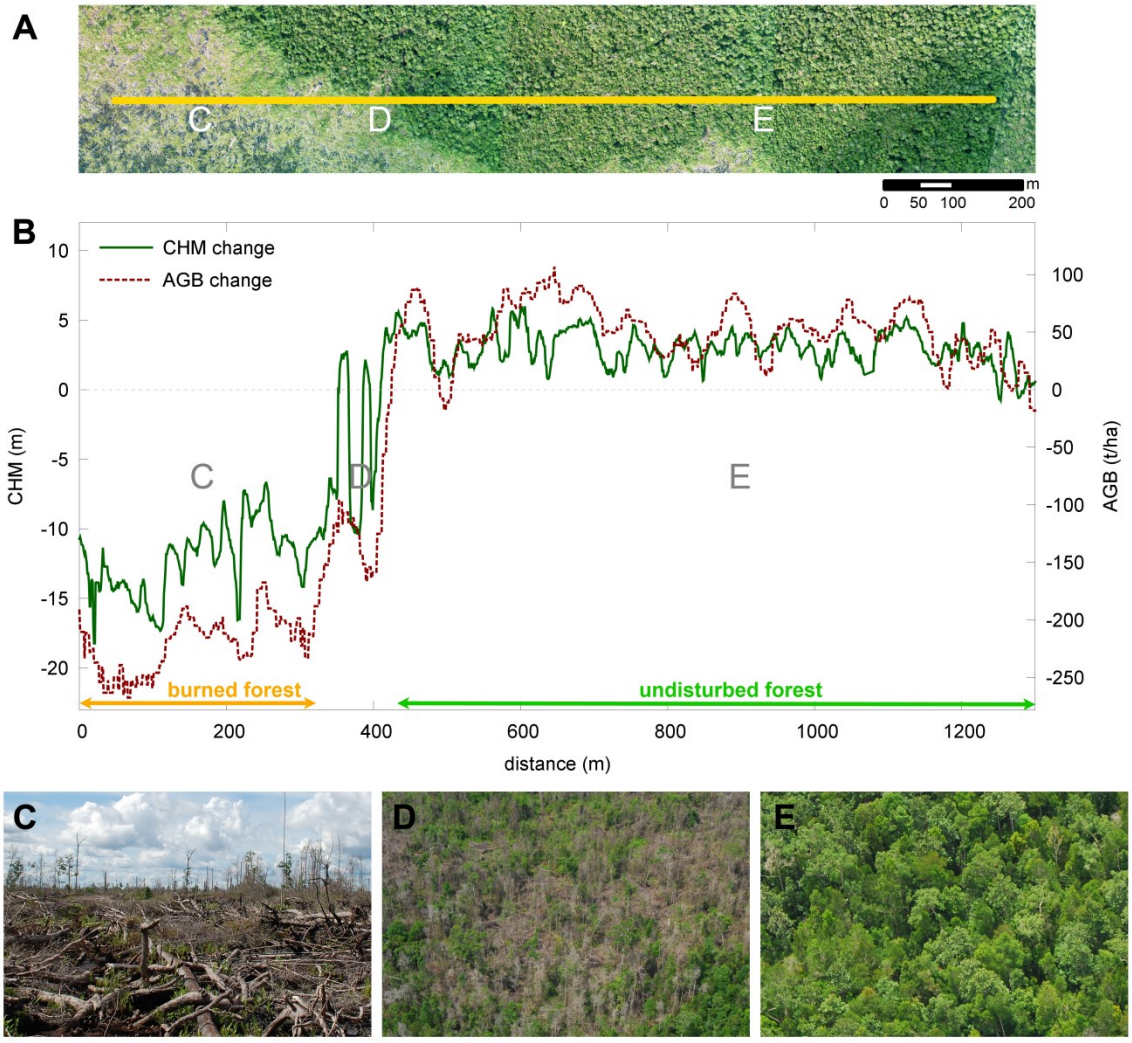

Figure VI-9: (A) Transect through a burned and adjacent unaffected peat swamp forest superimposed on a orthophoto from 11 October 2011. (B) Changes in canopy height and AGB. Photos of (C) a burned forest, (D) transition area of burned and unaffected forest and (E) undisturbed forest (© S. Englhart, F. Siegert). Locations of (C), (D), and (E) are indicated in the transect and graph. The location of the transect is shown in Figure VI-1.

Historical managed logged areas during the 1980s and early 1990s were identified on the basis of a Landsat scene from 30 June 1991. In total, 4,529 ha of the study area (39%) was affected by former managed logging of which 2,946 ha was degraded to shrubs, bushes, and grassland in 2007, whereby 110 ha were part of a large scale oil palm plantation. The remaining historical logged area (1,584 ha) was still forested in 2007 of which 1,211 ha remained unaffected between 2007 and 2011. The average biomass of these forests was 219 t/ha in 2007 and 238 t/ha in 2011 with a mean canopy height of 14.2 m and 16.8 m, respectively. In contrast, unlogged and undisturbed forests contained 194 t/ha with a mean canopy height of 13.9 m in 2007 and 214 t/ha with a mean canopy height of 16.0 m in 2011. These results demonstrate that historical logged forests have in general a higher forest biomass than unaffected forests, even though they were degraded 20 years ago. This comparison also revealed that historical logged forests experienced a higher growth rate (on average 2.6 m) during this four year time period than primary forests (on average 2.1 m), thereby accumulating a similar amount of AGB (19 t/ha and 20 t/ha, respectively).

5. Discussion

Canopy height and AGB dynamics were examined over a four year time period in a tropical peat swamp forest. Multi-temporal LiDAR measurements were investigated for their potential to detect changes in tropical peat swamp forests between 2007 and 2011. The data specifications and acquisition details of both datasets differed from each other, mostly in point density (Table VI-1). The results of this study revealed that both acquisitions are comparable when treated as independent assessments because the relative distribution of the LiDAR returns slightly differed over the different vegetation layers (Figure VI-4). By developing two independent AGB regression models for 2007 and 2011, the difference in point density does not affect the analysis. Hudak et al. (2012) also compared repetitive LiDAR measurements that had a 30-fold difference in point density and concluded that it does not affect biomass estimations and dynamics when treated as independent assessments with two independently developed regression models.

Changes in canopy height were evaluated on the basis of CHMs. We found that single high trees could be identified in both models in unaffected forests and even small scale impacts, e.g. felling of one or more trees, were visible (Figure VI-5). Several other

studies have shown the potential of repetitive LiDAR observations to detect small scale changes in the forest canopy and its dynamics. Dubayah et al. (2010) evaluated the different growth and AGB accumulation rates of old growth and secondary forests in Costa Rica. Jenkins et al. (2012) successfully monitored forest growth in an Australian scrubby forest-woodland and Kellner et al. (2009) analyzed canopy disturbance and regeneration in an old growth tropical forest for a 8.5 year time period and proved the short-term stability of the tropical forest.

AGB was quantified through regression modeling based on LiDAR CH and field inventory measurements. Two separate AGB regression models were developed for 2007 and 2011 due to the different LiDAR data specifications and acquisitions. Our study revealed an optimal AGB regression on the basis of a combined power and linear function. Although many studies obtained good results for estimating AGB from LiDAR height metrics on the basis of a power function (Asner et al. 2009; Lefsky et al. 2002; Saatchi et al. 2011a), we detected an extreme overestimation in the higher biomass range when using solely a power function. Additionally, AGB estimations derived from the power function were not as accurate as estimations derived from the combined power and linear function. The AGB regression model of 2007 solely based on the power function resulted in r^2=0.75 and *PPR*=65.1 t/ha whereas the regression model based on a combined power and linear function resulted in r^2=0.77 and *PPR*=54.2 t/ha. Similarly, the AGB model of 2011 based on the power function resulted in r^2=0.78 and *PPR*=52.3 t/ha and the combined power and linear function resulted in r^2=0.81 and *PPR*=47.4 t/ha. Mascaro et al. (2011a) developed a carbon estimation regression model on the basis of airborne LiDAR canopy height metrics in a tropical forest in Panama and also modified the power function of the AGB regression.

Forested areas that remained unaffected, were selective logged or burned between both LiDAR acquisitions were identified on the basis of RapidEye images and changes in canopy height and AGB were quantified. In unaffected peat swamp forests, canopy height increased on average 2.3 m and accumulated 5 t/ha y^{-1}. These unaffected forest areas included primary and secondary forests of different degradation levels as well as different peat swamp forest types. The growth and accumulation rates are an average of fast growth rates, e.g. in previously logged forests and slow growth rates, e.g. in primary forests. Sweda et al. (2012) and Boehm et al. (2012) analyzed some of the same 2007 LiDAR data in combination with another LiDAR dataset also acquired in 2011

within the study area. They found a canopy growth of 1.9 m and an AGB accumulation of 3.7 t/ha y^{-1}. The results might differ from each other mainly due to another spatial extent of the study area and also due to another LiDAR dataset of 2011.

Illegal selective logging activities were monitored on the basis of RapidEye data. AGB loss and canopy height change was quantified within 30 m and 50 m of detected logging trails. As no reference data could be found in literature, the extent of the analyzed area was based on repetitive field observations on ground and during flight surveys as well as long term experience within the study area. It is assumed that trees which are more than 50 m away from the trails are unlikely to be logged because new logging trails would then be constructed in order to overcome the access difficulties in peat swamp forests. Within the 30 m area of the trails, canopy height increased by 0.5 m and AGB was reduced by 55 t/ha which makes up 26% of initial biomass. The analysis of the 50 m area resulted in a canopy height increase of 1.0 m and AGB loss of 42 t/ha which is 20% of initial biomass. Although AGB was reduced in both cases, canopy height increased which is a result of the fast regrowth. Trees grow fast in height with thin trunks and thus slowly accumulate AGB. No other study on AGB loss due to selective logging in tropical peat swamp forests could be found. Mazzei et al. (2010) estimated AGB loss due to small impact logging in the eastern Amazon on the basis of field inventory data to 94.5 t/ha which is equivalent to 23% of the initial AGB. Other studies on managed selective logging also based on field measurements in dipterocarp forests reported an AGB loss between 33% and 56% of the initial forest biomass (Berry et al. 2010; Pinard et al. 1996). This comparison emphasizes the different degradation levels caused by selective logging in dipterocarp and peat swamp forests.

The quantitative assessment of burned peat swamp forests revealed that 92% of the initial 154 t/ha was lost. Three field inventory measurements were available within the study area before (2008) and after (2010) the fire in 2009. On average, 98% of 187 t/ha was lost due to fire. Hashimotio et al. (2000) and Hiratsuka et al. (2006) conducted field inventory measurements in East Kalimantan on a burned forest area and found remaining AGB of 8 - 10 t/ha and 9 -17 t/ha, respectively.

Managed logged areas in the 1980s and early 1990s were identified on the basis of Landsat. In total, 4,529 ha of the study area were affected by logging of which 65% were degraded to shrubs, bushes and grassland in 2007 demonstrating the high vulnerability of degraded peat swamp forests. Different growth but similar AGB

accumulation rates were detected in former logged (2.3 m and 19 t/ha) and completely unaffected forests (1.9 m and 20 t/ha) demonstrating faster growth rates of secondary forests. Unaffected and unlogged forests contained on average less biomass per hectare than former managed logged forests after 20 years of regrowth. This fact can be explained by different forest types with various species composition. For example, low pole peat swamp forests grow to a maximum height of 20 m. They contain very few commercial tree species and only few of these provide good quality timber (Shepherd et al. 1997). In contrast, tall interior and mixed peat swamp forests reach a maximum height of 45 m and 35 m, respectively, and comprise several tree species of commercial importance. Hence, these forest types are subjected to the most intense logging (Shepherd et al. 1997). A more detailed analysis of different and repetitive degradation levels would be helpful to assess the carbon stocks, growth and AGB accumulation rates of the different peat swamp forest types. A variability of AGB up to 140% was found in a peat swamp forest within the study area (Jubanski et al. 2012).

A next step could be the investigation of the variability of peat swamp forests considering different forest types and degradation levels leading to a better understanding of the forests and their environment. This study demonstrates the enormous potential of multi-temporal airborne LiDAR measurements for this kind of analyses by accurately estimating AGB dynamics and thereby meeting the requirements of REDD+.

6. Acknowledgements

The authors would like to thank Suwido Limin and his team from the Centre for International Co-operation in Management of Tropical Peatland (CIMTROP) in Palangka Raya for the logistical support during the field surveys. We would like to thank Sampang Gaman (CIMTROP) and Simon Husson (Orang Utan Tropical Peatland Project, OUTROP) for providing tree species lists. RapidEye data was provided by the German Aerospace Center (DLR) via the RESA - RapidEye Science Archive with funds from the Federal Ministry of Economics and Technology (proposal no 267) and by the European Space Agency (ESA) via EC/ESA GSC-DA. The LiDAR dataset of 2007 was acquired by Kalteng Consultants. The LiDAR measurements of 2011 were provided within Kalimantan Forests and Climate Partnership (KFCP) Project financed by AusAID (Australian Agency for International Development).

VII. Synthesis

1. Summary

This thesis evaluates the feasibility of SAR imagery to monitor the hydrological effects of restoration measurements in tropical peatlands. Furthermore, it examines the capability, accuracy, and limitations of different sensors, namely different SAR frequencies and polarizations, multispectral RapidEye imagery, and airborne LiDAR measurements, to retrieve AGB in Indonesian tropical peat swamp forests. Especially for climate change mitigation mechanisms, such as REDD+, accurate spatially explicit AGB estimations of carbon rich tropical forests are of high importance. In this context, tropical peat swamp forests are relevant, as they store carbon not only aboveground in forests but also belowground in thick peat deposits. Field inventories of remote and hardly accessible forests are very rare, as they are expensive, time consuming and laborious to collect. Hence, remote sensing has been identified as the most cost effective way to produce large scale AGB maps. Nevertheless, field inventory measurements are mandatory to calibrate and validate AGB estimations based on remote sensing data.

In a first step, the capability of multi-temporal ENVISAT ASAR (C-band) and ALOS PALSAR (L-band) imagery to monitor the hydrological effect of restoration measurements of peat was investigated. The restoration included blocking of drainage canals by dam building which is one of the most important measures to restore the hydrological and ecological functions of peat domes. The sensitivity of SAR to moisture was utilized to detect changes in peat soil moisture after dam construction. The rewetting of peat soils was successfully monitored, especially in deforested areas with a high density of dams resulting in a backscatter increase of up to 1.36 dB.

This thesis focuses mainly on the potential, accuracy, and limitations of AGB retrieval from multi-frequency SAR. Furthermore, multispectral RapidEye and multi-temporal airborne LiDAR measurements were evaluated, whereby SAR was most intensively investigated. Due to insufficient field inventory plots within SAR images, LiDAR based AGB estimations were used to examine the potential of TerraSAR-X (X-band) VV and ALOS PALSAR HV polarized data for AGB retrieval. This upscaling from field inventory derived AGB to LiDAR estimations provided numerous AGB reference data over the whole biomass range from woody regrowth to mature pristine forest, including

the spatial variation. This reference dataset offered a powerful basis for SAR analyses in terms of sufficient data for AGB model calibration and validation. Multi-temporal SAR imagery proved to be more accurate for AGB retrieval than mono-temporal imagery as the influences of extreme climatic conditions (e.g. heavy rainfall) are compensated. The study further revealed that AGB can be estimated with higher accuracy if TerraSAR-X and ALOS PALSAR data are combined than using only single-frequency data, i.e. either TerraSAR-X or ALOS PALSAR. The advantage of the synergistic use is the combination of the different penetration depths of the SAR signals into the vegetation. The multi-temporal combined AGB model saturated at approximately 300 t/ha. Based on the results achieved so far, a comparison of methods for AGB retrieval based on multi-temporal combined TerraSAR-X and ALOS PALSAR imagery was carried out. Multivariate linear regression (MLR), artificial neural network (ANN) and support vector regression (SVR) models were examined. Considering not only statistical measures but also large scale application, ANN proved to be a superior method to predict AGB. Upon closer analysis, the ANN models turned out to require plenty of AGB reference data for calibration. Further field inventories had been collected and were now directly linked to satellite signals. This reference data set was not suitable to apply ANNs. Thus, regression modeling was evaluated to estimate AGB in further analyses. AGB derived from field inventory measurements was correlated with multi-temporal TerraSAR-X HH, RADARSAT-2 (C-band) HH/HV, and ALOS PALSAR HH/HV polarized backscatter. Using directly field inventory derived AGB values instead of an upscaled reference dataset, a smaller grid size (40 m instead of 100 m) had was used because of the similarity to the size of the largest field inventory plot. No significant correlation between AGB and RADARSAT-2 HH and HV, and ALOS PALSAR HH polarized backscatter was retrieved. The regression modeling of TerraSAR-X HH polarized data and field inventory AGB resulted in a higher coefficient of determination (r^2=0.51) than the correlation between TerraSAR-X VV polarized imagery and LiDAR derived AGB (r^2=0.46). Furthermore, the regression modeling of ALOS PALSAR HV polarized backscatter and LiDAR derived AGB was more accurate (r^2=0.71) than using field inventory derived AGB (r^2=0.68). These results reveal that 1) TerraSAR-X HH polarized backscatter is more accurate for AGB estimation than TerraSAR-X VV polarized backscatter, and 2) AGB estimations with a spatial resolution of 100 m derived from LiDAR upscaled AGB reference data are more

accurate than AGB predictions with a resolution of 40 m derived from field inventory AGB values. In general, the resolution of AGB estimation influences the accuracy, the coarser the resolution, the more accurate are the predicted values (Mascaro et al. 2011b). Additionally, the upscaling of the AGB reference dataset includes error propagation. Hence, an evaluation of AGB estimations of the same resolution based on either upscaled or field inventory derived values would be important to conclude if numerous upscaled AGB reference data (including error propagation) outperform field inventory derived AGB values.

Furthermore, optical RapidEye imagery was analyzed for the capability to retrieve AGB and compared to SAR derived estimations. Spectral mixture analysis (SMA) was applied to obtain the amount of green vegetation (GV), non-photosynthetic vegetation (NPV) and soil in each pixel. The study revealed that AGB estimations based on RapidEye matched fractions are more accurate (r^2=0.92) than derived from multi-temporal combined TerraSAR-X and ALOS PALSAR data (r^2=0.68). AGB loss caused by small scale selective logging activities was visible within RapidEye derived AGB estimations, although the matched fractions saturated around 100 – 150 t/ha.

Airborne LiDAR measurements have already proven to allow very accurate AGB estimations during the upscaling of the AGB reference dataset for the SAR analyses. In a last step, multi-temporal airborne LiDAR tracks were investigated for the capability to monitor small scale dynamics in AGB and canopy height with a special focus on unaffected, selective logged and burned peat swamp forests. The effect of different point densities was evaluated first and it revealed no influence on the analyses when treated as two independent assessments. Accurate AGB regression models basing on LiDAR derived height histograms were developed for the years 2007 (r^2=0.77, n=79) and 2011 (r^2=0.81, n=53) taking also the different point densities into account. No constraint of saturation was detected in the higher biomass range. Unaffected peat swamp forests accumulated on average 20 t/ha and the canopy height increased by 2.3 m over this four year time period. Illegal selective logged forests lost on average 55 t/ha within 30 m and 42 t/ha within 50 m of detected logging trails, although the canopy height increased by 0.5 m and 1.0 m, respectively. The discrepancy between AGB loss and canopy height increase is explained by fast regrowth of vegetation in height with thin trunks thereby slowly accumulating AGB. Burned forests lost approximately 92% of the initial biomass. The results demonstrate the great potential of

airborne LiDAR measurements to monitor even small scale changes in AGB and canopy height with high accuracy.

2. Benefits and constraints of different sensors for AGB estimation

In this thesis, data of different sensors, namely SAR, optical, and airborne LiDAR were used to retrieve AGB of Indonesian tropical peat swamp forests. This chapter evaluates the benefits and constraints of the different sensors for AGB estimation.

The capability of SAR signals to penetrate clouds, haze or smoke is particularly advantageous in the frequently clouded tropics. SAR backscatter is generally sensitive to moisture. However, the use of multi-temporal SAR data compensates extreme climatic conditions, although annual variability due to extreme dry or wet years (particularly influenced by El Niño and La Niña periods) may remain. AGB estimation based on SAR is affected by saturation in the higher biomass ranges. In general, the saturation level strongly depends on SAR frequency and polarization, forest structure, and ground conditions (Lu 2006).

The acquisition of optical imagery is restrained by the frequent cloud cover in the tropics and is dependent on daylight. AGB estimations based on optical imagery are also affected by saturation in higher biomass ranges. High resolution RapidEye data proved to be more accurate than SAR data, especially when monitoring AGB loss due to logging activities. However, the saturation level of RapidEye unmixed fractions is with 100 – 150 t/ha lower than the saturation of SAR backscatter.

LiDAR does not penetrate clouds but has the unique capability to determine the three-dimensional structure of the vegetation in great detail (Goetz et al. 2009). LiDAR derived AGB estimations are widely based on airborne measurements, as only few LiDAR instruments operate from satellite platforms. Airborne LiDAR acquisition is very expensive and requires sophisticated technical equipment. In this thesis, airborne LiDAR derived AGB estimations yielded the most accurate predictions without the constraint of saturation in the higher biomass range. Even small scale changes in AGB, e.g. felling of one or more trees, could be monitored with high accuracy.

Regardless from which sensor AGB estimations are derived, there always exists a trade-off between costs, spatial extent, resolution, and accuracy. Nevertheless, it is very important to keep in mind that not always all requirements can be met. Other difficulties for monitoring long term AGB dynamics are the availability of repetitive acquisitions

and the comparability of multi-temporal datasets because the characteristics and conditions of vegetation are rarely stable.

3. Future research

Especially in the context of REDD+ and other climate change mitigation mechanisms, the importance of accurate carbon stock estimations of tropical forests is increasing. New technologies and satellites will provide opportunities for more accurate AGB estimations in future. For example, the ICESat-2 satellite is planned to be launched in 2015 and the ALOS-2 satellite with the PALSAR-2 sensor onboard in 2013. These satellites hold out the prospect of data continuity.

Irrespective of the sensor and its characteristics, the accuracy of AGB estimations depends on several other important factors which should be considered for future AGB monitoring. A major research topic is the correct choice of allometric equation to calculate AGB from field inventories. Several allometric equations have been developed for tropical forests (Chave et al. 2005; FAO 1997; IPCC 2006). Up to date, no allometric equation has been developed for tropical peat swamp forests. To generate one from destructive sampling would help to decrease the bias from generic models. The quality and quantity of field inventory plots emerged to be another crucial factor for both model calibration and validation. Ideally, plots are randomly distributed over the whole biomass range from woody regrowth to pristine mature forests. This is hardly possible due to the inaccessibility of tropical forests which would result in high field inventory costs. Furthermore, not all biomass ranges are equally distributed over the study area, for example regrowing areas containing biomass between 50 t/ha and 100 t/ha are hard to find and to access within the study area. Additionally, the time gap between field inventories and remote sensing data must be considered due to a potential regrowth or degradation of the vegetation. Furthermore, the quality and resolution of remote sensing data also influences the accuracy of AGB estimations.

This thesis emphasizes the importance to identify the needs, requirements, and capabilities of AGB estimations at the initial stage.

REFERENCES

Achard F., Eva H.D., Stibig H.J., Mayaux P., Gallego J., Richards T. et al. (2002) Determination of deforestation rates of the world's humid tropical forests. *Science,* **297,** pp. 999 - 1002.

Adams J.B., Smith M.O., and Johnson P.E. (1986) Spectral Mixture Modeling - A New Analysis of Rock and Soil Types at the Viking Lander-1 Site. *Journal of Geophysical Research-Solid Earth and Planets,* **91,** pp. 8098 - 8112.

Amini J. and Sumantyo J.T.S. (2009) Employing a Method on SAR and Optical Images for Forest Biomass Estimation. *IEEE Transactions on Geoscience and Remote Sensing,* **47,** pp. 4020 - 4026.

Asner G.P., Powell G.V.N., Mascaro J., Knapp D.E., Clark J.K., Jacobson J. et al. (2010) High-resolution forest carbon stocks and emissions in the Amazon. *Proceedings of the National Academy of Sciences of the United States of America,* **107,** pp. 16738 - 16742.

Asner G.P. (2011) Painting the world REDD: addressing scientific barriers to monitoring emissions from tropical forests. *Environmental Research Letters,* **6,** pp. 1 - 3.

Asner G.P., Knapp D.E., Balaji A., and Paez-Acosta G. (2009) Automated mapping of tropical deforestation and forest degradation: CLASlite. *Journal of Applied Remote Sensing,* **3,** pp. 1 - 24.

Asner G.P., Mascaro J., Muller-Landau H.C., Vieilledent G., Vaudry R., Rasamoelina M. et al. (2012) A universal airborne LiDAR approach for tropical forest carbon mapping. *Oecologia,* **168,** pp. 1147 - 1160.

Austin J.M., Mackey B.G., and Van Niel K.P. (2003) Estimating forest biomass using satellite radar: an exploratory study in a temperate Australian Eucalyptus forest. *Forest Ecology and Management,* **176,** pp. 575 - 583.

Avitabile V., Baccini A., Friedl M.A., and Schmullius C. (2012) Capabilities and limitations of Landsat and land cover data for aboveground woody biomass estimation of Uganda. *Remote Sensing of Environment,* **117,** pp. 366 - 380.

Aziz H.K. and White K. (2003) Using mimics to model L-band SAR backscatter from a peat swamp forest. *Journal of Tropical Forest Science,* **15,** pp. 546 - 556.

Baccini A., Goetz S., Walker W., Laporte N., Sun M., Sulla-Menashe D. et al. (2012) Estimated carbon dioxide emissions from tropical deforestation improved by carbon-density maps. *Nature Climate Change,* **2,** pp. 182 - 185.

Baccini A., Laporte N., Goetz S.J., Sun M., and Dong H. (2008) A first map of tropical Africa's above-ground biomass derived from satellite imagery. *Environmental Research Letters,* **3,** pp. 9 - 17.

Ballhorn U., Jubanski J., and Siegert F. (2011) ICESat/GLAS Data as a measurement tool for peatland topography and peat swamp forest biomass in Kalimantan, Indonesia. *Remote Sensing,* **3,** pp. 1957 - 1982.

Ballhorn U., Siegert F., Mason M., and Limin S. (2009) Derivation of burn scar depths and estimation of carbon emissions with LIDAR in Indonesian peatlands. *Proceedings of the National Academy of Sciences of the United States of America,* **106,** pp. 21213 - 21218.

Bater C.W., Wulder M.A., Coops N.C., Nelson R.F., Hilker T., and Naesset E. (2011) Stability of sample-based scanning-LiDAR-derived vegetation metrics for forest monitoring. *IEEE Transactions on Geoscience and Remote Sensing,* **49,** pp. 2385 - 2392.

Baup F., Mougin E., Hiernaux P., Lopes A., De Rosnay P., and Chenerie I. (2007) Radar signatures of Sahelian surfaces in Mali using ENVISAT-ASAR data. *IEEE Transactions on Geoscience and Remote Sensing,* **45,** pp. 2354 - 2363.

Berry N.J., Phillips O.L., Lewis S.L., Hill J.K., Edwards D.P., Tawatao N.B. et al. (2010) The high value of logged tropical forests: lessons from northern Borneo. *Biodiversity and Conservation,* **19,** pp. 985 - 997.

Bitterlich W. (1951) The angle counting sampling. *Zentralblatt für die gesamte Forst- und Holzwirtschaft,* **71,** pp. 191 - 205.

Boehm H.D.V. and Siegert F. (2004) The impact of logging and land use change in Central Kalimantan, Indonesia. *International Peat Journal,* **12,** pp. 3 - 10.

Boehm V., Liesenberg V., Sweda T., Tsuzuki H., and Limin S.H. (2012) Multi-temporal airborne LiDAR-surveys in 2007 and 2011 over tropical peat swamp forest environments in Central Kalimantan, Indonesia. *14th International Peat Congress, Stockholm, Sweden, 3-8 June.*

Boettcher H., Eisbrenner K., Fritz S., Kindermann G., Kraxner F., McCallum I. et al. (2009) An assessment of monitoring requirements and costs of 'Reduced Emissions from Deforestation and Degradation'. *Carbon Balance and Management,* **4,** pp. 1 - 14.

Boyd D.S., Foody G.M., and Curran P.J. (1999) The relationship between the biomass of Cameroonian tropical forests and radiation reflected in middle infrared wavelengths (3.0-5.0 mu m). *International Journal of Remote Sensing,* **20,** pp. 1017 - 1023.

Brown S. (1997) Estimation biomass and biomass change of tropical forests: a primer. *FAO Forestry Paper,* **134,** pp. 1 - 55.

Byrne K.A., Chojnicki B., Christensen T.R., Drösler M., Freibauer A., Friborg T., Frolking S., Lindroth A., Mailhammer J., Malmer N., Selin P., Turunen J., and Valentini R. (2004) EU peatlands: Current carbon stocks and trace gas fluxes. *Carbo GHG Europe, Report 4/2004.*

Campbell B.M. (2009) Beyond Copenhagen: REDD plus, agriculture, adaptation strategies and poverty. *Global Environmental Change-Human and Policy Dimensions,* **19,** pp. 397 - 399.

Camps-Valls G., Bruzzone L., Rojo-Alvarez J.L., and Melgani F. (2006) Robust support vector regression for biophysical variable estimation from remotely sensed images. *IEEE Geoscience and Remote Sensing Letters,* **3,** pp. 339 - 343.

Camps-Valls G., Munoz-Mari J., Gomez-Chova L., Richter K., and Calpe-Maravilla J. (2009) Biophysical Parameter Estimation With a Semisupervised Support Vector Machine. *IEEE Geoscience and Remote Sensing Letters,* **6,** pp. 248 - 252.

Castro K., Sanchez-Azofeifa G., and Rivard B. (2003) Monitoring secondary tropicals forests using space-borne data: implications for Central America. *International Journal of Remote Sensing,* **24,** pp. 1853 - 1894.

Chang C.-C. and Lin C.-J. (2001) LIBSVM: a Library for Support Vector Machines. *Software available at http://www.csie.ntu.edu.tw/~cjlin/libsvm.*

Chave J., Andalo C., Brown S., Cairns M.A., Chambers J.Q., Eamus D. et al. (2005) Tree allometry and improved estimation of carbon stocks and balance in tropical forests. *Oecologia,* **145,** pp. 87 - 99.

Chen W.J., Blain D., Li J.H., Keohler K., Fraser R., Zhang Y. et al. (2009) Biomass measurements and relationships with Landsat-7/ETM+ and JERS-1/SAR data over Canada's western sub-arctic and low arctic. *International Journal of Remote Sensing,* **30,** pp. 2355 - 2376.

Chudnoff M. (1984) Tropical Timbers of the World. *Agriculture Handbook 607,* US Department of Agriculture, Forest Service, Forest Product Labratory: Madison, WI, USA.

CKPP (2008) Provisional Report of the Central Kalimantan Peatland Project. *CKPP Consortium, Nov 2008, Palangka Raya, Indonesia, p 72. http://www.ckpp.org.*

Clark M.L., Roberts D.A., Ewel J.J., and Clark D.B. (2011) Estimation of tropical rain forest aboveground biomass with small-footprint lidar and hyperspectral sensors. *Remote Sensing of Environment,* **115,** pp. 2931 - 2942.

Clements T. (2010) Reduced Expectations: the political and institutional challenges of REDD. *Oryx,* **44,** pp. 309 - 310.

Couwenberg J., Dommain R., and Joosten H. (2010) Greenhouse gas fluxes from tropical peatlands in south-east Asia. *Global Change Biology,* **16,** pp. 1715 - 1732.

CPC (2009) Climate Prediction Center. *NOAA National Weather Service. http://cpc.noaa.gov.*

DeFries R., Achard F., Brown S., Herold M., Murdiyarso D., Schlamadinger B. et al. (2007) Earth observations for estimating greenhouse gas emissions from deforestation in developing countries. *Environmental Science & Policy,* **10,** pp. 385 - 394.

Del Frate F. and Solimini D. (2004) On neural network algorithms for retrieving forest biomass from SAR data. *IEEE Transactions on Geoscience and Remote Sensing,* **42,** pp. 24 - 34.

Dobson M.C., Pierce L., McDonald K., and Sharik T. (1991) Seasonal change in radar backscatter from mixed conifer and hardwood forests in northern Michigan. *International Geoscience and Remote Sensing Symposium (IGARSS),* **1-4,** pp. 1121 - 1124.

Dobson M.C., Ulaby F.T., Letoan T., Beaudoin A., Kasischke E.S., and Christensen N. (1992) Dependence of Radar Backscatter on Coniferous Forest Biomass. *IEEE Transactions on Geoscience and Remote Sensing,* **30,** pp. 412 - 415.

Dubayah R., Sheldon S., Clark D., Hofton M., Blair J., Hurtt G. et al. (2010) Estimation of tropical forest height and biomass dynamics using lidar remote sensing at La Selva, Costa Rica. *Journal of Geophysical Research-Biogeosciences,* **115,**

Dubois P.C., Vanzyl J., and Engman T. (1995) Measuring Soil-Moisture with Imaging Radars. *IEEE Transactions on Geoscience and Remote Sensing,* **33,** pp. 915 - 926.

Duncanson L., Niemann K., and Wulder M. (2010) Estimating forest canopy height and terrain relief from GLAS waveform metrics. *Remote Sensing of Environment,* **114,** pp. 138 - 154.

Eckert S. (2012) Improved Forest Biomass and Carbon Estimations Using Texture Measures from WorldView-2 Satellite Data. *Remote Sensing,* **4,** pp. 810 - 829.

Edwards D.P., Koh L.P., and Laurance W.F. (2012) Indonesia's REDD+ pact: Saving imperilled forests or business as usual? *Biological Conservation,* **151,** pp. 41 - 44.

Englhart S., Keuck V., and Siegert F. (2011) Aboveground biomass retrieval in tropical forests - The potential of combined X- and L-band SAR data use. *Remote Sensing of Environment,* **115,** pp. 1260 - 1271.

Englhart S., Keuck V., and Siegert F. (2012) Modeling Aboveground Biomass in Tropical Forests Using Multi-Frequency SAR Data-A Comparison of Methods. *IEEE Journal of Selected Topics in Applied Earth Observation and Remote Sensing,* **5,** pp. 298 - 306.

Envisat (2007) ASAR Product Handbook. *European Space Agency. http://envisat.esa.int/handbooks/asar.*

FAO (1997) Estimating biomass and biomass change of tropical forests: a primer. *FAO Forestry Paper - 134, Food and Agriculture Organization (FAO), Rome, Italy.*

FAO (2000) Global Forest Resources Assessment 2000. *FAO Forestry Paper - 140, Food and Agriculture Organization (FAO), Rome, Italy.*

FAO (2006) Global Forest Ressources Assessment 2005. *FAO Forestry Paper No. 147, UNFAO, Rome, Italy.*

FAO (2009) State of the World´s Forests 2009. *Food and Agriculture Organization of the United Nations, Rome, Italy, http://www.fao.org/docrep/011/i0350e/i0350e00.htm.*

Felton A.M., Engstrom L.M., Felton A., and Knott C.D. (2003) Orangutan population density, forest structure and fruit availability in hand-logged and unlogged peat swamp forests in West Kalimantan, Indonesia. *Biological Conservation,* **114,** pp. 91 - 101.

FIRMS (2009) Fire Information for Resource Management System. *University of Maryland at http://maps.geog.umd.edu/firms.*

Foody G.M., Boyd D.S., and Cutler M.E.J. (2003) Predictive relations of tropical forest biomass from Landsat TM data and their transferability between regions. *Remote Sensing of Environment,* **85,** pp. 463 - 474.

Foody G.M., Cutler M.E., McMorrow J., Pelz D., Tangki H., Boyd D.S. et al. (2001) Mapping the biomass of Bornean tropical rain forest from remotely sensed data. *Global Ecology and Biogeography,* **10,** pp. 379 - 387.

Franke J., Navratil P., Keuck V., Peterson K., and Siegert F. (2012) Monitoring fire and selective logging activities in tropical peat swamp forests. *IEEE Journal of Selected Topics in Applied Earth Observation and Remote Sensing,* **PP,** pp. 1 - 10.

Freitas S.R., Mello M.C.S., and Cruz C.B.M. (2005) Relationships between forest structure and vegetation indices in Atlantic Rainforest. *Forest Ecology and Management,* **218,** pp. 353 - 362.

Fritz T. (2009) TerraSAR-X Ground Segment Basic Product Specification Document. *Doc: TX-GS-DD-3302, http://sss.terrasar-x.dlr.de/pdfs/TX-GS-DD-3302.pdf.*

Furukawa Y., Inubushi K., Ali M., Itang A.M., and Tsuruta H. (2005) Effect of changing groundwater levels caused by land-use changes on greenhouse gas fluxes from tropical peat lands. *Nutrient Cycling in Agroecosystems,* **71,** pp. 81 - 91.

Gama F.F., dos Santos J.R., and Mura J.C. (2010) Eucalyptus biomass and volume estimation using interferometric and polarimetric SAR data. *Remote Sensing,* **2,** pp. 939 - 956.

Gibbs H.K., Brown S., Niles J.O., and Foley J.A. (2007) Monitoring and estimating tropical forest carbon stocks: making REDD a reality. *Environmental Research Letters,* **2,** pp. 1 - 13.

Gleason C.J. and Im J. (2011) A review of remote sensing of forest biomass and biofuel: options for small-area applications. *GIScience & Remote Sensing,* **48,** pp. 141 - 170.

Goetz S. and Dubayah R. (2011) Advances in remote sensing technology and implications for measuring and monitoring forest carbon stocks and change. *Carbon Management,* **2,** pp. 231 - 244.

Goetz S.J., Baccini A., Laporte N.T., Johns T., Walker W., Kellndorfer J. et al. (2009) Mapping and monitoring carbon stocks with satellite observations: a comparison of methods. *Carbon Balance and Management,* **4,** pp. 1 - 7.

GOFC-GOLD (2011) A sourcebook of methods and procedures for monitoring and reporting anthropogenic greenhouse gas emissions and removals caused by deforestation, gains and losses of carbon stocks in forests remaining forests, and forestation. *GOFC-GOLD Report version COP17-1; GOFC-GOLD Project Office, Natural Resources Canada, Alberta, Canada.*

Grassi G., Monni S., Federici S., Achard F., and Mollicone D. (2008) Applying the conservativeness principle to REDD to deal with the uncertainties of the estimates. *Environmental Research Letters,* **3,** pp. 1 - 12.

Grover K., Quegan S., and Freitas C.D. (1999) Quantitative estimation of tropical forest cover by SAR. *IEEE Transactions on Geoscience and Remote Sensing,* **37,** pp. 479 - 490.

Hadisuparto H. (1996) The effects of timber harvesting and forest conversion on peat swamp forest dynamics and environment in West Kalimantan. *Tropical Rainforest Research - Current Issues,* pp. 411 - 415.

Hamdan O., Aziz H., and bd Rahman K. (2011) Remotely Sensed L-Band Sar Data for Tropical Forest Biomass Estimation. *Journal of Tropical Forest Science,* **23,** pp. 318 - 327.

Hansen M.C., Stehman S.V., Potapov P.V., Arunarwati B., Stolle F., and Pittman K. (2009) Quantifying changes in the rates of forest clearing in Indonesia from 1990 to 2005 using remotely sensed data sets. *Environmental Research Letters,* **4,** pp. 1 - 12.

Hashim H., Busu I., Sim S.H., Jong T., Wan Kadir W., and Salam N. (2002) Soil moisture, depth of water table and peat decomposition in Sadong Simunjan river basin, Sarawak using AIRSAR/TOPSAR data. *3rd Malaysian Remote Sensing & GIS Conference and Exhibition, Kuala Lumpur, Malaysia.*

Hashimotio T., Kojima K., Tange T., and Sasaki S. (2000) Changes in carbon storage in fallow forests in the tropical lowlands of Borneo. *Forest Ecology and Management,* **126,** pp. 331 - 337.

Helmer E.H., Lefsky M.A., and Roberts D.A. (2009) Biomass accumulation rates of Amazonian secondary forest and biomass of old-growth forests from Landsat time series and the Geoscience Laser Altimeter System. *Journal of Applied Remote Sensing,* **3,** pp. 1 - 31.

Henderson F.M. and Lewis A.J. (1998) Principles and Applications of Imaging Radar - Manual of Remote Sensing. *John Wiley & Sons, Somerset, NJ, United States.*

Herold M. and Johns T. (2007) Linking requirements with capabilities for deforestation monitoring in the context of the UNFCCC-REDD process. *Environmental Research Letters,* **2,** pp. 1 - 7.

Hiratsuka M., Toma T., Diana R., Hadriyanto D., and Morikawa Y. (2006) Biomass recovery of naturally regenerated vegetation after the 1998 forest fire in East Kalimantan, Indonesia. *Jarq-Japan Agricultural Research Quarterly,* **40,** pp. 277 - 282.

Hoekman D.H. (2007) Satellite radar observation of tropical peat swamp forest as a tool for hydrological modelling and environmental protection. *Aquatic Conservation-Marine and Freshwater Ecosystems,* **17,** pp. 265 - 275.

Hooijer A., Page S., Canadell J.G., Silvius M., Kwadijk J., Wosten H. et al. (2010) Current and future CO_2 emissions from drained peatlands in Southeast Asia. *Biogeosciences,* **7,** pp. 1505 - 1514.

Hooijer A., Page S., Jauhiainen J., Lee W., Lu X., X, Idris A. et al. (2012) Subsidence and carbon loss in drained tropical peatlands. *Biogeosciences,* **9,** pp. 1053 - 1071.

Hooijer A., Silvius M., Wösten H., and Page S. (2006) PEAT-CO2, Assessment of CO2 emissions from drained peatlands in SE Asia. *Delft Hydraulics report Q3943.*

Höper H. (2007) Freisetzung klimarelevanter Gase aus deutschen Mooren. *Telma,* **37,** pp. 85 - 116.

Hoscilo A., Page S.E., Tansey K.J., and Rieley J.O. (2011) Effect of repeated fires on land-cover change on peatland in southern Central Kalimantan, Indonesia, from 1973 to 2005. *International Journal of Wildland Fire,* **20,** pp. 578 - 588.

Hudak A.T., Strand E.K., Vierling L.A., Byrne J.C., Eitel J.U.H., Martinuzzi S. et al. (2012) Quantifying aboveground forest carbon pools and fluxes from repeat LiDAR surveys. *Remote Sensing of Environment,* **123,** pp. 25 - 40.

Hughes R.F., Kauffman J.B., and Jaramillo V.J. (1999) Biomass, carbon, and nutrient dynamics of secondary forests in a humid tropical region of Mexico. *Ecology,* **80,** pp. 1892 - 1907.

Imhoff M.L. (1995) Radar Backscatter and Biomass Saturation - Ramifications for Global Biomass Inventory. *IEEE Transactions on Geoscience and Remote Sensing,* **33,** pp. 511 - 518.

Intergovernmental Panel on Climate Change (2006) 2006 IPCC guidelines for national greenhouse gas inventories. *Prepared by the National Greenhouse Gas Inventories Programme, Eggleston, H.S., Buendia, L., Miwa, k., Ngara, T.and Tanabe, K. (eds). Published: IGES, Japan.*

Intergovernmental Panel on Climate Change. (2006) 2006 IPCC guidelines for national greenhouse gas inventories. *Prepared by the National Greenhouse Gas Inventories Programme, Eggleston, H.S., Buendia, L., Miwa, k., Ngara, T.and Tanabe, K. (eds). Published: IGES, Japan.*

IPCC (2006) IPCC Guidelines for National Greenhouse Gas Inventories. *Prepared by the National Greenhouse Gas Inventories Programme, Eggleston, H.S., Buendia, L., Miwa, k., Ngara, T.and Tanabe, K.(Eds).Published: IGES, Japan.*

Jaenicke J., Englhart S., and Siegert F. (2011) Monitoring the effect of restoration measures in Indonesian peatlands by radar satellite imagery. *Journal of Environmental Management,* **92,** pp. 630 - 638.

Jaenicke J., Rieley J.O., Mott C., Kimman P., and Siegert F. (2008) Determination of the amount of carbon stored in Indonesian peatlands. *Geoderma,* **147,** pp. 151 - 158.

Jaenicke J., Wosten H., Budiman A., and Siegert F. (2010) Planning hydrological restoration of peatlands in Indonesia to mitigate carbon dioxide emissions. *Mitigation and Adaptation Strategies for Global Change,* **15,** pp. 223 - 239.

Jauhiainen J., Jaya A., Inoue T., Heikkinen J., and Vasander H. (2004) Carbon balance in managed tropical peat in Central Kalimantan. *Proceedings of the 12thInternationalPeat Congress, Tampere, Finnland,* 653 - 659.

Jauhiainen J., Limin S., Silvennoinen H., and Vasander H. (2008) Carbon Dioxide and Methane Fluxes in Drained Tropical Peat Before and After Hydrological Restoration. *Ecology,* **89,** pp. 3503 - 3514.

Jenkins R.B. (2012) Airborne laser scanning for vegetation structure quantification in a south east Australian scrubby forest-woodland. *Austral Ecology,* **37,** pp. 44 - 55.

Jubanski J., Ballhorn U., Kronseder K., Franke J., and Siegert F. (2012) Detection of large above ground biomass variability in lowland forest ecosystems by airborne LiDAR. *Biogeosciences Discuss.,* **9,** pp. 11815 - 11842.

Jung J. and Crawford M.M. (2012) Extraction of features from LIDAR waveform data for characterizing forest structure. *IEEE Geoscience and Remote Sensing Letters,* **9,** pp. 492 - 496.

Kellner J.R., Clark D.B., and Hubbell S.P. (2009) Pervasive canopy dynamics produce short-term stability in a tropical rain forest landscape. *Ecology Letters,* **12,** pp. 155 - 164.

Koch B. (2010) Status and future of laser scanning, synthetic aperture radar and hyperspectral remote sensing data for forest biomass assessment. *ISPRS Journal of Photogrammetry and Remote Sensing,* **65,** pp. 581 - 590.

Koh P.K., Butler R.A., and Bradshaw C.J. (2009) Conversion of Indonesia's peatlands. *Frontiers in Ecology and the Environment,* **7,** pp. 238 - 238.

Kronseder K., Ballhorn U., Böhm V., and Siegert F. (2012) Aboveground biomass estimation across forest types at different degradation levels in Central Kalimantan using LiDAR data. *International Journal of Applied Earth Observation and Geoinformation,* **18,** pp. 37 - 48.

Kuplich T.M., Curran P.J., and Atkinson P.M. (2005) Relating SAR image texture to the biomass of regenerating tropical forests. *International Journal of Remote Sensing,* **26,** pp. 4829 - 4854.

Kvalseth T.O. (1985) Cautionary Note About R2. *American Statistician,* **39,** pp. 279 - 285.

Langner A., Miettinen J., and Siegert F. (2007) Land cover change 2002-2005 in Borneo and the role of fire derived from MODIS imagery. *Global Change Biology,* **13,** pp. 2329 - 2340.

Langner A. and Siegert F. (2009) Spatiotemporal fire occurrence in Borneo over a period of 10 years. *Global Change Biology,* **15,** pp. 48 - 62.

Lasco R.D. (2002) Forest carbon budgets in Southeast Asia following harvesting and land cover change. *Science in China Series C-Life Sciences,* **45,** pp. 55 - 64.

Laur H., Bally P., Meadows P., Sanchez J., Schaettler B., Lopinto E., and Esteban D. (1998) Derivation of the backscattering coefficient ó0 in ESA ERS SAR PRI products. *ESA Document No. ES-TN-RS-PM-HL09, Issue 2, Rev. 5b.*

Le Quere C., Raupach M.R., Canadell J.G., Marland G., Bopp L., Ciais P. et al. (2009) Trends in the sources and sinks of carbon dioxide. *Nature Geoscience,* **2,** pp. 831 - 836.

Le Toan T., Beaudoin A., Riom J., and Guyon D. (1992) Relating Forest Biomass to Sar Data. *IEEE Transactions on Geoscience and Remote Sensing,* **30,** pp. 403 - 411.

Le Toan T., Picard G., Martinez J.M., Melon P., and Davidson M. (2001) On the relationship between Radar Measurements and Forest Structure and Biomass. *3rd International Symposium "Retrieval of Bio-and Geophysical Parameters from SAR Data for Land Applications", Sheffield, UK.*

Lefsky M.A., Cohen W.B., Harding D.J., Parker G.G., Acker S.A., and Gower S.T. (2002) Lidar remote sensing of above-ground biomass in three biomes. *Global Ecology and Biogeography,* **11,** pp. 393 - 399.

Lefsky M.A., Harding D.J., Keller M., Cohen W.B., Carabajal C.C., Espirito-Santo F.D. et al. (2005) Estimates of forest canopy height and aboveground biomass using ICESat. *Geophysical Research Letters,* **32,** pp. 1 - 4.

Li H., Mausel P., Brondizio E., and Deardorff D. (2010) A framework for creating and validating a non-linear spectrum-biomass model to estimate the secondary succession biomass in moist tropical forests. *ISPRS Journal of Photogrammetry and Remote Sensing,* **65,** pp. 241 - 254.

Lillesand T.M., Kiefer R.W., and Chipman J.W. (2008) Remote Sensing and Image Interpretation. *John Wiley & Sons, Inc. Hoboken, United States.*

Lu D., Chen Q., Wang G., Moran E., Batistella M., Zhang M. et al. (2012) ABoveground Forest Biomass Estimation with Landsat and LiDAR Data and Uncertainty Analysis of the Estimates. *International Journal of Forestry Research,* **2012,** pp. 1 - 16.

Lu D. (2005) Integration of vegetation inventory data and Landsat TM image for vegetation classification in the western Brazilian Amazon. *Forest Ecology and Management,* **213,** pp. 369 - 383.

Lu D.S. (2006) The potential and challenge of remote sensing-based biomass estimation. *International Journal of Remote Sensing,* **27,** pp. 1297 - 1328.

Lu D.S., Batistella M., and Moran E. (2005) Satellite estimation of aboveground biomass and impacts of forest stand structure. *Photogrammetric Engineering and Remote Sensing,* **71,** pp. 967 - 974.

Lucas R.M., Mitchell A.L., Rosenqvist A., Proisy C., Melius A., and Ticehurst C. (2007) The potential of L-band SAR for quantifying mangrove characteristics and change: case studies from the tropics. *Aquatic Conservation-Marine and Freshwater Ecosystems,* **17,** pp. 245 - 264.

Luckman A., Baker J., Kuplich T.M., Yanasse C.D.F., and Frery A.C. (1997) A study of the relationship between radar backscatter and regenerating tropical forest biomass for spaceborne SAR instruments. *Remote Sensing of Environment,* **60,** pp. 1 - 13.

Luscombe A. (2009) Image Quality and Calibration of Radarsat-2. *2009 Ieee International Geoscience and Remote Sensing Symposium, Vols 1-5,* pp. 1008 - 1011.

MacKinnon K., Hatta G., Halim H., and Mangalik A. (1996) The Ecology of Indonesia Series: Volume III: The Ecology of Kalimantan. *Periplus Edition.*

Malhi Y., Baker T.R., Phillips O.L., Almeida S., Alvarez E., Arroyo L. et al. (2004) The above-ground coarse wood productivity of 104 Neotropical forest plots. *Global Change Biology,* **10,** pp. 563 - 591.

Mas J.F. and Flores J.J. (2008) The application of artificial neural networks to the analysis of remotely sensed data. *International Journal of Remote Sensing,* **29,** pp. 617 - 663.

Mascaro J., Asner G., Muller-Landau H., van Breugel M., Hall J., and Dahlin K. (2011a) Controls over aboveground forest carbon density on Barro Colorado Island, Panama. *Biogeosciences,* **8,** pp. 1615 - 1629.

Mascaro J., Detto M., Asner G.P., and Muller-Landau H.C. (2011b) Evaluating uncertainty in mapping forest carbon with airborne LiDAR. *Remote Sensing of Environment,* **115,** pp. 3770 - 3774.

Mazzei L., Sist P., Ruschel A., Putz F.E., Marco P., Pena W. et al. (2010) Above-ground biomass dynamics after reduced-impact logging in the Eastern Amazon. *Forest Ecology and Management,* **259,** pp. 367 - 373.

Miettinen J. and Liew S.C. (2012) Two decades of destruction in Southeast Asia's peat swamp forests. *Frontiers in Ecology and the Environment,* **10,** pp. 124 - 128.

Mitchard E., Saatchi S., Lewis S., Feldpausch T., Woodhouse I., Sonke B. et al. (2011) Measuring biomass changes due to woody encroachment and deforestation/degradation in a forest-savanna boundary region of central Africa using multi-temporal L-band radar backscatter. *Remote Sensing of Environment,* **115,** pp. 2861 - 2873.

Mitchard E., Saatchi S., White L., Abernethy K., Jeffery K., Lewis S. et al. (2012) Mapping tropical forest biomass with radar and spaceborne LiDAR in Lope National Park, Gabon: overcoming problems of high biomass and persistent cloud. *Biogeosciences,* **9,** pp. 179 - 191.

Mitchard E.T.A., Saatchi S.S., Woodhouse I.H., Nangendo G., Ribeiro N.S., Williams M. et al. (2009) Using satellite radar backscatter to predict above-ground woody biomass: A consistent relationship across four different African landscapes. *Geophysical Research Letters,* **36,** pp. 1 - 6.

Monnet J.M., Chanussot J., and Berger F. (2011) Support Vector Regression for the Estimation of Forest Stand Parameters Using Airborne Laser Scanning. *IEEE Geoscience and Remote Sensing Letters,* **8,** pp. 580 - 584.

Morrogh-Bernard H., Husson S., Page S.E., and Rieley J.O. (2003) Population status of the Bornean orang-utan (Pongo pygmaeus) in the Sebangau peat swamp forest, Central Kalimantan, Indonesia. *Biological Conservation,* **110,** pp. 141 - 152.

Mountrakis G., Im J., and Ogole C. (2011) Support vector machines in remote sensing: A review. *ISPRS Journal of Photogrammetry and Remote Sensing,* **66,** pp. 247 - 259.

Muhamad N.Z. and Rieley J.O. (2002) Management of tropical peatlands in Indonesia: mega reclamation project in Central Kalimantan. In: Rieley J.O. and Page S.E. (eds) *Peatlands for people: natural resource functions and sustainable management*. Proceedings of the International Symposium on tropical peatland, Jakarta, 22-23 August 2001, pp. 155 - 162.

Mundt J., Streutker D., and Glenn N. (2007) Partial umixing of hyperspectral imagery: theory and methods. *In: ASPRS Annual Conference, Tampa, Florida.*

Murdiyarso D., Hergoualc'h K., and Verchot L., V (2010) Opportunities for reducing greenhouse gas emissions in tropical peatlands. *Proceedings of the National Academy of Sciences of the United States of America,* **107,** pp. 19655 - 19660.

Muukkonen P. and Heiskanen J. (2005) Estimating biomass for boreal forests using ASTER satellite data combined with standwise forest inventory data. *Remote Sensing of Environment,* **99,** pp. 434 - 447.

Nichol J.E. and Sarker M. (2011) Improved Biomass Estimation Using the Texture Parameters of Two High-Resolution Optical Sensors. *IEEE Transactions on Geoscience and Remote Sensing,* **49,** pp. 930 - 948.

NOAA Climate Prediction Center (2012) Historical El Nino/La Nina episodes (1950-present). *http://www.cpc.ncep.noaa.gov/products/analysis_monitoring/ensostuff/ensoyears.shtml*.

Page S.E., Hoscilo A., Langner A., Tansey K., Siegert F., Limin S. et al. (2009a) Chapter 9: Tropical peatland fires in Southeast Asia. In: Cochrane M.A. (eds) *Tropical Fire Ecology: Climate Change, Land Use, and Ecosystems Dynamics*. Springer-Praxis, Berlin, pp. 263 - 287.

Page S.E., Rieley J.O., and Banks C.J. (2011) Global and regional importance of the tropical peatland carbon pool. *Global Change Biology,* **17,** pp. 798 - 818.

Page S.E., Rieley J.O., Shotyk O.W., and Weiss D. (1999) Interdependence of peat and vegetation in a tropical peat swamp forest. *Philosophical Transactions of the Royal Society of London Series B-Biological Sciences,* **354,** pp. 1885 - 1897.

Page S.E., Rieley J.O., and Wuest R. (2006) Lowland tropical peatlands of Southeast Asia. In: Martini I.P., Martinez Cortizas A., and Chesworth W. (eds) *Peatlands: Evolution and Records of Environmental and Climate Changes*. Elsevier, New York, USA, pp. 145 - 172.

Page S.E., Siegert F., Rieley J.O., Boehm H.D.V., Jaya A., and Limin S. (2002) The amount of carbon released from peat and forest fires in Indonesia during 1997. *Nature,* **420,** pp. 61 - 65.

Page S., Hoscilo A., Wosten H., Jauhiainen J., Silvius M., Rieley J. et al. (2009b) Restoration Ecology of Lowland Tropical Peatlands in Southeast Asia: Current Knowledge and Future Research Directions. *Ecosystems,* **12,** pp. 888 - 905.

Paloscia S., Pampaloni P., Pettinato S., Poggi P., and Santi E. (2005) The retieval of soil moisture from ENVISAT/ASAR data. *EARSeL eProceedings,* **4,** pp. 44 - 51.

Pandey U., Kushwaha S.P.S., Kachhwaha T.S., Kunwar P., and Dadhwal V.K. (2010) Potential of Envisat ASAR data for woody biomass assessment. *Tropical Ecology,* **51,** pp. 117 - 124.

Pearson T., Walker S., and Brown S. (2005) Sourcebook for Land Use, Land-use Change and Forestry Projects. *Winrock International: Little Rock, AR, USA.*

Pfeifer N., Stadler P., and Briese C. (2001) Derivation of digital terrain models in the SCOP++ environment. *In Proceedings of OEEPE Workshop on Airborne Laserscanning and Interferometric SAR for Detailed Digital Terrain Models, Stockholm, Sweden.*

Pinard M.A. and Putz F.E. (1996) Retaining forest biomass by reducing logging damage. *Biotropica,* **28,** pp. 278 - 295.

Posa M.R.C. (2011) Peat swamp forest avifauna of Central Kalimantan, Indonesia: Effects of habitat loss and degradation. *Biological Conservation,* **144,** pp. 2548 - 2556.

Posa M.R.C., Wijedasa L.S., and Corlett R.T. (2011) Biodiversity and Conservation of Tropical Peat Swamp Forests. *Bioscience,* **61,** pp. 49 - 57.

Rabe A., van der Linden S., and Hostert P. (2009a) imageSVM, version 2.0. *software available at: http://www2.hu-berlin.de/hurs/projects/imageSVM.php.*

Rabe A., van der Linden S., and Hostert P. (2009b) Simplifying Support Vector Machines for Regression analysis of hyperspectral imagery. *First Workshop an Hyperspectral Image and Signal Processing: Evolution in Remote Sensing (WHISPERS), 26-28 August 2009, Grenoble, France.*

Rauste Y. (2005) Multi-temporal JERS SAR data in boreal forest biomass mapping. *Remote Sensing of Environment,* **97,** pp. 263 - 275.

Read D., Beerling D., Cannell M., Cox P., Curran P., Grace J. et al. (2001) The role of land carbon sinks in mitigating global climate change. *Policy document, The Royal Society, London,* **10,** 1 - 27.

Richter R. (1997) Correction of atmospheric and topographic effects for high spatial resolution satellite imagery. *International Journal of Remote Sensing,* **18,** pp. 1099 - 1111.

Rieley J.O. and Page S. (2005) Wise Use of Tropical Peatlands: Focus on Southeast Asia. *www.restorpeat.alterra.wur.nl.*

Rieley J.O., Page S.E., Limin S.H., and Winarti S. (1997) The Peatland Resource of Indonesia and the Kalimantan Peat Swamp Forest Research Project. In: Rieley J.O. and Page S.E. (eds) *Biodiversity and Sustainability of Tropical Peatlands*. Samara Publishing Limited, Cardigan, United Kingdom. pp. 37 - 44.

Romshoo S. (2004) Radar remote sensing for monitoring of dynamic ecosystem processes related to biogeochemical exchanges in tropical peatlands. *Visual Geosciences,* **9,** pp. 9 - 28.

Rosenqvist A., Milne A., Lucas R., Imhoff M., and Dobson C. (2003) A review of remote sensing technology in support of the Kyoto Protocol. *Environmental Science & Policy,* **6,** pp. 441 - 455.

Rosich B., Meadows P., Monti-Guarnieri A., D'Aria D., Tranfaglia M., Santuari M., and Navas I. (2007) Review of ASAR performance and product quality evolution after 5 years of operations. *Proc. Envisat Symposium 2007, Montreux, Switzerland.*

Rumelhart D.E., Hinton G.E., and Williams R.J. (1986) Learning Representations by Back-Propagating Errors. *Nature,* **323,** pp. 533 - 536.

Ryan C.M., Hill T., Woollen E., Ghee C., Mitchard E., Cassells G. et al. (2012) Quantifying small-scale deforestation and forest degradation in African woodlands using radar imagery. *Global Change Biology,* **18,** pp. 243 - 257.

Saatchi S.S., Harris N.L., Brown S., Lefsky L., Mitchard E.T.A., Salas W. et al. (2011a) Benchmark map of forest carbon stocks in tropical regions across three continents. *Proceedings of the National Academy of Sciences of the United States of America,* **108,** pp. 9899 - 9904.

Saatchi S.S., Houghton R.A., Alvala R.C.D.S., Soares J.V., and Yu Y. (2007) Distribution of aboveground live biomass in the Amazon basin. *Global Change Biology,* **13,** pp. 816 - 837.

Saatchi S., Marlier M., Chazdon R.L., Clark D.B., and Russell A.E. (2011b) Impact of spatial variability of tropical forest structure on radar estimation of aboveground biomass. *Remote Sensing of Environment,* **115,** pp. 2836 - 2849.

Salmah Z. (1992) Water management in deep peat soils in Malaysia. *Dissertation, Silsoe College, Cranfield Institute of Technology, UK.*

Santos J.R., Araujo L.S., Kuplich T.M., Freitas C.C., Dutra L.V., and Sant'Anna S.J.S. (2006) Tropical forest biomass and its relationship with P-band SAR data. *Revista Brasileira de Cartografia,* **58,** pp. 37 - 42.

Sarker L.R. and Nichol J.E. (2011) Improved forest biomass estimates using ALOS AVNIR-2 texture indices. *Remote Sensing of Environment,* **115,** pp. 968 - 977.

Sarker M., Nichol J., Ahmad B., Busu I., and Rahman A.A. (2012) Potential of texture measurements of two-date dual polarization PALSAR data for the improvement of forest biomass estimation. *ISPRS Journal of Photogrammetry and Remote Sensing,* **69,** pp. 146 - 166.

Schutz B.E., Zwally H.J., Shuman C.A., Hancock D., and DiMarzio J.P. (2005) Overview of the ICESat Mission. *Geophysical Research Letters,* **32,** pp. 1 - 4.

Shepherd P.A., Rieley J.O., and Page S.E. (1997) The relationship between forest vegetation and peat characteristics in the upper catchment of Sungai Sebangau, Central Kalimantan. In: Rieley J.O. and Page S.E. (eds) *Biodiversity and Sustainability of Tropical Peatlands*. Samara Publishing Limited, Cardigan, United Kingdom. pp. 191 - 207.

Shimada M., Isoguchi O., Tadono T., and Isono K. (2009) PALSAR Radiometric and Geometric Calibration. *IEEE Transactions on Geoscience and Remote Sensing,* **47,** pp. 3915 - 3932.

Siegert F., Ruecker G., Hinrichs A., and Hoffmann A.A. (2001) Increased damage from fires in logged forests during droughts caused by El Nino. *Nature,* **414,** pp. 437 - 440.

Sloan S., Edwards D.P., and Laurance W.F. (2012) Does Indonesia's REDD+ moratorium on new concessions spare imminently threatened forests? *Conservation Letters,* **5,** pp. 222 - 231.

Smola A.J. and Schölkopf B. (2004) A tutorial on support vector regression. *Statistics and Computing,* **14,** pp. 199 - 222.

Soenen S.A., Peddle D.R., Hall R.J., Coburn C.A., and Hall F.G. (2010) Estimating aboveground forest biomass from canopy reflectance model inversion in mountainous terrain. *Remote Sensing of Environment,* **114,** pp. 1325 - 1337.

Solberg S., Astrup R., Gobakken T., Naesset E., and Weydahl D. (2010) Estimating spruce and pine biomass with interferometric X-band SAR. *Remote Sensing of Environment,* **114,** pp. 2353 - 2360.

Sorensen K.W. (1993) Indonesian Peat Swamp Forests and Their Role As A Carbon Sink. *Chemosphere,* **27,** pp. 1065 - 1082.

Souza C.M., Roberts D.A., and Cochrane M.A. (2005) Combining spectral and spatial information to map canopy damage from selective logging and forest fires. *Remote Sensing of Environment,* **98,** pp. 329 - 343.

Stahlhut M. and Rieley J. (2005) Remote sensing for monitoring vegetation and hydrology of tropical peat swamp forests: the relationship between radar backscatter and precipitation. *Proceedings of the International Symposium and Workshop on Tropical Peatland, Palangka Raya, Indonesia.*

Strack M. (2008) Peatlands and Climate Change. *International Peat Society, Jyväskylä, Finnland.*

Streck S., OSullivan R., Janson-Smith T., and Tarasofky R. (2008) Climate Change and Forests: Emering Policy and Market Opportunities. *Royal Institute of International Affairs, London, UK.*

Sun G.Q., Simonett D.S., and Strahler A.H. (1991) A Radar Backscatter Model for Discontinuous Coniferous Forests. *IEEE Transactions on Geoscience and Remote Sensing,* **29,** pp. 639 - 650.

Suryadiputra N., Dohong A., Waspodo R., Lubis I., Hasudungan F., and Wibisono I.T. (2005) A Guide to Blocking of Canals and Ditches in Conjunction with the Community. *Wetlands International - Indonesia Programme, Bogor, Indonesia.*

Sweda T., Tsuzuki H., Maeda Y., Boehm V., and Limin S.H. (2012) Above- and below-ground carbon budget of degraded tropical peatland revealed by multi-temporal airborne laser altimetry. *14th International Peat Congress, Stockholm, Sweden, 3-8 June.*

Takahashi T., Usup A., Hayasaka H., and Limin S.H. (2003) Estimation of ground water levels in a peat swamp forest as an index of peat/forest fire. *Proceedings of the International Symposium on Land Management and Biodiversity in Southeast Asia, Bali, Indonesia.*

Tangki H. and Chappell N.A. (2008) Biomass variation across selectively logged forest within a 225-km(2) region of Borneo and its prediction by Landsat TM. *Forest Ecology and Management,* **256,** pp. 1960 - 1970.

Treuhaft R.N., Goncalves F.G., Drake J.B., Chapman B.D., dos Santos J.R., Dutra L.V. et al. (2010) Biomass estimation in a tropical wet forest using Fourier transforms of profiles from lidar or interferometric SAR. *Geophysical Research Letters,* **37,**

Ulaby F.T., Aslam A., and Dobson M.C. (1982) Effects of Vegetation Cover on the Radar Sensitivity to Soil-Moisture. *IEEE Transactions on Geoscience and Remote Sensing,* **20,** pp. 476 - 481.

Uryu Y., Mott C., Foead N., Yulianto K., Budiman A., Setiabudi, and Takakai F. (2008) Deforestation, Forest Degradation, Biodiversity Loss and CO_2 Emissions in Riau, Sumatra, Indonesia. *WWF Indonesia Technical Report, Jakarta, Indonesia.*

USGS (2009) SLC-off Gap-Filled Products - Gap-Fill Algorithm Methodology. *Geological Survey Earth Resources Observation System Data Center. http://landsat.usgs.gov/documents/L7SLCGapFilledMethod.pdf.*

Usup A., Hashimotio T., Takahashi T., and Hayasaka H. (2004) Combustion and thermal characteristics of peat fire in tropical peatland in Central Kalimantan, Indonesia. *Tropics,* **14,** pp. 1 - 19.

van der Werf G., Dempewolf J., Trigg S., Randerson J., Kasibhatla P., Gigliof L. et al. (2008) Climate regulation of fire emissions and deforestation in equatorial Asia. *Proceedings of the National Academy of Sciences of the United States of America,* **105,** pp. 20350 - 20355.

van der Werf G.R., Morton D.C., DeFries R.S., Olivier J.G.J., Kasibhatla P.S., Jackson R.B. et al. (2009) CO_2 emissions from forest loss. *Nature Geoscience,* **2,** pp. 829 - 829.

Vepakomma U., St-Onge B., and Kneeshaw D. (2008) Spatially explicit characterization of boreal forest gap dynamics using multi-temporal LiDAR data. *Remote Sensing of Environment,* **112,** pp. 2326 - 2340.

Vincent G., Sabatier D., Blanc L., Chave J., Weissenbacher E., Pélissier R. et al. (2012) Accuracy of small footprint airborne LiDAR in its predictions of tropical moist forest stand structure. *Remote Sensing of Environment,* **125,** pp. 23 - 33.

Waldes N.J.L. and Page S.E. (2001) Forest structure and tree diversity of a peat swamp forest in Central Kalimantan, Inodesia. *Jakarta symposium proceeding on peatlands or people natural resources function and sustainable management,* **Rieley, J. and Page S. (Eds),** pp. 16 - 22.

Wang J., Day J., and Sun G. (1993) Santa Barbara microwave backscattering model for woodlands. *International Journal of Remote Sensing,* **14,** pp. 1477 - 1493.

Watanabe M., Shimada M., Rosenqvist A., Tadono T., Matsuoka M., Romshoo S.A. et al. (2006) Forest structure dependency of the relation between L-band sigma(0) and biophysical parameters. *IEEE Transactions on Geoscience and Remote Sensing,* **44,** pp. 3154 - 3165.

Whitmore T.C. (1984) Tropical rain forests of the Far East. *Clarendon Press, Oxford.*

Wijaya A. and Gloaguen R. (2009) Fusion of ALOS PALSAR and Landsat ETM data for land cover classification and biomass modeling using non-linear methods. *IEEE International Geoscience and Remote Sensing Symposium IGARSS, Cape Twon, South Africa.*

Wijaya A., Liesenberg V., and Gloaguen R. (2010) Retrieval of forest attributes in complex successional forests of Central Indonesia: Modeling and estimation of bitemporal data. *Forest Ecology and Management,* **259,** pp. 2315 - 2326.

Williams A.P. and Hunt E.R. (2002) Estimation of leafy spurge cover from hyperspectral imagery using mixture tuned matched filtering. *Remote Sensing of Environment,* **82,** pp. 446 - 456.

World Agroforestry Centre (2011) Wood Density Database. *http://www.worldagroforestrycentre.org/Sea/Products/AFDbases/WD/Index.htm.*

Wösten J., Clymans E., Page S., Rieley J., and Limin S. (2008) Peat-water interrelationships in a tropical peatland ecosystem in Southeast Asia. *Catena,* **73,** pp. 212 - 224.

Wösten J.H.M., Ismail A.B., and vanWijk A.L.M. (1997) Peat subsidence and its practical implications: A case study in Malaysia. *Geoderma,* **78,** pp. 25 - 36.

Wösten J.H.M. and Ritzema H. (2001) Land and water management options for peatland development in Sarawak, Malaysia. *International Peat Journal,* **11,** pp. 59 - 66.

Wösten J.H.M. and Ritzema H. (2007) Subsidence and water management of tropical peatlands. *Peatlands International,* **2,** pp. 39 - 39.

Wosten J.H.M., Van der Berg J., Van Eijk P., Gevers G.J.M., Giesen W.B.J.T., Hooijer A. et al. (2006) Interrelationships between hydrology and ecology in fire degraded tropical peat swamp forests. *International Journal of Water Resources Development,* **22,** pp. 157 - 174.

Xie Y.C., Sha Z.Y., Yu M., Bai Y.F., and Zhang L. (2009) A comparison of two models with Landsat data for estimating above ground grassland biomass in Inner Mongolia, China. *Ecological Modelling,* **220,** pp. 1810 - 1818.

Yeager C., Marshall A., Stickler C., and Chapman C. (2003) Effect of fires on peat swamp and lowland dipterocarp forests in Kalimantan, Indonesia. *Tropical Biodiversity,* **8,** pp. 121 - 138.

Zhang Z. and Zang Run-Guo (2009) Modelling the Spatial Distribution of Aboveground Biomass Based on Vegetation Index in A Tropical Forest in Bawangling, Hainan Island, South China. *Chinese Journal of Plant Ecology,* **33,** pp. 833 - 841.

Zhao K.G., Popescu S., and Nelson R. (2009) LiDAR remote sensing of forest biomass: A scale-invariant estimation approach using airborne lasers. *Remote Sensing of Environment,* **113,** pp. 182 - 196.

STATEMENT AND DECLARATION OF HONOR

This PhD thesis has been supervised by Prof. Dr. Florian Siegert according to §6 promotion regulations. I hereby declare that this dissertation has not been submitted (as a whole or in parts) to any other commission and that I did not try to pass any other doctoral examination without success.

I confirm that this thesis was written exclusively by myself without the help of any illegal additives.

Munich, 15 November 2012 _____

Sandra Englhart